

# Nuclear-bound quarkonia and heavy-flavor hadrons

G. Krein,<sup>1</sup> A. W. Thomas,<sup>2</sup> K. Tsushima<sup>3</sup>

<sup>1</sup>Instituto de Física Teórica, Universidade Estadual Paulista,  
Rua Dr. Bento Teobaldo Ferraz, 271 - Bloco II, 01140-070 São Paulo, SP, Brazil

<sup>2</sup>ARC Centre of Excellence for Particle Physics at the Terascale and CSSM,  
School of Physical Sciences, Department of Physics, The University of Adelaide,  
Adelaide SA 5005, Australia

<sup>3</sup>Laboratório de Física Teórica e Computacional, Universidade Cruzeiro do Sul,  
Rua Galvão Bueno, 868, Liberdade 01506-000, São Paulo, SP, Brazil

June 9, 2017

## Abstract

In our quest to win a deeper understanding of how QCD actually works, the study of the binding of heavy quarkonia and heavy-flavor hadrons to atomic nuclei offers enormous promise. Modern experimental facilities such as FAIR, Jefferson Lab at 12 GeV and J-PARC offer exciting new experimental opportunities to study such systems. These experimental advances are complemented by new theoretical approaches and predictions, which will both guide these experimental efforts and be informed and improved by them. This review will outline the main theoretical approaches, beginning with QCD itself, summarize recent theoretical predictions and relate them both to past experiments and those from which we may expect results in the near future.

# Contents

<b>1</b>	<b>Introduction</b>	<b>2</b>
<b>2</b>	<b>Quantum chromodynamics</b>	<b>3</b>
2.1	QCD Lagrangian, quark masses and $\Lambda_{\text{QCD}}$	4
2.2	Symmetries and anomalies	7
2.3	Nonrelativistic QCD (NRQCD)	12
2.4	Potential nonrelativistic QCD (pNRQCD) and van der Waals forces	15
<b>3</b>	<b>Quark-meson coupling (QMC) model</b>	<b>19</b>
3.1	Nuclear matter and finite (hyper)nucleus	20
3.2	Hadron masses in nuclear matter	22
<b>4</b>	<b>Nuclear-bound <math>\eta_c</math> and <math>J/\Psi</math></b>	<b>27</b>
4.1	Quarkonium-nucleon potentials	28
4.2	$J/\Psi$ self-energy and $D\bar{D}$ loop	33
4.3	Predictions for $\eta_c$ - and $J/\Psi$ -nucleus binding energies	37
<b>5</b>	<b>Nuclear-bound <math>\phi</math></b>	<b>42</b>
5.1	$\phi$ self-energy	43
5.2	$\phi$ nuclear bound states	45
<b>6</b>	<b>Nuclear-bound of <math>\omega</math>, <math>\eta</math> and <math>\eta'</math> mesons</b>	<b>49</b>
6.1	In-medium masses of $\omega$ , $\eta$ and $\eta'$ mesons	49
6.2	$\omega$ -, $\eta$ - and $\eta'$ -nuclear bound states	49
<b>7</b>	<b>Nuclear-bound heavy-flavor hadrons</b>	<b>51</b>
7.1	Predictions for $D$ - and $\bar{D}$ -mesic nuclei in $^{208}\text{Pb}$	52
7.2	$\Lambda_c^+$ - and $\Lambda_b$ -hypernuclei	55
7.3	Description of $\Lambda_c^+$ - and $\Lambda_b$ -hypernuclei	55
7.4	Predictions for single-particle energies in $\Lambda_c^+$ - and $\Lambda_b$ -hypernuclei	56
<b>8</b>	<b>Conclusions and Perspectives</b>	<b>61</b>
<b>9</b>	<b>Acknowledgments</b>	<b>62</b>

## 1 Introduction

There is now overwhelming evidence that Quantum Chromodynamics (QCD) is indeed the fundamental theory of the strong interaction and yet we are very far from actually understanding how it works. Certainly lattice QCD has had remarkable success with ground state hadrons, mesons with a simple quark-anti-quark pair and baryons with three valence quarks [1]. Yet beyond that our ignorance is profound. After decades of speculation about, and searches for, colorless states with more than the minimal number of valence quarks we still have no idea whether such states exist or indeed whether QCD predicts them or not.

In the list of particles that have come and gone at various times we think of dibaryons [2, 3, 4], pentaquarks [5, 6] and exotic mesons [7]. Certainly, in the study of excited baryons it has recently become clear that the  $\Lambda(1405)$  is an anti-kaon-nucleon bound state [8] and that the Roper resonance is almost certainly dynamically generated through meson-baryon coupled channel dynamics [9], although

there is no consensus on this [10]. There is now a zoo of excited states of the  $c\bar{c}$  system that must involve more than a simple quark-anti-quark pair. Yet there is no consensus as to whether these are molecular states, threshold effects or genuine exotic states bound by gluonic forces [11]. Until we can find definitive answers to such issues, it is not possible to classify our understanding of QCD as more than superficial.

The study of the interactions of quarkonia with atomic nuclei is an extremely promising avenue for exploring such issues. Because of the Zweig rule, the mean fields generated by light meson exchange, which provide a natural explanation of the binding of atomic nuclei, cannot bind a  $c\bar{c}$  or  $b\bar{b}$  pair and *if* such states are indeed bound to nuclei one must look to other mechanisms, including gluon exchange.

Thus the key issues in this field are firstly whether quarkonia are indeed bound to nuclei, secondly by how much and what are the properties of such states and thirdly how can one quantitatively understand these observations in terms of QCD. This work aims to summarize the status of the theoretical and experimental work in this exciting area. It is complementary in some aspects to the recent review by A. Hosaka et al. in Ref. [12]; while the main focus of the latter is on properties of heavy hadrons in nuclear matter and few-body systems, the present review focuses on nuclear binding phenomena of quarkonia and heavy-flavor hadrons that are of direct relevance for the experiments planned at existing and forthcoming facilities that include FAIR, Jefferson Lab at 12 GeV and J-PARC.

The review begins with a reminder, in section 2, of QCD and especially its adaptation to heavy quark systems, with an emphasis on non-relativistic QCD, NRQCD, which has proven very successful in dealing with heavy quark systems. This is followed by a discussion of potential NRQCD, pNRQCD, which combines NRQCD with effective field theory to yield a Hamiltonian describing the gluon-mediated interactions of quarkonia with other colorless systems.

Section 3 is an outline of the quark-meson coupling (QMC) model. This model starts at the level of the quark structure of hadrons, focusing on the interactions between them mediated by meson exchange, including the change of the internal structure of a hadron immersed in a nuclear medium implied by the self-consistent solution of the field equations. The QMC model serves as a natural way to calculate the non-gluonic mechanisms which may contribute to the binding of quarkonia.

Section 4 deals with the ideal case of the interactions of the  $J/\Psi$  with nuclei. In terms of QCD this may be viewed as a small color dipole immersed in a nuclear medium and so goes to the heart of the issue elaborated earlier, namely how QCD actually works in systems with more than the smallest number of valence quarks. While the  $J/\Psi$  presents particular challenges because of its larger mass, any nuclear levels should be quite narrow and this should make their experimental identification, once formed, quite straightforward.

Although in the context of this review the strange quark is not particularly heavy, because the  $\phi$  meson is almost entirely  $s\bar{s}$ , with little light quark content, it serves as a promising way to access the physics at the heart of this review. In section 5 we outline the many experiments which have already given some hints of binding of the  $\phi$  to atomic nuclei as well as the more modern attempts in preparation. This experimental work is carefully placed in the context of modern theoretical expectations.

Although they are not strictly quarkonia, there has recently been quite a bit of experimental interest in the possible binding of  $\eta$ ,  $\eta'$  and  $\omega$  mesons and we devote section 6 to this topic. Section 7 deals with the natural extension of heavy flavored hadrons,  $D$ ,  $\bar{D}$  mesons and hypernuclei, namely bound states of  $D$ ,  $\bar{D}$  mesons as well as  $\Lambda_c^+$  and  $\Lambda_b$  baryons to nuclei. Finally, section 8 contains some concluding remarks.

## 2 Quantum chromodynamics

In this section we collect different pieces of common knowledge on QCD most relevant for the present review. Without aiming at being exhaustive or self-contained, the basic facts regarding QCD which

we have chosen to cover in this section are directly related to the material discussed in the rest of this review. We refer the reader to the indicated references throughout the text for a more complete and comprehensive account of the subjects discussed.

## 2.1 QCD Lagrangian, quark masses and $\Lambda_{\text{QCD}}$

We write the Lagrangian density of QCD as

$$\begin{aligned}\mathcal{L}_{\text{QCD}} &= \mathcal{L}_q^{(0)} + \mathcal{L}_Q^{(0)} + \mathcal{L}_g^{(0)} \\ &= \mathcal{L}_q + \mathcal{L}_Q + \mathcal{L}_g + \mathcal{L}_{\text{c.t.}},\end{aligned}\tag{1}$$

wherein the terms with or without the superscript (0) have the same structure and are given as follows.  $\mathcal{L}_q$  contains the light-flavor quark Dirac fields  $q = (u, d, s)$ ,  $\mathcal{L}_Q$  the heavy-flavor quark Dirac fields  $Q = (c, b, t)$ ,

$$\mathcal{L}_q = \bar{q}(x) (i\not{D} - m_q) q(x), \quad \mathcal{L}_Q = \bar{Q}(x) (i\not{D} - m_Q) Q(x),\tag{2}$$

and  $\mathcal{L}_g$  contains the pure-gluon part

$$\mathcal{L}_g = -\frac{1}{4} G_{\mu\nu}^a(x) G^{a\mu\nu}(x).\tag{3}$$

In Eq. (2),  $m_q$  and  $m_Q$  are the light and heavy quark mass matrices

$$m_q = \begin{pmatrix} m_u & 0 & 0 \\ 0 & m_d & 0 \\ 0 & 0 & m_s \end{pmatrix}, \quad m_Q = \begin{pmatrix} m_c & 0 & 0 \\ 0 & m_b & 0 \\ 0 & 0 & m_t \end{pmatrix}.\tag{4}$$

In addition,  $\not{D} = \gamma^\mu D_\mu$  and  $G_{\mu\nu}^a$ , with  $a = 1, \dots, 8$ , are respectively the SU(3) color covariant derivative and gluon field strength tensor,

$$D_\mu = \partial_\mu + ig A_\mu(x), \quad G_{\mu\nu}^a(x) = \partial_\mu A_\nu^a(x) - \partial_\nu A_\mu^a(x) - gf^{abc} A_\mu^b(x) A_\nu^c(x),\tag{5}$$

where  $A_\mu(x) = T^a A_\mu^a(x)$ ,  $f^{abc}$  are the structure constants of the color SU(3) group, defined through the commutator  $[T^a, T^b] = if^{abc} T^c$ , with  $T^a = \lambda^a/2$  and normalized as  $T^a T^a = 4/3$ , where  $\lambda^a$  are the SU(3) Gell-Mann matrices. Finally,  $\mathcal{L}_{\text{c.t.}}$  refers to the counterterm Lagrangian density that is required for renormalization; it contains terms of the same structure as those in the other three terms in the second line of Eq. (1). The relation between a field with and without a superscript (0) is through *wave-function renormalization* factors as  $\phi^{(0)}(x) = Z_\phi^{1/2} \phi(x)$ ; the renormalization procedure determines the relation between  $(m_q, m_Q, g)$  and  $(m_q^{(0)}, m_Q^{(0)}, g^{(0)})$ .  $\phi^{(0)}$  is a *bare* field and  $\phi$  is a *renormalized* field, and likewise for the mass and coupling parameters. The Lagrangian in Eq. (1) is not yet complete as gauge fixing terms are necessary for implementing the calculations; we have omitted them because they are not needed for the present discussions.

The separation into light and heavy quark sectors of QCD is dictated by the values of the quark masses. Since free quarks are not observed, their masses cannot be measured directly. When one refers to a value for the mass of a quark, it refers to a particular theoretical framework used to define it. For an observable particle, the position of the pole of the full propagator of the particle is taken as the definition of its mass—this is known as the pole mass. In QCD, the pole position of the quark propagator can be defined unambiguously in the context of perturbation theory only. In that context, the pole mass is infrared finite and gauge independent to all orders in perturbation theory [13].

Renormalization in a perturbative calculation in a field theory like QCD is based on subtraction schemes to handle ultraviolet divergences. Invariably, renormalization schemes introduce an arbitrary

mass scale, usually denoted by  $\mu$ . The counterterm Lagrangian density  $\mathcal{L}_{\text{c.t.}}$  in Eq. (1) is treated as part of the interaction and is used to cancel the ultraviolet divergences;  $\mu$  is a momentum at which one chooses to cancel the ultraviolet divergences and hence it is called the subtraction or renormalization scale. In this way, the values of the quark masses  $m_q$  and  $m_Q$  and the coupling constant  $\alpha_s \equiv g^2/4\pi$  depend on the scheme used to render amplitudes finite; they become *running* quantities, in that  $m_q = m_q(\mu)$ ,  $m_Q = m_Q(\mu)$ ,  $\alpha_s = \alpha_s(\mu)$ , with the running given by renormalization group (RG) equations. The most used renormalization scheme is the so-called  $\overline{\text{MS}}$  scheme [14]; in that scheme, the RG equation for a running quark mass  $m_f(\mu)$ , where  $f = (q, Q)$ , is given by (we present the one-loop contributions only) [15]

$$\mu^2 \frac{dm_f(\mu)}{d\mu^2} = \left[ -\frac{\alpha_s(\mu)}{\pi} + \mathcal{O}(\alpha_s^2) \right] m_f(\mu), \quad (6)$$

while the RG equation for  $\alpha_s(\mu)$  is

$$\mu^2 \frac{d\alpha_s(\mu)}{d\mu^2} = \beta(\alpha_s) = -b_0 \alpha_s^2 + \mathcal{O}(\alpha_s^3), \quad (7)$$

where  $b_0$  is the one-loop beta-function coefficient, given in terms of the number of flavors  $N_f$  as

$$b_0 = \frac{33 - 2N_f}{12\pi}, \quad (8)$$

where  $N_f$  is the number of light flavors with masses less than the scale  $\mu$ . Complications arise when heavy flavors need to be taken into account in the loops [14] but they are of no concern at the level of the present discussion. The essence of RG equations is that  $\mu$  is an extraneous parameter to the theory and physical quantities must be  $\mu$ -independent; when changing  $\mu$ , the running masses and coupling must be readjusted in compensation to leave observables invariant. These RG equations are commonly derived by using the fact that the bare parameters of the theory are  $\mu$ -independent. An intuitive meaning of  $\mu$  is given in an enlightened discussion in Ref. [14] in the context of a deep inelastic scattering process: for large values of  $\mu$ ,  $\mu$  plays the role of a cutoff on the transverse momentum in a loop integral contributing to such a process. In general,  $\mu$  is chosen to be of the same size as the typical momentum transfer involved in the process under study, and  $\alpha_s(\mu)$  at that scale gives the effective strength of the strong interaction in the process.

For  $\alpha_s(\mu)$  sufficiently small, one can obtain its explicit  $\mu$  dependence by integrating Eq. (7) from  $\mu_0$  to  $\mu$ :

$$\frac{1}{\alpha_s(\mu)} = \frac{1}{\alpha_s(\mu_0)} + b_0 \ln \left( \frac{\mu^2}{\mu_0^2} \right), \quad (9)$$

which can be rewritten in terms of a  $\mu$ -independent mass scale  $\Lambda_{\text{QCD}}$  as

$$\frac{1}{\alpha_s(\mu)} - b_0 \ln \left( \frac{\mu^2}{\Lambda_{\text{QCD}}^2} \right) = \frac{1}{\alpha_s(\mu_0)} - b_0 \ln \left( \frac{\mu_0^2}{\Lambda_{\text{QCD}}^2} \right). \quad (10)$$

This, on the other hand, means that

$$\Lambda_{\text{QCD}} = \mu e^{-1/[2b_0\alpha_s(\mu)]}, \quad (11)$$

or, equivalently

$$\alpha_s(\mu) = \frac{1}{b_0 \ln(\mu^2/\Lambda_{\text{QCD}}^2)} = \frac{12\pi}{(33 - 2N_f) \ln(\mu^2/\Lambda_{\text{QCD}}^2)}. \quad (12)$$

As  $\mu$  increases,  $\alpha_s(\mu)$  decreases, QCD becomes weakly coupled and perturbation is applicable. This feature is the renowned property of *asymptotic freedom* [16, 17]. Therefore, processes amenable to

perturbation theory are those involving large momentum transfers, or short distances. On the other hand, processes involving small momentum transfers are not amenable to perturbation theory because the effective coupling becomes large. From Eq. (12) one has that for  $\mu \sim \Lambda_{\text{QCD}}$ , the coupling increases substantially. Although Eq. (12) is not valid at such values of  $\mu$ , extractions of  $\alpha_s$  from different experimental sources show that it is a growing function of  $\mu$ , varying typically from  $\alpha_s \simeq 0.08$  at  $\mu = 1000$  GeV to  $\alpha_s \simeq 0.4$  at  $\mu = 2$  GeV [15].

The appearance of a mass scale in the theory due to the renormalization has deep consequences in the way a symmetry of the classical QCD Lagrangian is realized when taking into account quantum fluctuations. In general, when a symmetry of the classical Lagrangian of a theory is not realized in its quantum version, one says that there exists an *anomaly* in the theory. One particular anomaly that is of importance for the subject of quarkonia in nuclei, as we will discuss shortly, is related to scale invariance of (massless) QCD, known as the anomaly in the trace of the energy-momentum tensor (or, simply the *trace anomaly*) [18, 19, 20, 21, 22, 23, 24].

The mass scale  $\Lambda_{\text{QCD}}$  is a parameter of QCD; it is the value at which the theory becomes strongly coupled and nonperturbative. Its precise value depends on the renormalization scheme, on the number of active flavors, on the perturbative order at which the  $\beta$  function is evaluated and also on approximations used to solve the RG equation. That is, the determination of  $\Lambda_{\text{QCD}}$  from data involves the use of an  $\alpha_s(\mu)$  obtained from the solution of the RG equation in some renormalization scheme and calculated up to a certain number of loops; Equation (7), for example, is derived in the  $\overline{\text{MS}}$  scheme and a calculation that retains the first term only in that equation is a one-loop calculation. The present (central) values in the  $\overline{\text{MS}}$  scheme for different flavor numbers  $N_f$  are [15]

$$\Lambda_{\text{QCD}} = \begin{cases} 332 & \text{for } N_f = 3 \\ 292 & = 4 \\ 210 & = 5 \\ 89 & = 6 \end{cases} \quad (13)$$

Reference [25] is a very recent review of the present theoretical and empirical knowledge for  $\alpha_s$ . The review discusses several issues related to different definitions of  $\alpha_s$  and  $\Lambda_{\text{QCD}}$ , their scheme dependence and extraction of their values from experimental data. We strongly recommend this reference to the reader interested in more details on these fundamental parameters of QCD.

Knowing  $\alpha_s(\mu)$ , one can solve the RG equation for the quark masses  $m_f(\mu)$ . The PDG [15] quotes values of the masses of the light ( $u, d, s$ ) quarks in the  $\overline{\text{MS}}$  scheme at the renormalization scale  $\mu = 2$  GeV, and those of the heavy quarks ( $c, b, t$ ) as pole masses or as  $\overline{\text{MS}}$  masses evaluated at a scale equal to the mass, i.e.  $m_Q(\mu = m_Q)$ . The pole mass  $m_f$  and the  $\overline{\text{MS}}$  masses  $m_f(\mu)$  evaluated at  $\mu = m_f$  are related by

$$m_f = m_f(m_f) \left[ 1 + \frac{4\alpha_s(m_f)}{3\pi} + \mathcal{O}(\alpha_s^2) \right]. \quad (14)$$

Table 1 presents the values of  $\overline{\text{MS}}$  masses collected by the PDG [15]—for completeness, the electric charges and flavor quantum numbers (isospin I and third component of isospin  $I_3$ , strangeness S, charm C, bottom B and top T) of the quarks are also shown in the table. For the bottom quark, using the  $\overline{\text{MS}}$  mass given in the table leads to  $m_b = 1.18 \overline{m}_b(\overline{m}_b) = 4.93$  GeV for the bottom pole mass, when using Eq. (14) evaluated up to  $\alpha_s^3$  [15].

Inspection of Tab. 1 reveals that the ( $u, d, s$ ) quarks are clearly much lighter than the ( $c, b, t$ ) quarks. Although the  $s$  quark is much heavier than the ( $u, d$ ) quarks, still, it is an order of magnitude lighter than the lightest of the heavy quarks, the  $c$  quark. This large difference in the masses of light and heavy quarks has dramatic consequences in the dynamics governing the internal structure of quark-gluon bound states—the hadrons—containing different combinations of quarks of different flavors. In QCD, a hadron is described by a state in Hilbert space, the state being characterized by a set of quantum

Table 1: Quark masses (in GeV). The values of quark masses are central values (i.e. without uncertainties) from the PDG [15]—they are  $\overline{\text{MS}}$  masses,  $m_q = m_q(\mu = 2 \text{ GeV})$  for the light quarks  $q = (u, d, s)$ , and  $m_Q = m_Q(\mu = m_Q)$  for the heavy quarks  $Q = (c, b, t)$ , where  $\mu$  is the renormalization scale. Also shown are the electric charges (in units of the electron charge magnitude  $e$ ) and flavor quantum numbers of the quarks.

Quark	$u$	$d$	$s$	$c$	$b$	$t$
Mass	0.0022	0.0047	0.096	1.27	4.18	160
Charge	$+\frac{2}{3}$	$-\frac{1}{3}$	$+\frac{2}{3}$	$+\frac{2}{3}$	$+\frac{2}{3}$	$+\frac{2}{3}$
Flavor	$I=\frac{1}{2}, I_3=+\frac{1}{2}$	$I=\frac{1}{2}, I_3=-\frac{1}{2}$	$S=-1$	$C=+1$	$B=-1$	$T=+1$

numbers, such as spin, parity, flavor, etc. Hadron properties can be studied by analysing correlation functions (also known as propagators, or Green functions) of interpolators. Interpolators are gauge-invariant products of quark and gluon field operators having the quantum numbers of the hadron of interest. The mass spectrum of a hadron, for example, can be extracted by searching for isolated poles in such a correlation function. Let  $h$  denote a light-flavor hadron. Even though the interpolators for  $h$  contain gluon and light-flavor quark fields only, the heavy quark fields do contribute to the  $h$  correlation functions through quantum fluctuations. However, in view of their large mass, heavy quarks play a minor role in the properties of  $h$  in view of the *decoupling theorem* [26], which in its essence asserts that the contributions of a large mass in quantum fluctuations are suppressed when they appear in a finite amplitude, and when they appear in a divergent amplitude they can be eliminated through the renormalization of the parameters of the theory.

## 2.2 Symmetries and anomalies

Consider the hypothetical situation in which the light quarks are massless,  $m_q = 0$ , and the heavy quarks are infinitely heavy,  $m_Q = \infty$ . The heavy quarks do not contribute at all to the structure of the light-flavor hadron  $h$ . In this hypothetical situation, the only dimensionful parameters in the theory are  $\Lambda_{\text{QCD}}$  and the mass  $m_h$  and a typical size  $r_h$  of  $h$  would be

$$m_h = a_h \Lambda_{\text{QCD}}, \quad r_h = b_h \Lambda_{\text{QCD}}^{-1}, \quad (15)$$

where  $a_h$  and  $b_h$  are dimensionless numbers. Different hadrons have different values for  $a_h$  and  $b_h$ . The value of  $m_h$  is deeply connected with the breaking of the scale invariance of the QCD Lagrangian due to the renormalization. Let us consider a scale transformation of the spacetime coordinates  $x^\mu$  by a dimensionless parameter  $\lambda$

$$x^\mu \rightarrow x'^\mu = \lambda x^\mu, \quad (16)$$

and the associated transformations of the quark  $q(x)$  and gluon fields  $A_\mu(x)$

$$q(x) \rightarrow q'(x) = \lambda^{3/2} q(\lambda x), \quad A_\mu(x) \rightarrow A'_\mu(x) = \lambda A_\mu(\lambda x). \quad (17)$$

Under this scale transformation, while the the classical QCD (massless) Lagrangian would change as

$$\mathcal{L}_{\text{QCD}}(x) \rightarrow \mathcal{L}'_{\text{QCD}}(x) = \lambda^4 \mathcal{L}_{\text{QCD}}(\lambda x), \quad (18)$$

the action remains unchanged:

$$S_{\text{QCD}} = \int d^4x \mathcal{L}_{\text{QCD}}(x) \rightarrow \int d^4x \lambda^4 \mathcal{L}_{\text{QCD}}(\lambda x) = \int d^4x' \mathcal{L}_{\text{QCD}}(x') = S_{\text{QCD}}. \quad (19)$$

The associated Noether current, the dilatational current, is given by

$$J_{\text{dil}}^\mu(x) = T^{\mu\nu}(x) x_\nu, \quad (20)$$

where  $T^{\mu\nu}(x)$  is the energy-momentum tensor, which is a conserved quantity,  $\partial_\mu T^{\mu\nu}(x) = 0$ . The divergence of  $J_{\text{dil}}^\mu(x)$  is the trace of the energy-momentum tensor:

$$\partial_\mu J_{\text{dil}}^\mu(x) = T^\mu_\mu(x) = 0, \quad (21)$$

where the vanishing of  $T^\mu_\mu(x)$  follows from the classical equations of motion of the quark and gluon fields. On the other hand, since the expectation value of  $T^\mu_\mu$  in the state  $|h\rangle$  of a hadron at rest gives the mass of this state,

$$\langle h|T^\mu_\mu|h\rangle = m_h, \quad (22)$$

where we are using a nonrelativistic normalization for the hadron states  $|h\rangle$ , the result in Eq. (21) would suggest a vanishing mass for all hadrons.

A very simple, heuristic way to see how the situation changes due to quantum effects is as follows [27]. If one considers that the coupling  $g$  that appears in the Lagrangian is scale dependent,  $g = g(\mu)$ , the massless action is not scale invariant anymore. First, let us rescale the gluon field by  $g$  as  $\bar{A}_\mu^a \equiv g A_\mu^a$ , the massless Lagrangian becomes

$$\mathcal{L}_{\text{QCD}} = -\frac{1}{4g^2} \bar{G}_{\mu\nu}^a(x) \bar{G}^{a\mu\nu}(x) + \bar{q}(x) [i\gamma^\mu(\partial_\mu + i\bar{A}_\mu(x))] q(x), \quad (23)$$

so that one sees that all dependence on  $g$  appears as an overall factor in the pure-gluon term. Next, let us consider an infinitesimal scale transformation,  $\mu \rightarrow \lambda\mu$  with  $\lambda = 1 + \delta\lambda$ , so that

$$\delta S_{\text{QCD}} = \delta \left( -\frac{1}{4\pi\alpha_s} \frac{1}{4} \int d^4x \bar{G}_{\mu\nu}^a(x) \bar{G}^{a\mu\nu}(x) \right) = -\frac{2\beta(\alpha_s)}{\alpha_s} S_{\text{QCD}} \delta\lambda. \quad (24)$$

From Noether's theorem, one then has that the trace of the energy momentum tensor does not vanish, which is the statement of the trace anomaly [18, 19, 20, 21, 22, 23, 24]:

$$\begin{aligned} T^\mu_\mu(x) &= \frac{2\beta(\alpha_s)}{\alpha_s} \frac{1}{4} G_{\mu\nu}^a(x) G^{a\mu\nu}(x) = -\frac{1}{2} b_0 \alpha_s G_{\mu\nu}^a(x) G^{a\mu\nu}(x) \\ &= -\frac{9}{32\pi^2} g^2 G_{\mu\nu}^a(x) G^{a\mu\nu}(x), \end{aligned} \quad (25)$$

where we used the  $\beta$ -function at lowest order in perturbation theory. A more sophisticated proof of this result can be found in Ref. [28]. Therefore,

$$m_h = -\frac{9}{32\pi^2} \langle h|g^2 G_{\mu\nu}^a G^{a\mu\nu}|h\rangle. \quad (26)$$

That is, the entire mass of a hadron is due to gluons.

When  $m_q \neq 0$ , the trace of the energy-momentum tensor receives contributions from the mass term in the light-quark part of the QCD Lagrangian in Eq. (2) and  $m_h$  is given by

$$m_h = \frac{\beta(\alpha_s)}{2\alpha_s} \langle h|G_{\mu\nu}^a G^{a\mu\nu}|h\rangle + \langle h|\bar{q} m_q q|h\rangle. \quad (27)$$



The interesting point of this result is that the matrix element  $\langle h|g^2 G_{\mu\nu}^a G^{a\mu\nu}|h\rangle$  contributes to the amplitude of quarkonium-hadron scattering at threshold, as we discuss further ahead in this review. This means that one can probe the distribution of mass inside a hadron via close to threshold quarkonium-hadron scattering [29]. Also, the combined use of the trace anomaly and a deep-inelastic momentum sum rule allows to derive a separation of the nucleon mass into contributions of the quark and gluon kinetic and potential energies, quark masses, and the trace anomaly [30].

For  $m_q \neq 0$ , the parameters  $a_h$  and  $b_h$  receive contributions from  $m_q$ . Since  $m_q/\Lambda_{\text{QCD}} \ll 1$ , one can in principle calculate corrections to  $a_h$  and  $b_h$  by treating the mass term  $m_q \bar{q}(x)q(x)$  in the QCD Lagrangian in Eq. (1) as a perturbation and the results would be expressed in the form of (integer and noninteger) powers of  $m_q/\Lambda_{\text{QCD}}$  and of  $\ln(m_q/\Lambda_{\text{QCD}})$ . There is, however, a more practical way of implementing a calculation of this kind by using an EFT employing hadron degrees of freedom. When endowed with an appropriate power counting scheme, the EFT provides a powerful way of calculating quark-mass corrections to observables. The EFT is based on the fact that in the  $m_q \rightarrow 0$  limit, QCD acquires an  $SU(3)_R \times SU(3)_L$  chiral symmetry that is dynamically broken by the strong QCD interactions to an  $SU(3)_V$  flavor symmetry. Specifically, the light-quark part of the QCD Lagrangian in Eq. (2) can be rewritten in terms of the right-handed and left-handed quark field operators  $q_R(x) = 1/2(1 + \gamma_5)q(x)$  and  $q_L(x) = 1/2(1 - \gamma_5)q(x)$  as (we follow closely the presentation in Ref. [31]):

$$\mathcal{L}_q = \bar{q}(x) i\not{D} q(x) = \bar{q}_R(x) i\not{D} q_R(x) + \bar{q}_L(x) i\not{D} q_L(x), \quad (28)$$

which clearly is invariant under the transformations

$$q_R(x) \rightarrow q'_R = R q_R(x), \quad q_L(x) \rightarrow q'_L = L q_L(x), \quad (29)$$

with  $R \in SU_R(3)$  and  $L \in SU_L(3)$ . The dynamical breaking of the  $SU(3)_R \times SU(3)_L$  is commonly discussed in terms of the nonzero value of the vacuum expectation value (v.e.v.) of quark bilinears  $\bar{q}^f(x)q^{f'}(x) = \bar{q}_R^f q_L^{f'}(x) + \bar{q}_L^f q_R^{f'}(x)$ :

$$\langle \bar{q}_R^f(x)q_L^{f'}(x) \rangle = B \delta^{ff'}, \quad (30)$$

where  $B \sim \Lambda_{\text{QCD}}^3$  and  $f$  and  $f'$  are flavor indices. The v.e.v.  $\langle \bar{q}^f(x)q^f(x) \rangle$  is known as the quark condensate. In perturbation theory, it is trivially zero (in the massless limit) and its nonzero value is driven by nonperturbative gluon dynamics. There is a profound interrelationship between the trace anomaly and dynamical chiral symmetry breaking, in that the smallness of the pion mass would be difficult to reconcile with Eq. (27) were it not for the dynamical breaking of a symmetry, in the present case, chiral symmetry—for a very recent discussion on this, see Ref. [32]. A nonzero value of the condensate implies in a dynamically generated quark mass and thereof hadron masses can be understood as coming from massive quarks, as in the pre-QCD quark models. Our understanding on how this exactly happens and its impact on hadron observables has evolved tremendously during the last decades through numerical simulations of QCD discretized on a space-time Euclidean lattice [33] and also from studies in the continuum [34, 35].

Under the transformations in Eq. (29), this v.e.v. transforms as  $\langle \bar{q}_R^f q_L^{f'} \rangle = B (LR^\dagger)_{f'f}$ . Since for  $L = R$  the v.e.v. is unchanged, the  $SU(3)_R \times SU(3)_L$  symmetry of the Lagrangian is broken to its diagonal subgroup  $SU(3)_V$  and one identifies the eight pseudoscalar mesons  $\pi^0$ ,  $\pi^\pm$ ,  $K^0$ ,  $\bar{K}^0$ ,  $K^\pm$ , and  $\eta$  with the (pseudo-)Goldstone bosons with the fluctuations of  $\bar{q}_R q_L$ . The fields corresponding to these particles can be described by a special unitary  $3 \times 3$  matrix  $U(x)$

$$U = e^{i\Phi/f} \quad \Phi = \begin{pmatrix} \pi^0 + \eta/\sqrt{3} & \sqrt{2}\pi^+ & \sqrt{2}K^+ \\ \sqrt{2}\pi^- & -\pi^0 + \eta/\sqrt{3} & \sqrt{2}K^0 \\ \sqrt{2}K^- & \bar{K}^0 & -2\eta/\sqrt{3} \end{pmatrix}, \quad (31)$$

where  $f$  is the leptonic decay constant of the Goldstone bosons (with this normalization, the experimental value of the pion decay constant is  $f_\pi = 93$  MeV). This matrix transforms under  $SU(3)_R \times SU(3)_L$  as

$$U(x) \rightarrow L U(x) R^\dagger. \quad (32)$$

An effective Lagrangian density respecting  $SU(3)_R \times SU(3)_L$  can be constructed by using as building blocks products of  $U(x)$  and its derivative  $\partial_\mu U(x)$ . The leading order Lagrangian in the number of derivatives is

$$\mathcal{L}_{\text{GB}} = \frac{f^2}{4} \text{Tr} \left[ \partial_\mu U(x) \partial^\mu U^\dagger(x) \right]. \quad (33)$$

The factors  $1/f$  in Eq. (31) and  $f^2/4$  in the Lagrangian are chosen so that the kinetic-energy term of the fields in the Lagrangian have standard normalization.

The symmetry-breaking mass term in the QCD Lagrangian can be implemented in the EFT by using the trick of supposing that the mass matrix  $m_q$  transforms under  $SU(3)_R \times SU(3)_L$  as  $m_q \rightarrow L m_q R^\dagger$ , so that the mass term in the Lagrangian is invariant under  $SU(3)_R \times SU(3)_L$ . Then, to lowest order in  $m_q$ , the symmetry-breaking term in the EFT is

$$\mathcal{L}_{m_q} = \bar{q}(x) m_q q(x) = \bar{q}_R(x) m_q q_L(x) + \bar{q}_L(x) m_q q_R(x) \rightarrow \mathcal{L}_{\text{GB}-m_q} = B \text{Tr} \left[ U^\dagger(x) m_q + m_q^\dagger U(x) \right]. \quad (34)$$

The lowest order Lagrangian of this EFT is the sum of the two contributions, Eqs. (33) and (34). Higher order terms can be constructed in a similar fashion. There is a huge literature associated with the use of this EFT to study low-energy phenomena involving (pseudo)Goldstone bosons. The reader interested in knowing more on the techniques and applications of this and other chiral EFTs can find good guidance in the book of Ref. [36]. Of interest for the present review are two applications of this chiral EFT. One is related to the restoration of chiral symmetry at finite temperature  $T$  and baryon density  $\rho_B$ . The other is in connection with the derivation of the long-range part of the quarkonium-quarkonium interaction, that we discuss in subsection 2.4.

At very large temperatures, the relevant scale in QCD is the temperature and due to asymptotic freedom the coupling strength  $\alpha_s$  becomes small and so the quark condensate. The same can be expected for very large baryon densities, when the relative quark distances become small. For zero baryon density, recent lattice QCD simulations [37], employing a pion mass of  $m_\pi = 161$  MeV, have shown that there is a drastic decrease of the quark condensate around a temperature of  $T_{\text{pc}} = 154 \pm 9$  MeV. For finite baryon densities, the combined  $T$  and  $\rho_B$  behavior of the condensate is presently unknown in lattice QCD. However, for sufficiently low temperatures, the lowest mass excitations are pions and the chiral EFT just described can be used [38, 39] to obtain the temperature dependence of the condensate; to leading order,  $\langle \bar{q}q \rangle_T$  is given by (for two massless quark flavors):

$$\frac{\langle \bar{q}q \rangle_T}{\langle \bar{q}q \rangle} = 1 - \frac{T^2}{8f_\pi^2}. \quad (35)$$

For nonzero  $\rho_B$ , there are results from calculations using QCD sum rules that generalize this result for small values of  $\rho_B$  to [40, 41]:

$$\frac{\langle \bar{q}q \rangle_{T\rho_B}}{\langle \bar{q}q \rangle} = 1 - \sum_h \frac{\Sigma_h}{f_\pi^2 m_\pi^2} \rho_s^h = 1 - \frac{T^2}{8f_\pi^2} - \frac{1}{3} \frac{\rho_B}{\rho_0}, \quad (36)$$

where  $\Sigma_h = m_q \partial m_h / \partial m_q$ ,  $\rho_s^h$  is the scalar density of a hadron  $h$  in matter and  $\rho_0$  is the baryon saturation density of nuclear matter. These results point to a partial restoration of chiral symmetry and a large body of work has been devoted to extract signals of changes of the intrinsic structure of hadrons in nuclei due to this. In another direction, through experiments of heavy ion collisions, new phases of QCD matter are expected to be created which can teach us about the first stages of the evolution of

the Universe. Ref. [42] is a recent review on the theoretical and phenomenological understanding of selected topics on hadrons in medium.

The classical Lagrangian in Eq. (28) has two additional global  $U(1)$  symmetries: one is a vector  $U(1)$  symmetry where right- and left-handed quarks transform by a common phase, and the other is an axial  $U(1)$  symmetry where right- and left-handed quarks transform by the opposite phase. While the first remains a symmetry in the quantum version of the theory and is associated with baryon number conservation, the second does not. More specifically, the axial transformation is of the form

$$q_R(x) \rightarrow q'_R(x) = e^{-i\theta} q_R(x), \quad q_L(x) \rightarrow q'_L(x) = e^{+i\theta} q_L(x), \quad (37)$$

or, equivalently

$$q(x) \rightarrow q'(x) = e^{-i\theta \gamma_5} q(x). \quad (38)$$

Noether's theorem implies conservation of the flavor singlet current

$$\partial^\mu J_{5\mu}^{(0)}(x) = 0, \quad (39)$$

where

$$J_\mu^{(0)}(x) = \bar{q}(x) \gamma_\mu \gamma_5 q(x) = \bar{u}(x) \gamma_\mu \gamma_5 u(x) + \bar{s}(x) \gamma_\mu \gamma_5 s(x) + \bar{s}(x) \gamma_\mu \gamma_5 s(x). \quad (40)$$

There are various ways to demonstrate that this symmetry does not happen in the quantum version of the theory [43, 44]. The simplest to state but more elaborate to demonstrate is the assertion that the transformations in Eq. (37) (or in Eq. (38)) change the measure in the path integral [45]. One important consequence of this axial anomaly (also known as chiral anomaly) is that divergence of the flavor-singlet current is given by (now including the explicit symmetry-breaking mass term)

$$\partial^\mu J_{5\mu}^{(0)}(x) = \frac{3\alpha_s}{8\pi} \epsilon^{\mu\nu\alpha\beta} G_{\mu\nu}^a G_{\alpha\beta}^a + 2i \left[ m_u \bar{u}(x) \gamma_5 u(x) + m_d \bar{d}(x) \gamma_5 d(x) + m_s \bar{s}(x) \gamma_5 s(x) \right]. \quad (41)$$

We refer the reader to Ref. [27] for a modern textbook demonstration. As in the case of the trace anomaly, one sees that the nonconservation of the flavor-singlet current is driven by gluon dynamics.

In the absence of this axial anomaly, one would have one more pseudo Goldstone boson with flavor content  $\bar{u}u + \bar{d}d + \bar{s}s \equiv \eta_0$ , whose mass would vanish in the chiral limit. But the lightest candidate for a ninth pseudoscalar particle is  $\eta'(960)$ , which is much heavier than the other real eight pseudo Goldstone bosons [15]. Current understanding is that the physical pseudoscalar particles with an  $\bar{s}s$  content are  $\eta(549)$  and  $\eta'(960)$ , which are mixtures of the flavor singlet combination  $\eta_0$  and flavor octet  $\eta_8 = \bar{u}u + \bar{d}d - 2\bar{s}s$  combination, with  $\eta'(960)$  being predominantly composed by the  $\eta_0$  component. In section 6 we review studies of the formation of  $\eta$  and  $\eta'$  nuclear bound states. These are motivated [46, 47, 48] by the fact that the in-medium mass of the  $\eta$  and  $\eta'$  are modified by the interaction with the nuclear mean fields, in particular by the attractive scalar-isoscalar component. The study of these nuclear bound states provides a unique opportunity to learn about the interplay between dynamical chiral symmetry breaking and the axial anomaly.

We also review recent progress in studies of nuclear bound states of heavy-flavor hadrons. Hadrons containing light quarks and only one heavy quark (or antiquark) are very interesting QCD bound states. They are interesting as their internal dynamics is still determined by the light quarks and the presence of a heavy quark gives rise to a symmetry which is not apparent in the QCD Lagrangian. In the  $m_Q \rightarrow \infty$  limit, the heavy quark does not contribute with a (positive) kinetic energy to the bound state and the mass and typical size of the hadron are still governed by  $\Lambda_{\text{QCD}}$ . Moreover, the average velocity  $v_Q$  of the heavy quark in a heavy-light bound state is changed very little by the interactions, as  $\Delta v_Q = \Delta p_Q / m_Q \sim \Lambda_{\text{QCD}} / m_Q \ll 1$  and the interactions of a heavy quark, regardless of its flavor, within the hadron become independent of its spin. This gives rise to a spin-flavor heavy quark  $U(2N_Q)$  symmetry— $2N_Q = 2$  (spin)  $\times N_Q$  (heavy flavors). This means that the light quark dynamics occurs in

the background of a strong color field of an essentially static spectator. An EFT, known as HQET, can be constructed from the QCD Lagrangian by implementing a suitable  $1/m_Q$  expansion [31].

On the other hand, the internal dynamics of hadrons containing more than one heavy quark is very different from that of the previous two cases. Let us take the case of a heavy quarkonium  $Q\bar{Q}$ , which is one of the heavy hadrons of interest to the present review. For large values of  $m_Q$ , the bound-state is controlled by short-distance dynamics, which is weakly coupled and nonrelativistic. The interaction between the  $Q$  and  $\bar{Q}$  is essentially an attractive Coulomb force and the heavy quark must have a kinetic energy to balance this force and form a bound state. The mass and size of the  $Q\bar{Q}$  quarkonium are not at all controlled by  $\Lambda_{\text{QCD}}$ . Nonrelativistic QCD (NRQCD) [49] and potential nonrelativistic QCD (pNRQCD) [50, 51] are examples of EFTs that have been used to treat heavy quarkonia—for a comprehensive review, see Ref. [52]. These EFTs provide an adequate first-principles framework for studying the low energy interactions of quarkonia in nuclear matter as their Lagrangian (or Hamiltonian) can be cast into the form usually used to treat the nuclear many-body problem. We discuss this in the next section.

To finalize this section, we mention that the top quark  $t$  is of no interest in the present review. The top quark is the heaviest quark, its lifetime is very short,  $\tau_t = 5 \times 10^{-25}$  s, it decays with a probability close to 100% to a  $W$  boson and  $b$  quark, and has a width much larger than  $\Lambda_{\text{QCD}}$ , namely  $\Gamma_t \simeq 1.4$  GeV [15] and, because of this, it cannot form a QCD bound state like a toponium  $t\bar{t}$  or a heavy-light  $q\bar{t}$  meson [53].

## 2.3 Nonrelativistic QCD (NRQCD)

In this and in the following sections we outline the construction of nonrelativistic approximations to QCD that lead to EFTs adequate for studying quarkonium in free space. It is not our aim to give a full account of the field of nonrelativistic QCD or of the results obtained within such approximations; we direct the interested reader to excellent review articles available in the literature. We focus on concepts and techniques that we believe are useful for building EFTs for studying quarkonium in matter. A theoretical framework rooted in QCD and built on controllable approximations that can be systematically improved is not yet available for quarkonium in matter. It is our hope that the present and the following chapters will motivate readers to contribute to this endeavor.

As pointed out previously, when  $m_Q \gg \Lambda_{\text{QCD}}$ , the quark and antiquark in the rest frame of a heavy quarkonium are nonrelativistic, with relative velocities  $v \ll 1$ . This implies that relative momenta are given by  $|\vec{p}| \sim m_Q v \ll m_Q$ . A nonrelativistic approximation involves an expansion in powers of  $|\vec{p}|/m_Q$ ; since  $|\vec{p}|/m_Q \sim v \ll 1$ , the velocity  $v$  can be used as a small expansion parameter. The binding energy  $E_B$  is another important scale in the problem. From the virial theorem,  $E_B \sim m_Q v^2 \ll |\vec{p}|$ . Therefore, the heavy quarkonium bound state is characterized by three well-separated scales, traditionally named *hard*, *soft* and *ultrasoft*:

- Hard:  $m_Q$ , the heavy quark mass, it is the largest scale;
- Soft:  $|\vec{p}| \sim m_Q v$ , the relative momentum;
- Ultrasoft:  $E_B \sim m_Q v^2$ , the binding energy.

NRQCD is an EFT designed to accurately reproduce the low momentum behavior of QCD in the heavy quark sector, where  $m_Q \gg \Lambda_{\text{QCD}}$ . NRQCD is obtained from QCD by *integrating out* the hard scale  $m_Q$ . The heavy-quark field operators are two-component nonrelativistic Pauli spinors,  $\psi$  for the quark and  $\chi$  for the antiquark, and gluons are kept fully relativistic. The field  $\psi$  annihilates a heavy quark and  $\chi$  creates a heavy antiquark. For simplicity, we consider a single heavy flavor quark, so there is no need for flavor indices in  $\psi$  and  $\chi$  and  $m_Q$ . Here we will follow the simplest path to

construct the lowest-order terms of the Lagrangian: one writes down the most general gauge-invariant, rotationally symmetric and Hermitian local Lagrangian that respects P (parity), T (time-reversal) and Galilean invariances—here we follow closely the presentation in Ref. [54]. Moreover, the Lagrangian is built using a power counting scheme, whose meaning will become clear in the next discussions. We concentrate on the part of the effective Lagrangian that describes the couplings of the heavy quark and antiquark fields ( $\psi, \chi$ ) to gluon fields; they are written as an expansion in powers  $1/m_Q$ . The NRQCD Lagrangian density can be written generically as

$$\mathcal{L}_{\text{NRQCD}} = \mathcal{L}_{\text{light}} + \mathcal{L}_{\psi\psi} + \mathcal{L}_{\chi\chi} + \mathcal{L}_{\psi\psi\chi\chi} + \dots, \quad (42)$$

where  $\mathcal{L}_{\text{light}}$  collects the contributions containing only soft and ultrasoft light-quark and gluon fields. Let us start discussing the quadratic terms in ( $\psi, \chi$ ); they are of the form

$$\begin{aligned} \mathcal{L}_{\psi\psi} &= \sum_n C_n \psi^\dagger(x) \frac{O_n(x)}{m_Q^n} \psi(x) \\ &= \mathcal{L}_{\psi\psi}^{(0)} + \mathcal{L}_{\psi\psi}^{(1)} + \mathcal{L}_{\psi\psi}^{(2)} + \dots, \end{aligned} \quad (43)$$

with the  $O_n$  built from gluon fields, their derivatives with respect to time and space coordinates and contractions with spin matrices  $\vec{\sigma}$ . The Lagrangian  $\mathcal{L}_{\chi\chi}$  is of same form as Eq. (43), but with  $\psi \rightarrow \chi$  and a global sign change in some of the terms due to charge-conjugation symmetry. In addition, the  $\dots$  in Eq. (42) include pure-gluon terms and of course multiquark interactions, beyond the four-quark term. The mass dimension of fermion fields is  $[\psi] = [\chi] = 3/2$ . The factors of  $m_Q$  are introduced in order the coefficients  $C_n$  be dimensionless. Since  $[\mathcal{L}] = 4$ , therefore  $[O_n] = n + 1$ . The coefficients  $C_n$  are functions of  $\alpha_s$ , the quark mass  $m_Q$  and a regularization cutoff like the scale  $\mu$  of dimensional regularization; they are determined by a *matching procedure*: this amounts to calculating a low-energy heavy-quark on-shell scattering amplitude in NRQCD at a given order in  $\alpha_s$  and up to some order in the small parameter expansion  $v$ , and equating the result to the same calculation in full QCD at some matching scale, e.g. at  $\mu = m_Q$ . That perturbation theory can be used follows from the fact that corrections to the coefficients from quantum fluctuations are from short-distances.

To build gauge-invariant expressions, one can use the covariant derivatives, written as Hermitean operators as  $iD_t = i\partial/\partial t - gA_0$ ,  $i\vec{D} = i\vec{\nabla} + g\vec{A}$ . Whenever convenient, one can use the relation of the covariant derivatives to the color electric and magnetic fields:  $E^i = G^{i0} = -(i/g)[D_t, D^j]$  and  $B^i = \epsilon^{ijk} G_{jk} = (i/g)\epsilon^{ijk} [D_j, D_k]$ . Their mass dimensions are  $[D_t] = [\vec{D}] = 1$ , and  $[\vec{E}] = [\vec{B}] = 2$ . One last ingredient in the construction of the effective Lagrangian is field redefinition, in that some terms in  $O_n$  that are in principle allowed by the symmetries can be eliminated by redefining the fields [55]—for a very recent discussion on field redefinitions in EFTs, see Ref. [56]. Table 2 summarizes the dimensions and transformation properties under  $P$  and  $T$  of all the building blocks.

Table 2: Mass dimension and transformation properties under parity  $P$  and time-reversal  $T$  of the basic quantities used to build the Lagrangian of NRQCD.

	$iD_t$	$i\vec{D}$	$\vec{E}$	$\vec{B}$	$\vec{\sigma}$
Mass dim.	1	1	2	2	0
P	+	-	-	+	+
T	+	-	+	-	-

Starting with the lowest-dimension operator  $O_0$ , one has two operators that can be used:  $m_Q$  and  $iD_t$ . The first can be eliminated by using the field redefinition  $\psi \rightarrow e^{im_Q t}\psi$ ; the presence of such a term

would spoil the power-counting scheme in  $1/m_Q$ . What remains is then the second operator, leading to  $C_0 \psi^\dagger(x) iD_t \psi(x)$ . To obtain the canonical  $i\partial/\partial t$  term in the equation of motion for  $\psi$  (i.e. the Schrödinger equation), one needs to choose  $C_0 = 1$ . Therefore, the zeroth-order Lagrangian is given by

$$\mathcal{L}_{\psi\psi}^{(0)} = \psi^\dagger(x) iD_t \psi(x). \quad (44)$$

The Lagrangian  $\mathcal{L}_{\chi\chi}^{(0)}$  is of the same form as this with  $\psi \rightarrow \chi$ .

At the next order, there are in principle three terms of dimension 2 contributing to  $O_1$ :  $(iD_t)^2$ , and terms proportional to the product of  $iD^i$  and  $iD^j$ . The first leads to an interaction of the form  $C_1 \psi^\dagger (iD_t)^2 \psi$ . This term can be eliminated by using the field redefinition  $\psi \rightarrow \psi - C_1 (iD_t/2m_Q) \psi$ , as can be verified very easily. To obtain an Hermitean operator, the  $iD^i$  and  $iD^j$  must be combined in the form of a commutator  $i[iD^i, iD^j]$  or anticommutator  $\{iD^i, iD^j\}$ ; these must be contracted with  $\sigma^i$ ,  $\delta^{ij}$  and  $\epsilon^{ijk}$  to obtain operators respecting rotational and  $T$  symmetries. Since the commutator gives the magnetic field, one can write the first-order Lagrangian as

$$\mathcal{L}_{\psi\psi}^{(1)} = \psi^\dagger(x) \left( \frac{\vec{D}^2}{2m_Q} + c_F g \frac{\vec{\sigma} \cdot \vec{B}}{2m_Q} \right) \psi(x), \quad (45)$$

where we used the fact the coefficient of the first term is equal to unity [55] and the index  $F$  in  $c_F$  stands for Fermi, motivated by the equivalent term that gives the Fermi hyperfine splitting in QED [57].  $\mathcal{L}_{\chi\chi}^{(1)}$  is of the same form but with an overall minus sign multiplying both terms.

Construction of  $O_2$  is also straightforward, though a bit more involved [54]. We will not use them here, but they are given next for completeness [58]:

$$\mathcal{L}_{\psi\psi}^{(2)} = \psi^\dagger(x) \left[ c_D g \frac{(\vec{D} \cdot \vec{E} - \vec{E} \cdot \vec{D})}{8m_Q^2} + c_S g \frac{i\vec{\sigma} \cdot (\vec{D} \times \vec{E} - \vec{E} \times \vec{D})}{8m_Q^2} \right] \psi(x), \quad (46)$$

where here  $D$  and  $S$  in  $c_D$  and  $c_S$  stand for Darwin and spin-orbit.  $\mathcal{L}_{\chi\chi}^{(2)}$  is the same as this with  $\psi \rightarrow \chi$ . The coefficients  $c_s$  and  $c_F$  are related to each other by [55]  $c_S = 2c_F - 1$ .

From dimensional analysis, one has that the four-fermion contact interaction terms  $\mathcal{L}_{\psi\psi\chi\chi}$  demand a factor  $1/m_Q^2$  to obtain a dimensionless coefficient; we write these constant interactions as [59]:

$$\begin{aligned} \mathcal{L}_{\psi\psi\chi\chi} &= \frac{d_{ss}}{m_Q^2} \psi^\dagger(x) \psi(x) \chi^\dagger(x) \chi(x) + \frac{d_{sv}}{m_Q^2} \psi^\dagger(x) \vec{\sigma} \psi(x) \cdot \chi^\dagger(x) \vec{\sigma} \chi(x) \\ &+ \frac{d_{vs}}{m_Q^2} \psi^\dagger(x) T^a \psi(x) \chi^\dagger(x) T^a \chi(x) + \frac{d_{vv}}{m_Q^2} \psi^\dagger(x) T^a \vec{\sigma} \psi(x) \cdot \chi^\dagger(x) T^a \vec{\sigma} \chi(x). \end{aligned} \quad (47)$$

We refer to Ref. [55] for a complete list of operators up to  $1/m_Q^3$  in the NRQCD Lagrangian.

As mentioned previously, the dimensionless parameters  $c_F, c_D, d_{ss}, \dots$  are determined by a matching procedure. The factors of 2 and 8 in Eqs. (46) and (46) were introduced to reproduce tree-level matching, so that a generic coefficient is given as  $C_n \sim 1 + \mathcal{O}(\alpha_s)$  when loop corrections are calculated. As examples, we quote the  $\mathcal{O}(\alpha_s)$  expressions for the coefficients of the bilinear terms, determined in Ref. [55] by using dimensional regularization

$$c_F = 1 + \frac{\alpha_s}{2\pi} (C_A + C_F), \quad c_D = 1 + \frac{\alpha_s}{2\pi} C_A, \quad (48)$$

where  $C_F = 4/3$  and  $C_A = 3$  are the eigenvalues in the fundamental representation of the SU(3) Casimir operators. The four-fermion contact interactions were calculated at  $\mathcal{O}(\alpha_s^2)$  in Ref. [59], also in

dimensional regularization:

$$\begin{aligned} d_{ss} &= \frac{2}{3}C_F \left( \frac{C_A}{2} - C_F \right) \alpha_s^2, & d_{sv} &= C_F \left( \frac{C_A}{2} - C_F \right) \alpha_s^2, \\ d_{vs} &= \left( \frac{4}{3}C_F + \frac{11}{12}C_A \right) \alpha_s^2, & d_{vv} &= \left( 2C_F - \frac{1}{4}C_A \right) \alpha_s^2. \end{aligned} \quad (49)$$

In the above, we have chosen the matching scale to be  $\mu = m_Q$ .

It is important to note that we have not written down the contributions of the light quark degrees in the above. They, of course, cannot be neglected in any realistic QCD calculation. As we discuss in the next section, in some applications their contributions to quarkonium properties can be introduced by coupling the nonrelativistic field to effective hadron degrees of freedom, like Goldstone boson fields.

NRQCD is rigorously derived from QCD in a systematic manner and has been adapted to lattice QCD [60], where it has shown to provide an efficient framework for simulating heavy quarks [61]. For analytical calculations, however, NRQCD still has too many active degrees of freedom, that is, it contains degrees that never appear as asymptotic states, only through virtual fluctuations. For example, while the binding energy, the ultrasoft scale, is a property of the asymptotic state, the relative momentum, the soft scale, is not; they are entangled in NRQCD. This makes difficulties with the power counting, as discussed in-depth in the reviews in Refs. [52, 62]. The solution within the framework of an EFT is that if one is interested in physics at the scale of the binding energy, the degrees of freedom at scales higher than the binding energy should be integrated out. This idea was implemented in Ref. [50] and further elaborated in Ref. [51]. The resulting EFT is named potential nonrelativistic QCD, pNRQCD, and will be discussed next.

## 2.4 Potential nonrelativistic QCD (pNRQCD) and van der Waals forces

pNRQCD gives a natural connection of QCD with a nonrelativistic Hamiltonian and the Schrödinger equation and it has proven to provide an adequate framework for describing heavy quarkonium dynamics. Its resemblance to nuclear many-body potential models makes it an adequate starting point for constructing EFTs for heavy quarkonia in a nuclear medium, particularly when treating nuclei within an independent-particle approximation.

As discussed in the previous section, the largest scale in a quarkonium bound state is the heavy quark mass  $m_Q$ . Other two relevant scales are the relative momentum  $|\vec{p}| \sim m_Q v$  and the relative kinetic energy  $E \sim m_Q v^2$ , where  $v$  is the relative velocity  $v$  between  $Q$  and  $\bar{Q}$ . These scales must be compared to  $\Lambda_{\text{QCD}}$ , which sets the scale of strong coupling. If one *assumes* that they satisfy the following hierarchy

$$m_Q \gg m_Q v \gg m_Q v^2 \gg \Lambda_{\text{QCD}}, \quad (50)$$

then  $v \sim \alpha_s$  and the integration of degrees of freedom at the scale  $m_Q v$  out can be carried out using perturbation theory. NRQCD can be matched to an EFT whose fields describe the ultrasoft (US) degrees of freedom. This gives rise to pNRQCD in the weak coupling regime, the matching coefficients being potentials that depend on the relative coordinate and momentum between  $Q$  and  $\bar{Q}$ . Moreover, the pNRQCD Lagrangian density can be written in terms of color singlet and color octet fields representing the  $Q\bar{Q}$  pair, and fields representing the US gluons and light quarks. We refer the reader to the reviews in Refs. [52, 62] for the technical aspects involved in the derivations. The  $Q\bar{Q}$  fields depend on two coordinates, which are conveniently chosen to be the center-of-mass  $\vec{R}$  and relative  $\vec{r}$  coordinates. The US gauge and light-quark fields depend only on  $\vec{R}$ ; in practice, this corresponds to a multipole expansion of the US fields. At leading order in  $1/m_Q$  and at  $\mathcal{O}(R)$  in the multipole expansion, one has that the action of pNRQCD can be written as [50, 51]

$$S_{\text{pNRQCD}} = \int dt d^3R \mathcal{L}_{\text{pNRQCD}}, \quad (51)$$

with  $\mathcal{L}_{\text{pNRQCD}}$  given by

$$\begin{aligned} \mathcal{L}_{\text{pNRQCD}} = & \mathcal{L}_{\text{light}} + \int d^3r \left\{ \text{Tr} \left[ S^\dagger (i\partial_0 - h_s) S + O^\dagger (iD_0 - h_o) O \right] \right. \\ & \left. + gV_A(r) \text{Tr} \left[ O^\dagger (\vec{r} \cdot \vec{E}) S + S^\dagger (\vec{r} \cdot \vec{E}) O \right] + \frac{g}{2} V_B(r) \text{Tr} \left[ O^\dagger (\vec{r} \cdot \vec{E}) O + O^\dagger O (\vec{r} \cdot \vec{E}) \right] \right\}, \end{aligned} \quad (52)$$

where  $S = S(t, \vec{R}, \vec{r})$  and  $O = O(t, \vec{R}, \vec{r})$  are respectively quark-antiquark matrix-valued singlet and octet fields, normalized with respect to color,  $S = \mathbf{1}S/\sqrt{N_c}$  and  $O = T^a O^a/\sqrt{T_F}$ , with  $N_c = 3$  the number of colors and  $T_F = 1/2$ , and  $h_s$  and  $h_o$  are the singlet and octet Hamiltonians

$$h_s = -\frac{\nabla_r^2}{m_Q} - \frac{\nabla_R^2}{4m_Q} + V_s(r), \quad h_o = -\frac{\nabla_r^2}{m_Q} - \frac{D_R^2}{4m_Q} + V_o(r), \quad (53)$$

and

$$V_s(r) = -C_F \frac{\alpha_s}{r}, \quad V_o(r) = \frac{\alpha_s}{2N_c} \frac{1}{r}, \quad V_A(r) = V_B(r) = 1. \quad (54)$$

We recall that the light-quark and gauge fields, including those gauge fields in  $\mathcal{L}_{\text{pNRQCD}}$ , are functions of time and  $\vec{R}$ :  $q_i = q_i(t, \vec{R})$ ,  $\bar{q}_i = \bar{q}_i(t, \vec{R})$ ,  $G^{\mu\nu} = G^{\mu\nu}(t, \vec{R})$ ,  $\vec{E}^i \equiv G^{i0}(\vec{R}, t)$ ,  $iD_0 O \equiv i\partial_0 O - g[A_0(\vec{R}, t), O]$ . At order  $1/m_Q^2$  there appear retardation terms and spin-dependent potentials, all of them calculable analytically.

A heavy quarkonium injected in a nucleus at low energies interacts by exchanging gluons with the light quarks of the nucleons. When this energy is much smaller than the quarkonium binding energy  $E_B \sim m_Q v^2 \approx m_Q \alpha_s^2 \gg \Lambda_{\text{QCD}}$ , the internal structure of the quarkonium is not resolved. Therefore, one can treat the quarkonium state in terms of an independent color-singlet field. This is equivalent to the statement that one can integrate out the ultra-soft scale  $m_Q \alpha_s^2$  and match pNRQCD to another EFT whose degrees of freedom are color-singlet quarkonium states, described by a field generically denoted by  $\varphi$  and gluon fields at the scale  $\Lambda_{\text{QCD}}$  [63]. Such an EFT is known as gluonic van der Waals EFT (gWEFT), the name being motivated by its original construction [63] aiming at deriving long range color van der Waals interactions in quarkonium-quarkonium interactions. Very recently, gWEFT was applied in Ref. [64] to the concrete case of the  $\eta_b$ - $\eta_b$  system. A similar van der Waals EFT was recently developed in Ref. [65] to describe the low-energy dynamics of an atom pair. In an earlier publication [66], effective field theory theories were used to treat the electromagnetic scattering of two massive particles, wherein one particle (or both) is electrically neutral.

Gluons at the scale  $\Lambda_{\text{QCD}}$  interact nonperturbatively with quarkonium states and the quarks of light hadrons. In the case of quarkonium-quarkonium interactions, such ultrasoft (US) gluons can be hadronized in terms of (pseudo) Goldstone bosons (GB) and gWEFT can be matched to a chiral EFT whose degrees of freedom are described by the  $\varphi$  fields and pseudoscalar GB fields [64]. The values of the couplings of the matching to the chiral EFT can be determined from the anomaly in the trace of the QCD energy-momentum tensor [18, 19, 20, 21, 22, 23, 24, 67, 68]. Although the quarkonium-quarkonium interaction is not our focus in this review, we discuss in the following a systematic procedure for obtaining its long-range van der Waals component by matching gWEFT Lagrangian to a chiral EFT [64]. Our aim in presenting such a discussion here is twofold. First, to motivate its possible extension to study quarkonium interactions with light hadrons that couple to pions and other hadronic degrees of freedom, with couplings fixed phenomenologically or by lattice QCD results [69]. Second, to emphasize the close connection of such an EFT approach with model calculations of quarkonium binding in medium using phenomenological Lagrangians; in particular with those based on evaluations meson-antimeson loop contributions to quarkonium in-medium self-energies that we discuss in sections ahead [70, 71, 72, 73, 74, 75, 76].

The following discussion is based on the presentation in Ref. [77]; further details can be found in Ref. [64]. As mentioned above, gWEFT is an EFT at the scale  $\Lambda_{\text{QCD}}$  and it is not difficult to convince



ourselves by using dimensional analysis that its lowest order Lagrangian can be written as (for simplicity of notation, we omit labels referring to spin and other eventually required quantum numbers):

$$\mathcal{L}_{\text{gWEFT}} = \mathcal{L}_{\text{light}} + \varphi^\dagger(t, \vec{R}) \left( i\partial_0 - E_\varphi + \frac{\nabla_{\vec{R}}^2}{4m_Q} + \frac{1}{2}\alpha_\varphi g^2 \vec{E}^2 + \dots \right) \varphi(t, \vec{R}), \quad (55)$$

where  $\dots$  stands for relativistic kinetic corrections or other higher-order operators coupling  $\varphi$  to gluons and  $\beta$  is the matching coefficient, which is the chromopolarizability of the quarkonium, given by [78, 79, 80]

$$\alpha_\varphi = -\frac{2V_A^2 T_F}{3N_c} \langle \varphi | r^i \frac{1}{E_\varphi - h_o} r^i | \varphi \rangle, \quad (56)$$

with  $|\varphi\rangle$  being the quarkonium bound-state wave function. If the hierarchy in Eq. (50) is strictly valid, then, at order  $1/m_Q$  and at  $\mathcal{O}(R)$ ,  $|\varphi\rangle$  is an  $1S$  Coulombic state and the polarizability  $\beta$  can be evaluated in closed form [78, 81]. Note that in Ref. [64] the polarizability is denoted by  $\beta$ . In the evaluation of  $\alpha_\varphi$ , one inserts a complete set of intermediate states that are eigenstates of the octet Hamiltonian  $h_o(\vec{r})$ . Since  $h_o(\vec{r})$  is a repulsive Coulomb potential, the octet intermediate states correspond to Coulombic continuum eigenstates. A commonly employed approximation [71, 79, 80, 82] in the evaluation of  $\alpha_\varphi$  is to use plane waves in place of the Coulombic continuum eigenstates. This corresponds to the  $N_c \rightarrow \infty$  limit.

At energies of order  $m_\pi \ll \Lambda_{QCD}$ , the relevant degrees of freedom are the quarkonium states and the pseudo GB and it is natural to integrate out the gluons in favor of pions, and match gWEFT to a chiral EFT, denoted  $\chi EFT$ , in which the pseudo GB enter as explicit degrees of freedom. Specifically, limiting the discussion to the case that quarkonium field  $\varphi$  is a scalar under chiral symmetry, the interaction operators with Goldstone bosons can be easily constructed making use as building blocks the unitary matrix  $U(x)$ , that parametrizes the Goldstone boson fields and that involving the light-quark masses, Eqs. (33) and (34). To leading order, the Lagrangian density of  $\chi EFT$  can be written as (we limit the discussion to the pion sector of the  $U(x)$  matrix) [64]

$$\begin{aligned} \mathcal{L}_{\chi EFT}^\varphi &= \varphi^\dagger \left( i\partial_0 + \frac{\nabla^2}{2m_\varphi} \right) \varphi + \mathcal{L}_{GB} + \mathcal{L}_{GB-m_q} \\ &+ \frac{f^2}{4} \varphi^\dagger \varphi \left[ c_{d0} \text{Tr} \left( \partial_0 U \partial_0 U^\dagger \right) + c_{di} \text{Tr} \left( \partial_i U \partial^i U^\dagger \right) + c_m \text{Tr} \left( \chi^\dagger U + \chi U^\dagger \right) \right] + V_{\text{cont.}}(\varphi^\dagger, \varphi), \end{aligned} \quad (57)$$

where  $V_{\text{cont.}}(\varphi^\dagger, \varphi)$  are  $\varphi$ -contact interactions—they do not play any role in the long-distance properties of the quarkonium-quarkonium interaction in lowest order, although they are needed in the renormalization of ultraviolet divergences coming from chiral loops. The  $c_{d0}$ ,  $c_{di}$  and  $c_m$  are matching coefficients that can be obtained from the matrix element [68]

$$g^2 \langle \pi^+(p_1) \pi^-(p_2) | \vec{E}_a^2 | 0 \rangle = \frac{8\pi^2}{b} \left( \kappa_1 E_1 E_2 - \kappa_2 \vec{p}_1 \cdot \vec{p}_2 + 3m_\pi^2 \right), \quad (58)$$

where  $p_1 = (E_1, \vec{p}_1)$  and  $p_2 = (E_2, \vec{p}_2)$  are the pion four-momenta,  $\kappa_1 = 2 - 9\kappa/2$ ,  $\kappa_2 = 2 + 3\kappa/2$ ,  $b = b_0/4\pi$ , with  $b_0$  given in Eq. (8), and  $\kappa \simeq 0.2$ , as extracted from pionic transitions of quarkonium states [68]. More specifically, the matching coefficients can be obtained by equating the amplitudes for two-pion production calculated in gWEFT and  $\chi EFT$  [64]:

$$\frac{4\pi^2 \alpha_\varphi}{b} \left( \kappa_1 E_1 E_2 - \kappa_2 \vec{p}_1 \cdot \vec{p}_2 + 3m_\pi^2 \right) = -c_{d0} E_1 E_2 + c_{di} \vec{p}_1 \cdot \vec{p}_2 - c_m m_\pi^2, \quad (59)$$

which yields

$$c_{d0} = -\frac{4\pi^2 \alpha_\varphi}{b} \kappa_1, \quad c_{di} = -\frac{4\pi^2 \alpha_\varphi}{b} \kappa_2, \quad c_m = -\frac{12\pi^2 \alpha_\varphi}{b}. \quad (60)$$

Once the matching coefficients appearing in Eq. (57) are determined, one can obtain an effective potential describing  $\varphi\varphi$  interactions at low momentum transfers. For momentum transfers of the order of the pion mass,  $k_{\varphi\varphi} \sim m_\pi$ , the relative  $\varphi\varphi$  kinetic energy is much smaller than the pion mass:  $\vec{k}_{\varphi\varphi}^2/m_\varphi \sim m_\pi^2/m_\varphi \ll m_\pi$ . Under such circumstances, the pions can be integrated out and the  $\varphi\varphi$  potential appears as a matching coefficient in an effective  $\varphi\varphi$  Lagrangian, the leading order of which can be written as

$$L_{\varphi\varphi} = \int d^3R \varphi^\dagger(t, \vec{R}) \left( i\partial_0 + \frac{\nabla^2}{2m_\varphi} \right) \varphi(t, \vec{R}) - \frac{1}{2} \int d^3R d^3R' \varphi^\dagger(t, \vec{R}) \varphi^\dagger(t, \vec{R}') W_{\varphi\varphi}(\vec{R}, \vec{R}') \varphi(t, \vec{R}') \varphi(t, \vec{R}), \quad (61)$$

where  $W_{\varphi\varphi}(\vec{R}, \vec{R}')$  contains short- and long-distance contributions. Details on the derivations and explicit formulae for the pion contribution to  $W(\vec{R}, \vec{R}')$  can be found in Ref. [64]; here we simply quote the final result for its long-distance part ( $r = |\vec{R}_1 - \vec{R}_2|$ ):

$$W_{\varphi\varphi}^{\text{vdW}}(r) = \lim_{r \gg 1/2m_\pi} W_{\varphi\varphi}(r) = -\frac{3(3 + \kappa_2)^2 \pi^{3/2} \alpha_\varphi^2 m_\pi^{9/2}}{4b^2 r^{5/2}} e^{-2m_\pi r}, \quad (62)$$

which is identified as a color van der Waals contribution to the  $\varphi\varphi$  interaction. An earlier result derived in Ref. [67] using a similar method to ours is contained in Eq. (62) if one takes  $\kappa_2 = 2$  in that equation and also neglects contributions proportional to  $m_\pi^2$  in the expression coming from the trace anomaly, Eq. (58). Neglecting such terms does not change the functional dependence on  $r$  and  $m_\pi$  of  $W_{\varphi\varphi}^{\text{vdW}}(r)$ , but does make it weaker by a factor of  $16/25$ . Explicit numerical results for the case of the  $\eta_b$ - $\eta_b$  system are presented in Ref. [64]. In particular, for future reference, we mention that the numerical value for the polarizability of  $\eta_b$ , for a bottom mass of  $m_Q = 5$  GeV, was obtained to be

$$\alpha_{\eta_b} = 0.50_{-0.38}^{+0.42} \text{ GeV}^{-3}. \quad (63)$$

where the central value refers to  $\alpha_s(1.5 \text{ GeV}) = 0.35$ , the largest to  $\alpha_s(2 \text{ GeV}) = 0.3$  and the smallest to  $\alpha_s(1 \text{ GeV}) = 0.5$ . We mention that the effect of using continuum Coulomb wave functions instead of plane waves [71, 79, 80, 82] in the evaluation of the integral in Eq. (56) is to increase  $\alpha_{\eta_b}$  by at most 5% [64, 77].

The results show very clearly that as the attraction from the Coulomb potential weakens, the polarizability increases. This is because the size of the color charge distribution increases. One consequence of the larger value of the polarizability is that the van der Waals interaction becomes stronger. Excited quarkonia states are expected to have larger polarizabilities and therefore interact with stronger van der Waals forces. On the other hand, a calculation of  $\alpha_\varphi$  for such states with Eq. (56) might not be reliable, as excited states of charmonia or bottomonia are not Coulomb bound states and, most likely, nonperturbative physics plays an important role in the determination of the polarizability of such states.

It is remarkable that one is able to derive from QCD an analytic expression for a hadron-hadron interaction. One should, however, recall that such a derivation was made possible by assuming the validity of the hierarchy of scales in Eq. (50). Amongst the most important implications of the hierarchy is the weakly coupled nature of the quarkonium bound states, which allows the use of perturbation theory to integrate out the high-energy scales. Now, when the relative position of the scales  $m_Q v$  and  $\Lambda_{\text{QCD}}$  are inverted in Eq. (50), QCD becomes strongly coupled and an entire new strategy is required to derive EFT for treating low-energy heavy quarkonium interactions. To describe the physics below  $\Lambda_{\text{QCD}}$ , the use of explicit hadronic degrees of freedom is one possibility and hence the appropriate degrees of freedom in this regime are described by quarkonium singlet fields, (pseudo) Goldstone boson fields and other hadron fields representing heavy-light mesons and light baryons. An advantage of using explicit

hadron degrees of freedom is that the correct chiral non-analytic behavior of observables as a function of the pion mass is obtained more easily [83, 84, 85, 86]. The construction of such an EFT would need input from phenomenology and lattice QCD simulations to fix parameters [69]. In particular, to describe e.g. the quarkonium states  $\eta_c$  and  $J/\Psi$ , one would need to include in addition to the color Coulomb potential discussed above, nonperturbative interactions associated with confinement. While great progress has been achieved recently in constructing such an EFT to describe heavy quarkonium hybrids by using as degrees of freedom heavy quarks and excited glue degrees of freedom [87], the treatment of light quarks remains challenging. The use of models is an essential part of contemporary research in the field. Recent studies of interactions of heavy quarkonia wherein nonperturbative forces are involved have been conducted in Refs. [88, 89, 90, 91].

In summary, the study of heavy quarkonium in a nucleus requires the use of different pieces of theoretical tools. The use of EFTs for treating heavy quarkonium states in free space allows us to constrain many of their properties, but to describe their interactions with light hadrons requires the use of models. In particular, for making reliable predictions for experimental searches of possible bound states of heavy quarkonium with atomic nuclei, no matter how well a heavy quarkonium is understood in free space, one still needs a well-constrained nuclear many-body model. Most of the predictions presented in this review rely on one of such models, the quark-meson coupling (QMC) model, a self-consistent quark-based model that has proven to successfully describe a great variety of nuclear phenomena. The model is particularly suitable, as we discuss in sections ahead, for studying nuclear binding of the light quarkonium  $\phi$  and also the  $\eta$  and  $\omega$  mesons, as well as of heavy-flavored hadrons, the  $D$  and  $\bar{D}$  mesons, and  $\Lambda_c$  and  $\Lambda_b$  baryons. The foundations of QMC model and its predictions for hadron properties in medium are the subject of the next section.

### 3 Quark-meson coupling (QMC) model

In this section we briefly review the quark-meson coupling (QMC) model, the quark-based model for nuclear matter and finite nuclei invented by Guichon [92] and further developed and applied to finite nuclei in Ref. [93].

Many nuclear phenomena now seem to indicate that the traditional approach, omitting any consideration of the underlying quark and gluon degrees of freedom, may have its limitations, and suggest a need for subnucleonic and subhadronic degrees of freedom. There is no doubt that hadrons consist of quarks, antiquarks and gluons and that they can respond to the environment and change their character in matter. The basic working hypothesis and assumption of the QMC model is that quarks play an important role in nuclei and nuclear matter.

Based on the QMC model, various nuclear phenomena have been successfully studied [94] starting at the quark level, using a self-consistent model for nuclear physics. Although there are many kinds of relativistic mean-field theory for nuclear physics, very few are built from the quark level. We emphasise especially the wide success of the QMC model which has been applied systematically to many nuclear phenomena. Specially relevant for the present review, are nuclear bound states of heavy and light quarkonium and light hadrons, and heavy-baryon hypernuclei. The model incorporates explicit quark degrees of freedom into nuclear many-body systems. It is shown that at the *hadronic* level, it is certainly possible to cast the QMC model into a form similar to that of a quantum hadrodynamics (QHD) [95, 96], or a similar type of mean-field model by re-defining the scalar field. However, at the same time, the QMC model can describe how the internal structure of hadrons changes in a nuclear medium. That is the greatest advantage of the QMC model and it has opened a tremendous number of new lines of investigation.

Since the discovery of QCD as the fundamental theory of the strong interaction, numerous attempts have been made to derive the nuclear force within quark models. The QMC model stands between the

traditional meson-exchange picture and the hard core quark models, namely, it is a mean-field model in the sense of QHD but with the couplings of  $\sigma$  and  $\omega$  mesons to confined quarks, rather than to the point-like nucleon. After a considerable amount of work, one finds that the effect of the internal, quark structure of the nucleon is absorbed into the scalar polarizability in the effective nucleon mass in matter. It is the dependence of the scalar polarizability on the scalar field in matter (or it is numerically equivalent to the dependence on nuclear density) that is the heart of the QMC model and leads to the novel saturation mechanism of the binding energy of nuclear matter as a function of density.

Because the scalar polarizability plays such an important role in the QMC model, it is of great interest to study whether the dependence of the scalar polarizability on the scalar field can be extracted from the fundamental theory, i.e., QCD. In Ref. [97], it is shown that the remarkable progress in resolving the problem of chiral extrapolation of lattice QCD data gives one confidence that the pion loop contributions are under control. In the case of the nucleon, one can then use this control to estimate the effect of applying a chiral invariant scalar field to the nucleon, i.e., to estimate the scalar polarizability of the nucleon. The resulting value is in excellent agreement with the range found in the QMC model, which is vital to describe many phenomena in nuclear physics. Thus, in a very real sense, the results presented in Ref. [97] provide a direct connection between the growing power to compute hadron properties from QCD itself and fundamental properties of atomic nuclei. Further work in this direction is certainly necessary.

### 3.1 Nuclear matter and finite (hyper)nucleus

Using the Born-Oppenheimer approximation, a relativistic Lagrangian density which gives the same mean-field equations of motion for a nucleus or a hypernucleus, in which the quasi-particles moving in single-particle orbits are three-quark clusters with the quantum numbers of a strange, charm or bottom hyperon or a nucleon, when expanded to the same order in velocity, is given by QMC [93, 94, 98, 99, 100, 101]:

$$\mathcal{L}_{QMC}^Y = \mathcal{L}_{QMC}^N + \mathcal{L}_{QMC}^Y, \quad (64)$$

$$\begin{aligned} \mathcal{L}_{QMC}^N \equiv & \bar{\psi}_N(\vec{r}) \left[ i\gamma \cdot \partial - m_N^*(\sigma) - (g_\omega \omega(\vec{r}) + g_\rho \frac{\tau_3^N}{2} b(\vec{r}) + \frac{e}{2}(1 + \tau_3^N) A(\vec{r})) \gamma_0 \right] \psi_N(\vec{r}) \\ & - \frac{1}{2} [(\nabla \sigma(\vec{r}))^2 + m_\sigma^2 \sigma(\vec{r})^2] + \frac{1}{2} [(\nabla \omega(\vec{r}))^2 + m_\omega^2 \omega(\vec{r})^2] \\ & + \frac{1}{2} [(\nabla b(\vec{r}))^2 + m_\rho^2 b(\vec{r})^2] + \frac{1}{2} (\nabla A(\vec{r}))^2, \end{aligned} \quad (65)$$

$$\begin{aligned} \mathcal{L}_{QMC}^Y \equiv & \bar{\psi}_Y(\vec{r}) \left[ i\gamma \cdot \partial - m_Y^*(\sigma) - (g_\omega^Y \omega(\vec{r}) + g_\rho^Y I_3^Y b(\vec{r}) + e Q_Y A(\vec{r})) \gamma_0 \right] \psi_Y(\vec{r}), \\ & (Y = \Lambda, \Sigma^{0,\pm}, \Xi^{0,+}, \Lambda_c^+, \Sigma_c^{0,+}, \Xi_c^{0,+}, \Lambda_b), \end{aligned} \quad (66)$$

where, for a normal nucleus,  $\mathcal{L}_{QMC}^Y$  in Eq. (64), namely Eq. (66) is not needed. In the above  $\psi_N(\vec{r})$  and  $\psi_Y(\vec{r})$  are respectively the nucleon and hyperon (strange, charm or bottom baryon) fields. The mean meson fields represented by,  $\sigma, \omega$  and  $b$  which are directly coupled to the quarks self-consistently, are the scalar-isoscalar, vector-isoscalar and third component of vector-isovector fields, respectively, while  $A$  stands for the Coulomb field. When we consider the situation where a hadron  $h$  is embedded in a nucleus or in nuclear matter, we may add the corresponding Lagrangian  $\mathcal{L}^h$  instead of  $\mathcal{L}_{QMC}^Y$ .

In an approximation where the  $\sigma$ ,  $\omega$  and  $\rho$  mean fields couple only to the  $u$  and  $d$  light quarks, the coupling constants for the hyperon are obtained as  $g_\omega^Y = (n_q/3)g_\omega$ , and  $g_\rho^Y \equiv g_\rho = g_\rho^q$ , with  $n_q$  being the total number of valence light quarks in the hyperon  $Y$ , where  $g_\omega$  and  $g_\rho$  are the  $\omega$ - $N$  and  $\rho$ - $N$  coupling constants.  $I_3^Y$  and  $Q_Y$  are the third component of the hyperon isospin operator and its electric charge in units of the proton charge,  $e$ , respectively. The field dependent  $\sigma$ - $N$  and  $\sigma$ - $Y$

coupling strengths respectively for the nucleon  $N$  and hyperon  $Y$ ,  $g_\sigma(\sigma) \equiv g_\sigma^N(\sigma)$  and  $g_\sigma^Y(\sigma)$ , appearing in Eqs. (65) and (66), are defined by

$$m_N^*(\sigma) \equiv m_N - g_\sigma(\sigma)\sigma(\vec{r}), \quad (67)$$

$$m_Y^*(\sigma) \equiv m_Y - g_\sigma^Y(\sigma)\sigma(\vec{r}), \quad (68)$$

where  $m_N$  ( $m_Y$ ) is the free nucleon (hyperon) mass. Note that the dependence of these coupling strengths on the applied scalar field ( $\sigma$ ) must be calculated self-consistently within the quark model [92, 93, 94, 98, 99, 100, 101, 102]. Hence, unlike quantum hadrodynamics (QHD) [95, 96], even though  $g_\sigma^Y(\sigma)/g_\sigma(\sigma)$  may be 2/3 or 1/3 depending on the number of light quarks  $n_q$  in the hyperon in free space,  $\sigma = 0$  (even this is true only when their bag radii in free space are exactly the same), this will not necessarily be the case in a nuclear medium.

The Lagrangian density Eq. (64) [or (65) and (66)] leads to a set of equations of motion for the finite (hyper)nuclear system:

$$[i\gamma \cdot \partial - m_N^*(\sigma) - (g_\omega\omega(\vec{r}) + g_\rho\frac{\tau_3^N}{2}b(\vec{r}) + \frac{e}{2}(1 + \tau_3^N)A(\vec{r}))\gamma_0]\psi_N(\vec{r}) = 0, \quad (69)$$

$$[i\gamma \cdot \partial - m_Y^*(\sigma) - (g_\omega^Y\omega(\vec{r}) + g_\rho I_3^Y b(\vec{r}) + eQ_Y A(\vec{r}))\gamma_0]\psi_Y(\vec{r}) = 0, \quad (70)$$

$$\begin{aligned} (-\nabla_r^2 + m_\sigma^2)\sigma(\vec{r}) &= - \left[ \frac{\partial m_N^*(\sigma)}{\partial \sigma} \right] \rho_s(\vec{r}) - \left[ \frac{\partial m_Y^*(\sigma)}{\partial \sigma} \right] \rho_s^Y(\vec{r}), \\ &\equiv g_\sigma C_N(\sigma)\rho_s(\vec{r}) + g_\sigma^Y C_Y(\sigma)\rho_s^Y(\vec{r}), \end{aligned} \quad (71)$$

$$(-\nabla_r^2 + m_\omega^2)\omega(\vec{r}) = g_\omega\rho_B(\vec{r}) + g_\omega^Y\rho_B^Y(\vec{r}), \quad (72)$$

$$(-\nabla_r^2 + m_\rho^2)b(\vec{r}) = \frac{g_\rho}{2}\rho_3(\vec{r}) + g_\rho^Y I_3^Y \rho_B^Y(\vec{r}), \quad (73)$$

$$(-\nabla_r^2)A(\vec{r}) = e\rho_p(\vec{r}) + eQ_Y\rho_B^Y(\vec{r}), \quad (74)$$

where,  $\rho_s(\vec{r})$  ( $\rho_s^Y(\vec{r})$ ),  $\rho_B(\vec{r}) = \rho_p(\vec{r}) + \rho_n(\vec{r})$  ( $\rho_B^Y(\vec{r})$ ),  $\rho_3(\vec{r}) = \rho_p(\vec{r}) - \rho_n(\vec{r})$ ,  $\rho_p(\vec{r})$  and  $\rho_n(\vec{r})$  are the nucleon (hyperon) scalar, nucleon (hyperon) baryon, third component of isovector, proton and neutron densities at the position  $\vec{r}$  in the (hyper)nucleus. On the right hand side of Eq. (71),  $-[\partial m_N^*(\sigma)/\partial \sigma] \equiv g_\sigma C_N(\sigma)$  and  $-[\partial m_Y^*(\sigma)/\partial \sigma] \equiv g_\sigma^Y C_Y(\sigma)$ , where  $g_\sigma \equiv g_\sigma(\sigma = 0)$  and  $g_\sigma^Y \equiv g_\sigma^Y(\sigma = 0)$ . At the hadronic level, the entire information on the quark dynamics is condensed into the effective couplings  $C_{N,Y}(\sigma)$  of Eq. (71), which are characteristic new features of QMC. Furthermore, when  $C_{N,Y}(\sigma) = 1$ , which corresponds to a structureless nucleon or hyperon, the equations of motion given by Eqs. (69)-(74) can be identified with those derived from QHD [95, 96].

We note here that, for the Dirac equation Eq. (70) for  $Y = \Lambda_{c,b}$  baryons to be discussed in section 7.2, the effects of Pauli blocking at the quark level is introduced by adding a repulsive potential. This is the same as that used for the strange  $\Lambda$ -hyperon case. This was extracted by the fit to the  $\Lambda$ - and  $\Sigma$ -hypernuclei taking into account the  $\Sigma N - \Lambda N$  channel coupling [99]. The modified Dirac equation for the  $Y = \Lambda_{c,b}$  is,

$$[i\gamma \cdot \partial - M_Y(\sigma) - (\lambda_Y\rho_B(\vec{r}) + g_\omega^Y\omega(\vec{r}) + g_\rho I_3^Y b(\vec{r}) + eQ_Y A(\vec{r}))\gamma_0]\psi_Y(\vec{r}) = 0, \quad (75)$$

where  $\rho_B(\vec{r})$  is the baryon density at the position  $\vec{r}$  in the  $\Lambda_{c,b}$ -hypernucleus. The value of  $\lambda_Y = \lambda_{c,b}$  is 60.25 MeV (fm)<sup>3</sup>. The details about the effective Pauli blocking at the quark level can be found in Refs. [94, 99].

The effective mass of the nucleon  $N$  and hyperon  $Y$  are calculated by Eq. (88) to be shown later, by replacing  $h \rightarrow N$ , and  $h \rightarrow Y$ , respectively. The explicit expressions for  $C_{N,Y}(\sigma) \equiv S_{N,Y}(\sigma)/S_{N,Y}(0)$ , are related by,

$$\frac{\partial m_{N,Y}^*(\sigma)}{\partial \sigma} = -n_q g_\sigma^q \int_{bag} d\vec{y} \bar{\psi}_q(\vec{y})\psi_q(\vec{y}) \equiv -n_q g_\sigma^q S_{N,Y}(\sigma) = -\frac{\partial}{\partial \sigma} [g_\sigma^{N,Y}(\sigma)\sigma], \quad (76)$$

where  $g_\sigma^q$  is the light-quark- $\sigma$  coupling constant. By the above relation, we may define the  $\sigma$ - $N$  and  $\sigma$ - $Y$  coupling constants:

$$g_\sigma^{N,Y} = n_q g_\sigma^q S_{N,Y}(0). \quad (77)$$

Note that, the same as that for  $C_{N,Y}(\sigma)$ ,  $S_N(0)$  and  $S_Y(0)$  values are different, because the ground state light quark wave functions in the nucleon  $N$  and hyperon  $Y$  are different in vacuum as well as in medium. (That is, the bag radii of the  $N$  and  $Y$  are different in vacuum as well as in medium.)

In the calculations summarised here the parameters which are used for the study of infinite nuclear matter and finite nuclei [98], are  $m_\omega = 783$  MeV,  $m_\rho = 770$  MeV,  $m_\sigma = 418$  MeV and  $e^2/4\pi = 1/137.036$ . The corresponding meson-nucleon coupling constants are given in next subsection.

### 3.2 Hadron masses in nuclear matter

Below we consider the rest frame of infinitely large symmetric nuclear matter, a spin and isospin saturated system with only strong interactions. To do so, one first keeps only  $\mathcal{L}_{QMC}^N$  in Eq. (64), or correspondingly drops all the quantities with the super- and under-script  $Y$ , and set the Coulomb field  $A(\vec{r}) = 0$  in Eqs. (69)-(74). Next one sets all the terms with any derivatives of the density to be zero. Then, within Hartree mean-field approximation, the nuclear (baryon),  $\rho_B$ , and scalar,  $\rho_s$ , densities are respectively given by,

$$\rho_B = \frac{4}{(2\pi)^3} \int d\vec{k} \theta(k_F - |\vec{k}|) = \frac{2k_F^3}{3\pi^2}, \quad (78)$$

$$\rho_s = \frac{4}{(2\pi)^3} \int d\vec{k} \theta(k_F - |\vec{k}|) \frac{m_N^*(\sigma)}{\sqrt{m_N^{*2}(\sigma) + k^2}}. \quad (79)$$

Here,  $m_N^*(\sigma)$  is the value (constant) of the effective nucleon mass at the given density (see also Eq. (67)) and  $k_F$  the Fermi momentum. In the standard QMC model [92, 94], the MIT bag model is used for describing nucleons and hyperons (hadrons). The use of this quark model is an essential ingredient for the QMC model, as similar results can be obtained using the Nambu–Jona-Lasinio model [102] or a constituent quark model [103].

Then, the Dirac equations for the quarks and antiquarks in nuclear matter, in bags of hadrons,  $h$ , ( $q = u$  or  $d$ , and  $Q = s, c$  or  $b$ , hereafter) neglecting the Coulomb force in nuclear matter, are given by ( $|\mathbf{x}| \leq$  bag radius) [100, 104, 105, 106, 107]:

$$\left[ i\gamma \cdot \partial_x - (m_q - V_\sigma^q) \mp \gamma^0 \left( V_\omega^q + \frac{1}{2} V_\rho^q \right) \right] \begin{pmatrix} \psi_u(x) \\ \psi_{\bar{u}}(x) \end{pmatrix} = 0, \quad (80)$$

$$\left[ i\gamma \cdot \partial_x - (m_q - V_\sigma^q) \mp \gamma^0 \left( V_\omega^q - \frac{1}{2} V_\rho^q \right) \right] \begin{pmatrix} \psi_d(x) \\ \psi_{\bar{d}}(x) \end{pmatrix} = 0, \quad (81)$$

$$[i\gamma \cdot \partial_x - m_Q] \psi_Q(x) \text{ (or } \psi_{\bar{Q}}(x)) = 0. \quad (82)$$

The (constant) mean-field potentials for a bag in nuclear matter are defined by  $V_\sigma^q \equiv g_\sigma^q \sigma$ ,  $V_\omega^q \equiv g_\omega^q \omega$  and  $V_\rho^q \equiv g_\rho^q b$ , with  $g_\sigma^q$ ,  $g_\omega^q$  and  $g_\rho^q$  the corresponding quark-meson coupling constants. We assume  $SU(2)$  symmetry,  $m_{u,\bar{u}} = m_{d,\bar{d}} \equiv m_{q,\bar{q}}$ . The corresponding effective quark masses are defined by,  $m_{u,\bar{u}}^* = m_{d,\bar{d}}^* = m_{q,\bar{q}}^* \equiv m_{q,\bar{q}} - V_\sigma^q$ . In symmetric nuclear matter within Hartree approximation, the  $\rho$ -meson mean field is zero,  $V_\rho^q = 0$  in Eqs. (80) and (81) and we ignore it. (This is not true in a finite nucleus, even with equal numbers of protons and neutrons, since the Coulomb interactions among the protons induces an asymmetry between the proton and neutron densities to give  $\rho_3 = \rho_p - \rho_n \neq 0$ .)

The same meson mean fields  $\sigma$  and  $\omega$  for the quarks in Eqs. (80) and (81), satisfy self-consistently the following equations at the nucleon level (together with the effective nucleon mass  $m_N^*(\sigma)$  of Eq. (67)

calculated by Eq. (88) below):

$$\omega = \frac{g_\omega \rho_B}{m_\omega^2}, \quad (83)$$

$$\sigma = \frac{g_\sigma}{m_\sigma^2} C_N(\sigma) \frac{4}{(2\pi)^3} \int d\vec{k} \theta(k_F - |\vec{k}|) \frac{m_N^*(\sigma)}{\sqrt{m_N^{*2}(\sigma) + \vec{k}^2}} = \frac{g_\sigma}{m_\sigma^2} C_N(\sigma) \rho_s, \quad (84)$$

where

$$C_N(\sigma) \equiv \frac{-1}{g_\sigma(\sigma=0)} [\partial m_N^*(\sigma)/\partial \sigma]. \quad (85)$$

Because of the underlying quark structure of the nucleon used to calculate  $m_N^*(\sigma)$  in nuclear medium,  $C_N(\sigma)$  decreases significantly as  $\sigma$  increases, whereas in the usual point-like nucleon-based models it is constant,  $C_N(\sigma) = 1$ . It is this variation of  $C_N(\sigma)$  (or equivalently dependence of the scalar coupling on density,  $g_\sigma(\sigma)$ ) that yields a novel saturation mechanism for nuclear matter in the QMC model, and contains the important dynamics which originates in the quark structure of the nucleon and hyperon. It is this variation through the scalar polarisability which yields three-body or density dependent effective forces, as has been demonstrated by constructing an equivalent energy density functional [108]. As a consequence of the *derived*, nonlinear couplings of the meson fields in the Lagrangian density at the nucleon (hyperon) and meson level, the standard QMC model yields the nuclear incompressibility of  $K \simeq 280$  MeV with  $m_q = 5$  MeV. This is in contrast to a naive version of QHD [95, 96] (the point-like nucleon model of nuclear matter), results in the much larger value,  $K \simeq 500$  MeV; the empirically extracted value falls in the range  $K = 200 - 300$  MeV. (See Ref. [109] for a recent, extensive analysis of this issue.)

Table 3: Current quark masses (input), coupling constants and the bag constant obtained with the nucleon bag radius  $R_N = 0.8$  fm in vacuum.

$m_{u,d}$	5 MeV	$g_\sigma^q$	5.69
$m_s$	250 MeV	$g_\omega^q$	2.72
$m_c$	1300 MeV	$g_\rho^q$	9.33
$m_b$	4200 MeV	$B^{1/4}$	170 MeV

Once the self-consistency equation for the  $\sigma$  field, Eq. (84), has been solved, one can evaluate the total energy per nucleon:

$$E^{\text{tot}}/A = \frac{4}{(2\pi)^3 \rho} \int d\vec{k} \theta(k_F - |\vec{k}|) \sqrt{m_N^{*2}(\sigma) + \vec{k}^2} + \frac{m_\sigma^2 \sigma^2}{2\rho} + \frac{g_\omega^2 \rho}{2m_\omega^2}. \quad (86)$$

We then determine the coupling constants,  $g_\sigma$  and  $g_\omega$ , so as to fit the binding energy of 15.7 MeV at the saturation density  $\rho_0 = 0.15 \text{ fm}^{-3}$  ( $k_F^0 = 1.305 \text{ fm}^{-1}$ ) for symmetric nuclear matter. The determined quark-meson coupling constants, and the current quark mass values used are listed in Tab. 3. The coupling constants at the nucleon level are  $g_\sigma^2/4\pi = 3.12$ ,  $g_\omega^2/4\pi = 5.31$  and  $g_\rho^2/4\pi = 6.93$ . (See Eq. (77).)

We show in Fig. 1 the modulus of the binding energy per nucleon  $E^{\text{tot}}/A - m_N$  (left panel) and the effective nucleon mass,  $m_N^*$  (right panel) obtained using the determined quark-meson coupling constants. The corresponding mean field potentials felt by the light quarks,  $V_\omega^q$  and  $V_\sigma^q$ , are shown in Fig. 2.

In the following, let us consider the situation that a hadron  $h$  is immersed in nuclear matter. The normalized, static solution for the ground state quarks or antiquarks with flavor  $f$  in the hadron  $h$  may be written,  $\psi_f(x) = N_f e^{-i\epsilon_f t/R_h^*} \psi_f(\vec{r})$ , where  $N_f$  and  $\psi_f(\vec{r})$  are the normalization factor and corresponding

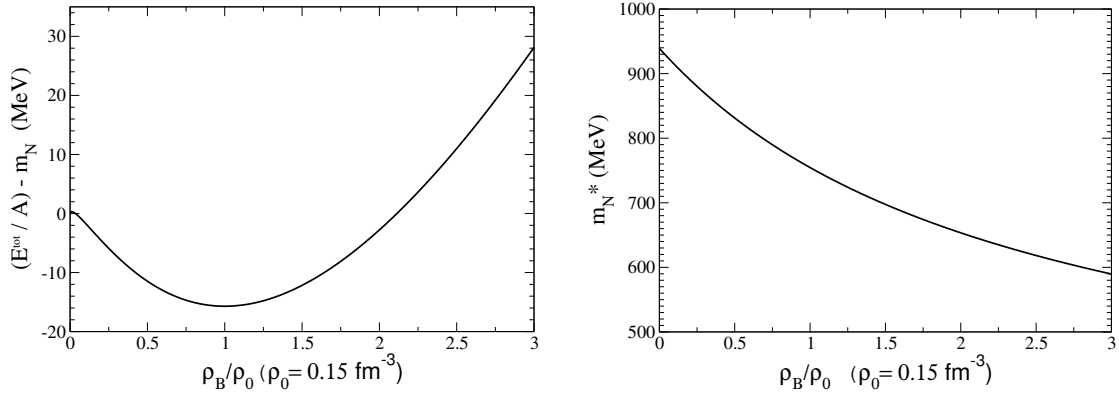


Figure 1: Negative of the binding energy per nucleon for symmetric nuclear matter,  $(E^{\text{tot}}/A) - m_N$ , v.s.  $\rho_B/\rho_0$  ( $\rho_0 = 0.15 \text{ fm}^{-3}$ ) with the vacuum light quark mass  $m_q = m_{\bar{q}} = 5 \text{ MeV}$  ( $q = u, d$ ), calculated using the QMC model (left panel), as well as the effective nucleon mass  $m_N^*$  (right panel). The incompressibility  $K$  obtained is  $K = 279.3 \text{ MeV}$ .

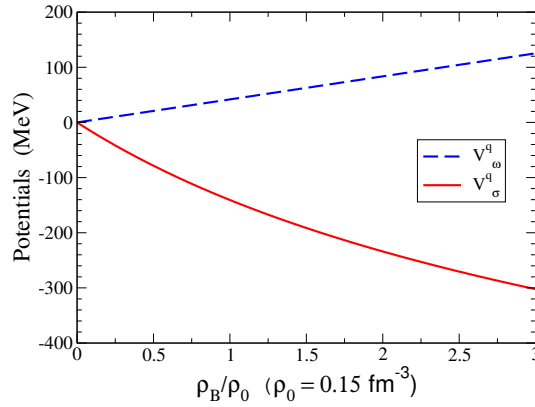


Figure 2: Light quark potentials.

spin and spatial part of the wave function. The bag radius in medium for hadron  $h$ , denoted  $R_h^*$ , is determined through the stability condition for the mass of the hadron against the variation of the bag radius [92, 94, 93, 98] (see also Eq. (88)). The eigenenergies in units of  $1/R_h^*$  are given by,

$$\begin{pmatrix} \epsilon_u \\ \epsilon_{\bar{u}} \end{pmatrix} = \Omega_q^* \pm R_h^* \left( V_\omega^q + \frac{1}{2} V_\rho^q \right), \quad \begin{pmatrix} \epsilon_d \\ \epsilon_{\bar{d}} \end{pmatrix} = \Omega_q^* \pm R_h^* \left( V_\omega^q - \frac{1}{2} V_\rho^q \right), \quad \epsilon_Q = \epsilon_{\bar{Q}} = \Omega_Q. \quad (87)$$

The hadron masses in a nuclear medium  $m_h^*$  (free mass will be denoted by  $m_h$ ), are calculated by

$$m_h^* = \sum_{j=q,\bar{q},Q,\bar{Q}} \frac{n_j \Omega_j^* - z_h}{R_h^*} + \frac{4}{3} \pi R_h^{*3} B, \quad \left. \frac{\partial m_h^*}{\partial R_h} \right|_{R_h=R_h^*} = 0, \quad (88)$$

where  $\Omega_q^* = \Omega_{\bar{q}}^* = [x_q^2 + (R_h^* m_q^*)^2]^{1/2}$  ( $q = u, d$ ), with  $m_q^* = m_q - g_\sigma^q \sigma$ ,  $\Omega_Q^* = \Omega_{\bar{Q}}^* = [x_Q^2 + (R_h^* m_Q)^2]^{1/2}$  ( $Q = s, c, b$ ), and  $x_{q,Q}$  are the bag eigenfrequencies.  $B$  is the bag constant,  $n_q(n_{\bar{q}})$  and  $n_Q(n_{\bar{Q}})$  are the lowest mode quark (antiquark) numbers for the quark flavors  $q$  and  $Q$  in the hadron  $h$ , respectively, while  $z_h$  parametrizes the sum of the center-of-mass and gluon fluctuation effects, which (following Ref. [93]) are assumed to be independent of density. Concerning the sign of  $m_q^*$  in nuclear medium, it reflects nothing but the strength of the attractive scalar potential as in Eqs. (80) and (81), and thus naive interpretation of the mass for a (physical) particle, which is positive, should not be applied. The parameters are determined to reproduce the corresponding masses in free space. The quark-meson



coupling constants,  $g_\sigma^q$ ,  $g_\omega^q$  and  $g_\rho^q$ , have been already determined. Exactly the same coupling constants,  $g_\sigma^q$ ,  $g_\omega^q$  and  $g_\rho^q$ , are used for the light quarks in the mesons and baryons as in the nucleon. (See Tab. 3.)

However, in studies of the kaon system, we found that it was phenomenologically necessary to increase the strength of the vector coupling to the non-strange quark in the  $K^+$  (by a factor of  $1.4^2$ , i.e.,  $g_{K\omega}^q \equiv 1.4^2 g_\omega^q$ ) in order to reproduce the empirically extracted repulsive  $K^+$ -nucleus interaction [104]. This may be related to the fact that kaon is a pseudo-Goldstone boson, where treatment of the Goldstone bosons in a naive quark model should not be expected to be satisfactory. We also discuss this possibility,  $g_\omega^q \rightarrow 1.4^2 g_\omega^q$ , for the  $D$ - and  $\bar{D}$ -meson nuclear bound states [107] in subsection 7.1. The scalar ( $V_s^h$ ) and vector ( $V_v^h$ ) potentials felt by the hadrons  $h$ , in nuclear matter are given by,

$$V_s^h = m_h^* - m_h, \quad (89)$$

$$V_v^h = (n_q - n_{\bar{q}})V_\omega^q + I_3^h V_\rho^q, \quad (V_\omega^q \rightarrow 1.4^2 V_\omega^q \text{ for } K, \bar{K}), \quad (90)$$

where  $I_3^h$  is the third component of isospin projection of the hadron  $h$ . Thus, the vector potential felt by a heavy baryon with a charm or bottom quark, is equal to that of the hyperon with the same light quark configuration in QMC.

In Tab. 4 we present the input (vacuum masses  $m_h$ ) bag parameters  $z_h$ , and the bag radius obtained in vacuum (at  $\rho_0 = 0.15 \text{ fm}^{-3}$ )  $R_h$  ( $R_h^*$ ) for various hadrons. Note that the bag radius in vacuum for the nucleon,  $R_N = 0.8 \text{ fm}$  is the input. For a more recent study of the  $\eta$ - $\eta'$  system, which takes into account the role of the  $U_A(1)$  axial anomaly, we refer to Refs. [46, 47, 48].

Table 4: The bag parameters, various hadron masses and the bag radii in free space [at normal nuclear matter density,  $\rho_0 = 0.15 \text{ fm}^{-3}$ ]  $z_h, R_h$  and  $m_h$  [ $m_h^*$  and  $R_h^*$ ].  $m_h$  and  $R_N = 0.8 \text{ fm}$  in free space are inputs. Note that the quantities for the physical  $\omega$ ,  $\phi$ ,  $\eta$  and  $\eta'$  are calculated including the octet-singlet mixing effect (see subsection 6.1), and that  $\omega$  and  $\rho$  below stand for the physical particles, and are different from those appearing in the Lagrangian density of QMC.

$h$	$z_h$	$m_h$ (MeV)	$R_h$ (fm)	$m_h^*$ (MeV)	$R_h^*$ (fm)
$N$	3.295	939.0	0.800	754.5	0.786
$\Lambda$	3.131	1115.7	0.806	992.7	0.803
$\Sigma$	2.810	1193.1	0.827	1070.4	0.824
$\Xi$	2.860	1318.1	0.820	1256.7	0.818
$\Lambda_c$	1.766	2284.9	0.846	2162.5	0.843
$\Sigma_c$	1.033	2452.0	0.885	2330.2	0.882
$\Xi_c$	1.564	2469.1	0.853	2408.0	0.851
$\Lambda_b$	-0.643	5624.0	0.930	5502.9	0.928
$\omega$	1.866	781.9	0.753	658.7	0.749
$\rho$	1.907	770.0	0.749	646.2	0.746
$K$	3.295	493.7	0.574	430.4	0.572
$K^*$	1.949	893.9	0.740	831.9	0.738
$\eta$	3.131	547.5	0.603	483.9	0.600
$\eta'$	1.711	957.8	0.760	896.5	0.758
$\phi$	1.979	1019.4	0.732	1018.9	0.732
$D$	1.389	1866.9	0.731	1804.9	0.730
$D^*$	0.849	2000.8	0.774	1946.7	0.772
$B$	-1.136	5279.2	0.854	5218.1	0.852

In Fig. 3 we show ratios of effective masses (free masses + scalar potentials) versus those of the free particles, for mesons (left panel) and baryons (right panel), respectively. With increasing density the

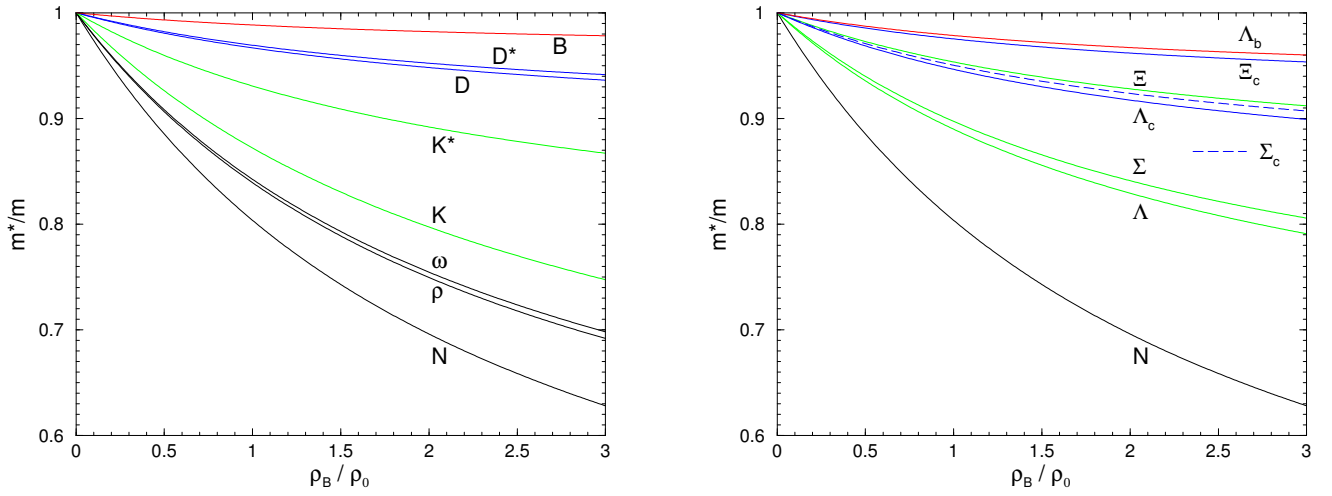


Figure 3: Effective mass ratios for mesons (left panel) and baryons (right panel) in symmetric nuclear matter, where,  $\rho_0 = 0.15 \text{ fm}^{-3}$ .  $\omega$  and  $\rho$  stand for physical mesons which are treated in the quark model, and should not be confused with the fields appearing in the QMC model.

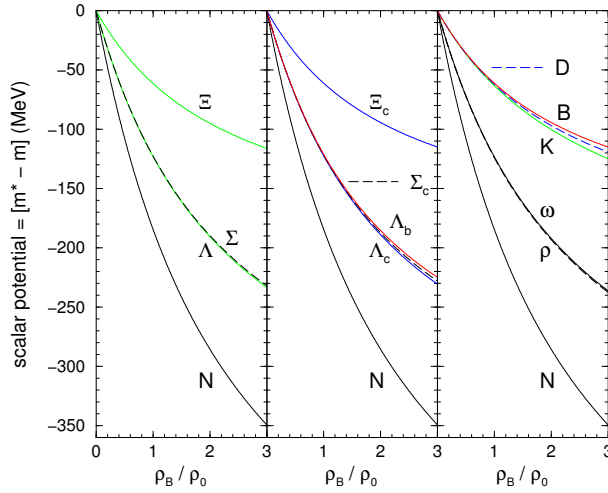


Figure 4: Scalar potentials for various hadrons in nuclear matter, where,  $\rho_0 = 0.15 \text{ fm}^{-3}$ . (See also caption of Fig. 3.)

ratios decrease as usually expected, but the magnitude of this reduction is reduced as we move from hadrons with only light quarks to those with one strange quark, with one charm quark, and with one bottom quark. This is because their masses in free space are in the order from light to heavy. Thus, the net ratios for the decrease in masses (developing of scalar masses) compared to that of the free masses becomes smaller. In Fig. 3 one may notice the somewhat anomalous behavior of the ratio for the kaon ( $K$ ). This is related to what we meant by the pseudo-Goldstone boson nature, i.e., its mass in free space is relatively light,  $m_K \simeq 495 \text{ MeV}$ , and the relative ratio for the reduction in mass in a nuclear medium is large.

Probably it is simpler and clearer to compare the scalar potentials felt by each hadron in nuclear matter. Calculated results are shown in Fig. 4. From the results one can confirm that the scalar potential felt by the hadron  $h$ ,  $V_s^h$ , follows a simple light quark number scaling rule:

$$V_s^h \simeq \frac{n_q + n_{\bar{q}}}{3} V_s^N, \quad (91)$$

where  $n_q$  ( $n_{\bar{q}}$ ) is the number of light quarks (antiquarks) in the hadron  $h$ , and  $V_s^N$  is the scalar potential

Table 5: The slope parameters,  $a_B$  ( $B = N, \Lambda, \Sigma, \Xi, \Lambda_c, \Sigma_c, \Xi_c, \Lambda_b$ ).

$a_B$	$\times 10^{-4} \text{ MeV}^{-1}$	$a_B$	$\times 10^{-4} \text{ MeV}^{-1}$
$a_N$	8.8	$a_{\Lambda_b}$	10.9
$a_\Lambda$	9.3	$a_{\Lambda_c}$	9.8
$a_\Sigma$	9.5	$a_{\Sigma_c}$	10.3
$a_\Xi$	9.4	$a_{\Xi_c}$	9.9

felt by the nucleon. It is interesting to notice that baryons with a charm and a bottom quark ( $\Xi_c$  is a quark configuration,  $qsc$ ), show very similar features to those of hyperons with one or two strange quarks.

It has been found that the function  $C_B(\sigma)$  ( $B = N, \Lambda, \Sigma, \Xi, \Lambda_c, \Sigma_c, \Xi_c, \Lambda_b$ ) (see Eq. (76) and two lines above), can be parameterized as a linear form in the  $\sigma$  field,  $g_\sigma\sigma$ , for practical calculations [93, 98, 99, 100, 101]:

$$C_B(\sigma) = 1 - a_B \times (g_\sigma\sigma), \quad (B = N, \Lambda, \Sigma, \Xi, \Lambda_c, \Sigma_c, \Xi_c, \Lambda_b). \quad (92)$$

The values obtained for  $a_B$  are listed in Tab. 5. This parameterization works very well up to about three times of normal nuclear matter density  $3\rho_0$ . Then, the effective masses for the baryons,  $B$ , in nuclear matter are well approximated by:

$$m_B^* \simeq m_B - \frac{n_q}{3} g_\sigma \left[ 1 - \frac{a_B}{2} (g_\sigma\sigma) \right] \sigma, \quad (B = N, \Lambda, \Sigma, \Xi, \Lambda_c, \Sigma_c, \Xi_c, \Lambda_b), \quad (93)$$

with  $n_q$  the number of light quarks in the baryon  $B$ .

## 4 Nuclear-bound $\eta_c$ and $J/\Psi$

As remarked in the Introduction, the mean fields generated by light meson exchange, which provide a natural explanation of the binding of atomic nuclei, cannot bind heavy  $c\bar{c}$  (or  $b\bar{b}$ ) quarkonia. Their interactions with the medium necessarily involve other mechanisms, including those based on multigluon-gluon exchange [79, 110, 112] and excitation of charmed hadronic intermediate states with light quarks created from the vacuum [71, 72, 73, 74, 75]. Reference [68] presents a recent review of the properties of charmonium states and compiles a fairly complete list of references on theoretical studies concerning a great variety of physics issues related to these states. On the experimental side, one of the major challenges is to find appropriate kinematical conditions to produce these hadrons essentially at rest, or with small momentum relative to the nucleus, as effects of the nuclear medium are driven by low energy interactions. The studies of in-medium charmonia present advantages compared to those of the  $\phi$ -meson, to be discussed in section 5. First, they have a very small decay width in vacuum, and they are expected to have a small width in a nucleus too. Second, since they are heavier than the  $\phi$ -meson, they are expected to move slower than the  $\phi$ -meson once produced near threshold in a nucleus. Therefore, one can hope that they can form nuclear bound states more easily than the  $\phi$ -meson.

Since the earlier suggestion [110, 111] that heavy charmonia states may form bound states with nuclei, a large literature on this subject has accumulated along the years. Many different methods have been used to investigate the possible existence of such exotic states. These include QCD-based approaches, the most prominent examples being calculations based on the color polarizability of quarkonium [68, 71, 82, 112, 113, 114, 115], QCD sum rules [116, 117, 118], meson loops [71, 72, 73, 74, 75], phenomenological approaches [119, 120], and, more recently, lattice QCD simulations [121, 122].

Knowledge of the low-energy quarkonium-nucleon interaction in free space is an important input for the study of quarkonium binding to nuclei. As for now, there is no direct experimental information

on the interaction of heavy quarkonium with the nucleon; practically all of our knowledge on this interaction comes from lattice QCD simulations. All available lattice results on quarkonium-nucleon interaction [122, 123, 124, 125, 126] indicate that it is attractive and not very strong. The crucial question is whether the strength is strong enough to form a bound state with the nucleon; if not, the important issue then becomes whether it is strong enough to bind a quarkonium to a sufficiently large nucleus.

In this section, we present predictions for  $\eta_c$  and  $J/\Psi$  bound states with nuclei of different sizes. We concentrate on two main approaches to the problem of quarkonium binding to nuclei. One approach is based on nonrelativistic effective quarkonium-nucleon potentials. Such potentials are either obtained by making use, in one way or another, of the ideas underlying pNRQCD through the multipole expansion of color fields and the concept of chromopolarizability of quarkonium, or by fits from lattice QCD simulations. The other approach considers the self-energy of a charmonium due to  $D\bar{D}$  loops in nuclear matter. The self-energy depends on the nuclear matter density which, through a local density approach, provides an effective potential for the charmonium in a finite nucleus.

Both approaches make use in an essential way of the independent-particle nature of the nucleus. The average baryon number density in the center of a large nucleus is close to the saturation density of nuclear matter,  $\rho_0 = 0.16 \text{ fm}^{-3}$  (in QMC  $\rho_0 = 0.15 \text{ fm}^{-3}$  has commonly been adopted); thereby the average separation distance of two two nearest neighbour nucleons in such a nucleus is  $d_{\text{av}} \sim \rho^{-1/3} \sim 1.8 \text{ fm}$ . Taking for the typical size of a nucleon the r.m.s. charge radius of the proton,  $r_p \equiv \langle r_p^2 \rangle^{1/2} \simeq 0.88 \text{ fm} \sim \Lambda_{\text{QCD}}^{-1}$ , as extracted from measurements of electric form factors in electron-proton scattering experiments [127], one obtains  $2r_p \sim d_{\text{av}}$ . On the other hand, the nucleon-nucleon interaction has a strong short-range repulsion (hard-core), which prevents substantial superposition of the quark cores of different nucleons in the nucleus. The interplay between the hard-core repulsion and the Pauli Exclusion Principle is at the basis of the nuclear shell model [128], in that nucleons move almost independently from each other with a well-defined angular momentum in an average mean field. The fact that  $2r_p \sim d_{\text{av}}$  does not spoil this picture of the nucleus [129, 130] as being a close-packed system of nucleons moving almost independently from each other.

## 4.1 Quarkonium-nucleon potentials

Let us imagine a heavy quarkonium  $Q\bar{Q}$  injected with low momentum into a close-packed nucleus. When the quark mass  $m_Q$  is large, i.e.  $m_Q \gg \Lambda_{\text{QCD}}$ , the heavy quarkonium is, as discussed in section 2, essentially a Coulomb bound state, with a Bohr radius  $r_0 = (m_Q \alpha_s)^{-1}$ , with  $\alpha_s = \alpha_s(m_Q) \ll 1$ . The quarkonium interacts by exchanging gluons with the light quarks of the nucleons, the typical wavelengths of the gluons being  $\lambda_g \sim r_p$ . For  $J/\Psi$ , for example, which is not a Coulomb bound state, potential models inspired by the Cornell model [131, 132] predict a r.m.s. radius of the order of  $r_{J/\Psi} \sim 0.2 \text{ fm} \ll r_p$ . Therefore, since  $\lambda_g \gg r_{J/\Psi}$ , the  $J/\Psi$  in the nucleus behaves like a small color dipole interacting with a uniform gluon field.

Having such a picture in mind for a quarkonium in a nucleus, one can describe the quarkonium-nucleus system using standard mean-field techniques of nonrelativistic many-body physics [133]. Given a nonrelativistic two-body quarkonium-nucleon potential,  $W_{\varphi N}$ , motivated either by a pNRQCD calculation or by phenomenological fits to lattice results, one can embed such a potential in a nonrelativistic many-body Hamiltonian of the form

$$H = H_N + H_{\varphi N}, \quad (94)$$

where  $H_N$  contains the kinetic energy of the nucleons and nucleon-nucleon (and multi-nucleon) interactions, and

$$H_{\varphi N} = \int d^3r \varphi^\dagger(t, \vec{r}) \left( -\frac{1}{2m_\varphi} \nabla^2 \right) \varphi(t, \vec{r})$$

$$+ \int d^3r d^3r' N^\dagger(t, \vec{r}) \varphi^\dagger(t, \vec{r}') W_{\varphi N}(\vec{r} - \vec{r}') \varphi(t, \vec{r}') N(t, \vec{r}), \quad (95)$$

where  $N(t, \vec{r})$  and  $\varphi(t, \vec{r})$  are the nucleon and quarkonium nonrelativistic quantum field operators—for simplicity of presentation, we omit flavor and spin indices. Let  $\{\varphi_\alpha(\vec{r})\}$  be a complete set of single-particle states of a quarkonium  $\varphi$ , and  $\{N_n(\vec{r})\}$  a corresponding set for the nucleons, where  $\alpha$  and  $n$  collect all quantum numbers necessary to specify the corresponding single-particle states. Taking the expectation value of  $H$  in a state with  $A$  independent nucleons and one quarkonium and varying the expectation value with respect to a  $\varphi_\alpha^*(\vec{r})$ , one obtains [133]

$$-\frac{1}{2m_\varphi} \nabla^2 \varphi_\alpha(\vec{r}) + W_{\varphi A}(\vec{r}) \varphi_\alpha(\vec{r}) = \epsilon_\alpha \varphi_\alpha(\vec{r}), \quad (96)$$

where  $\epsilon_\alpha$  are the single-particle energy states of a quarkonium in the system,  $W_{\varphi A}(\vec{r})$  is the  $\varphi$ -nucleus mean-field potential, given by

$$W_{\varphi A}(\vec{r}) = \int d^3r' W_{\varphi N}(\vec{r} - \vec{r}') \rho_A(\vec{r}'), \quad (97)$$

with  $\rho_A(\vec{r})$  being the nuclear density

$$\rho_A(\vec{r}) = \langle A | N^\dagger(\vec{r}) N(\vec{r}) | A \rangle = \sum_{n=1}^A N_n^*(\vec{r}) N_n(\vec{r}). \quad (98)$$

If one makes the assumption that the quarkonium in the nucleus does not change the density of nucleons, i.e. that the single-nucleon states are not modified by the interactions of the quarkonium with the nucleons, we have that, given a nuclear density profile  $\rho_A(\vec{r})$ , from a model or from experiment, Eq. (96) is an ordinary Schrödinger equation for a particle  $\varphi$  in a potential  $W_{\varphi A}(\vec{r})$ .

For nuclei composed of two or three nucleons only, the mean field treatment discussed above is not appropriate. For those nuclei, few-body methods are required. A few of these include the Green's function Monte Carlo, Faddeev-Yakubovsky equations, hyperspherical coordinates, Gaussian-basis variational, and the stochastic variational methods—Ref. [134] presents a comparison of results obtained with those methods for four-body nuclei using a particular  $NN$  potential. In this review, the smallest nucleus considered is  ${}^4\text{He}$ ; although it is a very dense nucleus, the mean field approximation might give only a first estimate for what one can expect with an accurate few-body calculation. We refer the reader to the recent review in Ref. [12] for a presentation on the use of Gaussian expansion method [135, 136] to charmonium binding to two- and four-nucleon nuclei [120]. We also remark that in a mean field treatment of a many-body system, the center of mass motion is not removed, but for a large nucleus this is not a severe problem. For  ${}^4\text{He}$  we follow the prescription used in the QMC model, where we use the  $\varphi$ - ${}^4\text{He}$  reduced mass in Eq. (96) instead of  $m_\varphi$ .

A quarkonium-nucleon potential  $W_{\varphi N}(\vec{r})$  can be constructed from the forward scattering amplitude of a quarkonium off a nucleon. The scattering amplitude can be written as a product of two terms: (1) a matrix element of gluon fields in the nucleon state, which can be obtained from the anomaly in the trace of the QCD energy-momentum tensor [18, 20], and (2) a quarkonium-gluon interaction, which can be evaluated using the multipole expansion [68, 82, 114, 115], or the operator product expansion of a current-current correlation function in an one-nucleon state [29], or an effective Lagrangian for quarkonium-gluon fields [113]. Specifically, the forward elastic  $\varphi N$  scattering matrix can be evaluated from the gWEFT Lagrangian in Eq. (55) as the expectation value of the  $\varphi$ -gluon term in an one-nucleon state

$$\mathcal{A}_{\varphi N} = \frac{1}{2} \alpha_\varphi \langle N | (g\vec{E})^2 | N \rangle, \quad (99)$$

where we use a nonrelativistic normalization for the states  $|N\rangle$ , and the expression for the quarkonium polarizability  $\beta$  is given in Eq. (56). From Eq. (100), one then has that this corresponds to a scattering length  $a_{\varphi N}$  given by<sup>1</sup>

$$a_{\varphi N} = - \left( \frac{\mu_{\varphi N}}{2\pi} \right) \mathcal{A}_{\varphi N} = - \left( \frac{\mu_{\varphi N}}{4\pi} \right) \alpha_{\varphi} \langle N | (g\vec{E})^2 | N \rangle. \quad (101)$$

where  $\mu_{\varphi N}$  is the reduced mass

$$\mu_{\varphi N} = \frac{m_{\varphi} m_N}{m_{\varphi} + m_N}. \quad (102)$$

One can obtain an estimate for the the matrix element  $\langle N | (g\vec{E})^2 | N \rangle$  by relating it to the nucleon mass via the anomaly in the trace of the energy momentum tensor (in the chiral limit). First, note that [68]:

$$\langle N | \left[ (g\vec{E})^2 - (g\vec{B})^2 \right] | N \rangle = -\frac{1}{2} \langle N | g^2 G_{\mu\nu}^a G^{a\mu\nu} | N \rangle = \frac{16\pi^2}{9} m_N \leq \langle N | (g\vec{E})^2 | N \rangle, \quad (103)$$

where we used Eq. (26) and the last inequality follows from the fact that  $\langle N | (g\vec{B})^2 | N \rangle \geq 0$ . Therefore, one obtains the following estimate for the scattering length

$$a_{\varphi N} \leq - \left( \frac{\mu_{\varphi N}}{4\pi} \right) \frac{16\pi^2}{9} m_N \alpha_{\varphi} = - \frac{4\pi m_N}{9} \mu_{\varphi N} \alpha_{\varphi}. \quad (104)$$

This shows that the color polarization force is attractive.

To investigate the binding of  $\varphi$  in a nucleus due to such a polarization force one would need a potential to be used in Eq. (97). Knowledge of the momentum-independent forward scattering amplitude  $\mathcal{A}_{\varphi N}$  is not enough for constructing such a potential. One can, however, construct a  $\varphi N$  contact interaction, which we denote by  $W_{\varphi N}^{\text{pol}}(\vec{r})$ , that reproduces that forward scattering amplitude; namely:

$$W_{\varphi N}^{\text{pol}}(\vec{r}) = \frac{4\pi}{2\mu_{\varphi N}} a_{\varphi N} \delta(\vec{r}) = - \frac{8\pi^2}{9} m_N \alpha_{\varphi} \delta(\vec{r}), \quad (105)$$

where, for definiteness, we have taken the equality in Eq. (104). Using this into Eq. (97), one obtains for the  $\varphi$ -nucleus potential due to the color polarizability force the following expression:

$$W_{\varphi A}^{\text{pol}}(\vec{r}) = \frac{4\pi}{2\mu_{\varphi N}} a_{\varphi N} \rho_A(\vec{r}) = - \frac{8\pi^2}{9} m_N \alpha_{\varphi} \rho_A(\vec{r}). \quad (106)$$

Although the full  $\varphi N$  potential is of finite range and includes a long-range tail of the form of a van der Waals force, this interaction already provides interesting insight into the problem of quarkonium binding to nuclei. It is clear that the strength of the polarization force in Eq. (106) is controlled by the value of the polarizability  $\alpha_{\varphi}$ . The estimates in Refs. [68, 115] find that the binding energy of  $J/\Psi$  in nuclear matter (taking  $\rho_0 = 0.17 \text{ fm}^{-3}$ ), is 21 MeV for  $\alpha_{J/\Psi} = 2 \text{ GeV}^{-3}$ , which corresponds to a scattering length of  $a_{J/\Psi N} = -0.37 \text{ fm}$ . This is a rather strong binding energy on the nuclear scale; recall that the binding energy of a nucleon in nuclear matter is 16 MeV. On the other hand, a very recent extraction [137] based on a global fit to both differential and total cross sections from available data on  $J/\Psi p$  scattering

<sup>1</sup>Our conventions for the relationships involving the (on-shell)  $S$ -matrix, scattering amplitude  $\mathcal{A}(k)$ , phase shift  $\delta(k)$ , scattering length  $a$ , and effective range  $r_e$ , for  $s$ -waves are

$$S = 1 + i \frac{2\mu k}{2\pi} \mathcal{A}(k) = e^{2i\delta(k)}, \quad \mathcal{A}(k) = \frac{2\pi/\mu}{k \cotan \delta(k) - ik}, \quad k \cotan \delta(k) = -\frac{1}{a} + \frac{1}{2} r_e k^2 + \dots, \quad (100)$$

where  $\mu$  is the reduced mass of the two-body system.

leads for the spin-averaged  $J/\Psi p$   $s$ -wave scattering length the value  $a_{J/\Psi p} = -0.046 \pm 0.005$  fm, which is consistent with the value  $a_{\eta_c N} = -0.05$  fm from Ref. [82] but smaller by almost an order of magnitude than the value estimated in Refs. [68, 115]. A scattering length of  $a_{J/\Psi p} = -0.046$  fm leads to a  $J/\Psi$  binding energy in nuclear matter (taking  $\rho_0 = 0.17 \text{ fm}^{-3}$ ) of  $2.7 \pm 0.3$  MeV, which is of the order of the deuteron binding energy. Estimates based on lattice hybrid potentials [138] lead to even smaller values for the strength of the  $\varphi N$  interaction. Reference [139] investigated the existence of bound states in elastic and inelastic channels of charmonium-nucleon and bottomonium-nucleon systems using an extended local hidden gauge formalism and incorporating constraints from heavy quark spin-flavor symmetry, but no scattering lengths and effective range parameters were provided.

A first estimate on the required attraction to bind a quarkonium to a nucleus can be obtained from the condition for the existence of a nonrelativistic  $s$ -wave bound state of a particle of mass  $m$  trapped in an attractive spherical well of radius  $R$  and depth  $V_0$  [140]:

$$V_0 > \frac{\pi^2 \hbar^2}{8mR^2}. \quad (107)$$

Taking  $m = m_{J/\Psi}$  and  $R = 5$  fm (radius of a relatively large nucleus), one obtains  $V_0 > 1$  MeV. Based on such an estimate, one may say that the prospects for a quarkonium to form bound states with a nucleus seem to be very good. Real nuclei, however, have a surface and, as we show shortly, the above estimate can be quite misleading. A full calculation, using realistic density profiles of nuclei is required for a more reliable estimate. Single-particle bound-state energies will be presented for a few nuclei in subsection 4.3

Next, we consider the charmonium-nucleon system from the perspective of the lattice results of Refs. [125, 126]. Those references present a fit of the lattice data in terms of a finite-range nucleon-charmonium effective nonrelativistic potential  $W_{\varphi N}(\vec{r})$ . In addition, results are presented for  $\eta_c N$  and  $J/\Psi N$  scattering lengths and effective range parameters extracted from evaluations of scattering phase shifts through Lüscher's method [141] adapted to twisted boundary conditions [142]. Most of the results are from quenched lattice data, but Ref. [126] also presents selected results for the  $\eta_c N$  system using unquenched lattice data. The quenched results are obtained with a lattice size of  $L^3 \times T = 32^3 \times 48$  and lattice spacing  $a \approx 0.094$  fm. The simulations are for three pion masses,  $m_\pi = 640, 720, 870$  MeV, which correspond to nucleon masses  $m_N = 1430, 1520, 1700$  MeV, quarkonium masses  $m_{\eta_c} = 2920$  MeV and  $m_{J/\Psi} = 3000$  MeV. For the  $J/\Psi N$  system, there are two spin states, spin-1/2 and spin-3/2. The  $s$ -wave scattering lengths found are [126]:  $(a_{J/\Psi N})_{\text{SAV}} \sim 0.35$  fm  $>$   $a_{\eta_c N} \sim 0.25$  fm, where SAV means spin average, with very little dependence on the pion mass within the range of masses used. In addition, the  $s$ -wave effective range  $r_e$  is of similar value for both  $\eta_c N$  and  $J/\Psi N$  systems,  $r_e \sim 1.0$  fm, also with very little pion mass dependence but with errors of the order of 50%.

The extraction of an effective potential in Refs. [125, 126] is based on the method introduced in Ref. [143] for the  $NN$  interaction. In general terms, an equal-time Bethe-Salpeter amplitude is calculated on the lattice through nucleon and charmonium interpolators. An appropriate projection with respect to the discrete elements of cubic rotation group is made to obtain a Bethe-Salpeter wave function that corresponds in the continuum to an  $s$ -wave. The effective charmonium-nucleon potential is then defined as the equivalent appearing in a Schrödinger equation with stationary energy  $E$ , namely:

$$V_{\varphi N}(r) = E_{\varphi N} + \frac{1}{2\mu_{\varphi N}} \frac{\nabla_{\text{latt}}^2 \phi_{\varphi N}(r)}{\phi_{\varphi N}(r)}, \quad (108)$$

where  $\nabla_{\text{latt}}^2$  is a lattice Laplacian and  $\mu_{\varphi N}$  is the reduced mass of the  $\varphi N$  two-body system. The fit provided for the  $\eta_c N$  potential from simulations using  $m_\pi = 640$  MeV gives a very good fit of the data in the range  $r \sim 0.3$  fm to  $r = 2.5$  fm. It is given in the form of a Yukawa potential with a strength  $\gamma$  and range  $\alpha$ :

$$V_{\eta_c N}^{\text{fit}}(r) = -\gamma \frac{e^{-\alpha r}}{r}, \quad (109)$$

with  $\gamma = 0.1$  and  $\alpha = 0.6 \text{ GeV} \sim 3 \text{ fm}^{-1}$ . Interestingly, the lattice results for large  $r$  cannot be fitted with a  $1/r^n$  falloff, with  $n > 1$ , as one would expect from a typical van der Waals force. The authors of Ref. [126] argue that this might be indication of a screening effect of nonperturbative nature.

As mentioned, the lattice values for the scattering lengths reported in Ref. [126] are extracted from Lüscher's formula for the phase shifts and, therefore, they contain information on the full  $\varphi N$  interaction and not only from the fitting region  $r \sim 0.3 \text{ fm}$  to  $r = 2.5 \text{ fm}$ . One can assess the importance of the interaction coming from the region  $r < 0.3 \text{ fm}$  by calculating the scattering length with  $V_{\eta_c N}^{\text{fit}}(r)$  and comparing the result with the value from the lattice simulation. One can extract the scattering length and effective range by calculating the scattering phase shift  $\delta(k)$  and fitting  $k \cotan \delta(k)$  for small values of  $k$  to the formula given in Eq. (100). To calculate the phase shifts we have used the variable phase approach [144]. We have calculated the scattering length with the fitted potential given in Eq. (109), using the lattice values  $m_N = 1430 \text{ MeV}$  and  $m_{\eta_c} = 2920 \text{ MeV}$ . We obtained for the  $s$ -wave scattering length  $a_{\eta_c N} = -0.13 \text{ fm}$ , which is smaller by a factor of two in comparison with the value obtained with Lüscher's formula. For orientation, we mention that in Born approximation, the scattering length from the Yukawa fit in Eq. (109) is  $a^{\text{Born}} = -\gamma(2\mu_{\eta_c N}/\alpha^2) = -0.1 \text{ fm}$ . This indicates that the full  $\eta_c N$  potential receives substantial contributions from relative distances shorter than  $r < 0.3 \text{ fm}$ , i.e. when the  $\eta_c$  is immersed in the nucleon, a situation resembling very much the hadrocharmonium picture suggested in Ref. [145]. In this picture, a heavy quarkonium is bound as a compact object within the volume of a light hadron; in the case the light hadron is a nucleon, the hadrocharmonium would be a charmed pentaquark. A recent lattice QCD simulation tested this picture with a variety of light quark hadrons and found binding energies ranging from  $-1$  to  $-2.5 \text{ MeV}$ . The simulations were performed with pion and kaon masses given by  $m_\pi = 223 \text{ MeV}$  and  $m_K = 476 \text{ MeV}$ , and the charm quark mass was taken  $m_c = 1269 \text{ MeV}$ .

Because the data of Refs. [125, 126] show a very mild pion mass dependence within the range of masses used in the lattice simulations, the extrapolation of the potential extracted in that references to physical masses and short distances with the use of a chiral EFT is virtually impossible. In view of this, here we simply take a phenomenological approach, in that we cut off the lattice potential of Eq. (109) at some prescribed distance, that we suggestively denote by  $r_{\text{vdW}}$ , and add to it a constant piece,  $W_0$ , which extends from  $r = 0$  to  $r_{\text{vdW}}$ . The constant potential mimics the feature of the interaction being of a small color dipole interacting with a uniform gluon field. The value of  $W_0$  is fixed by fitting the lattice value for the scattering length—we make no effort to fit the effective range  $r_e$  due to the large errors associated with its extraction from the lattice data. For the  $J/\Psi N$  system we refit  $W_0$  to reproduce the spin-averaged lattice value for  $a_{J/\Psi N}$ . Since we are unable to perform an extrapolation of the potentials to physical masses due to the large pion masses used in the lattice simulations, we simply use the physical masses of the nucleon and quarkonia in the fitting procedure. Specifically, we write for the full  $\varphi N$  potential

$$W_{\varphi N}^{\text{latt}}(r) = -W_0 [1 - f(r, r_{\text{vdW}})] + V_{\eta_c N}^{\text{fit}}(r) f(r, r_{\text{vdW}}), \quad (110)$$

with a  $f(r, r_{\text{vdW}})$  that resembles a step function:

$$f(r, r_{\text{vdW}}) = \frac{1}{1 + (r_{\text{vdW}}/r)^{10}}. \quad (111)$$

To avoid proliferation of uncontrolled parameters, in fitting  $W_0$  for the  $J/\Psi N$  system we use the  $\eta_c N$  values for  $\gamma$  and  $\alpha$  given above. The  $\varphi$ -nucleus potential is then obtained by inserting Eq. (110) in Eq. (97); we denote this potential by  $W_{\varphi A}^{\text{latt}}(\vec{r})$

$$W_{\varphi A}^{\text{latt}}(\vec{r}) = \int d^3 r' W_{\varphi N}^{\text{latt}}(\vec{r} - \vec{r}') \rho_A(\vec{r}'). \quad (112)$$

We have chosen two typical values for  $r_{\text{vdW}}$ : one is  $r_{\text{vdW}} = 0.3 \text{ fm}$ , which corresponds roughly to the lowest value of  $r$  used in the fitting of the lattice data with the Yukawa form  $V_{\eta_c N}^{\text{fit}}(r)$ , and the other is



$r_{\text{vdW}} = 0.5$  fm, which is a little larger than one half of the radius of the proton. The resulting values for  $W_0$  are shown in Tab. 6; they reveal that as  $r_{\text{vdW}}$  decreases,  $W_0$  must increase to fit the scattering length. This is expected, as the strength of the Yukawa,  $\gamma = 0.1$ , is not enough to describe the lattice values of the scattering lengths when  $r_{\text{vdW}} = 0$ . The values of effective range parameter that are obtained with  $W_{\varphi N}^{\text{latt}}(r)$  for both  $\eta_c N$  and  $J/\Psi$  systems are compatible, within errors, with the lattice results. Of course, by adjusting simultaneously  $W_0$  and  $r_{\text{vdW}}$ , both the scattering length and effective range could be fitted, but the errors are large for  $r_e$  and there is not much to be gained with a fit to a quantity not well constrained by data. Given the potential, the important issue is to know how large must a nucleus be to bind a charmonium. This will be discussed in the first part of subsection 4.3, where we present numerical results for the  $\varphi$ -nucleus potentials and single-particle energy levels.

## 4.2 $J/\Psi$ self-energy and $D\bar{D}$ loop

Based on the QMC model explained in section 3,  $J/\Psi$  mass shift in nuclear matter and  $J/\Psi$ -nucleus bound states were studied in Refs. [72, 73, 74], using the effective Lagrangian approach with the in-medium  $D$  and  $\bar{D}$  meson masses calculated by the QMC model [94]. In these studies the  $J/\Psi$  self-energy in the intermediate states involved the  $D, \bar{D}, D^*$  and  $\bar{D}^*$  mesons. It turned out that the  $J/\Psi$  self-energy has larger contributions from the loops involving the  $D^*$  and  $\bar{D}^*$  mesons. This is unexpected, since the mass of the  $D^*$  ( $\bar{D}^*$ ) is heavier than that of  $D$  ( $\bar{D}$ ) by about 140 MeV in vacuum, and the decrease of the masses in nuclear matter are nearly the same for the  $D$  and  $D^*$  mesons [72, 72, 74] (also to be shown later). Thus, the relative enhancement of these meson loop contributions to the  $J/\Psi$  self-energy in medium should be similar to that in vacuum, or the loop involving only the  $D^*$  and  $\bar{D}^*$  mesons in the  $J/\Psi$  self-energy is not expected to give a larger contribution than that involving only the  $D$  and  $\bar{D}$  mesons. This is because, between the  $D\bar{D}$ - and  $D^*\bar{D}^*$ -loops, the energy necessary to excite the latter loop needs, at least twice the mass difference of the  $D$  and  $D^*$ .

At least two issues may be considered for this unexpected result: (i) coupling constants used for the  $J/\Psi$ - $DD^*$  and  $J/\Psi$ - $D^*D^*$  were assumed to be the same as that for  $J/\Psi$ - $DD$ , and (ii) ambiguity in the effective Lagrangian adopted. Considering these, we have chosen to update [75] our previous works of the  $J/\Psi$ -nucleus bound states [72, 73, 74] in this subsection. Thus, similarly to the  $\phi$ -meson case to be discussed in section 5, we update the  $J/\Psi$  mass shift and  $J/\Psi$ -nuclear bound states including only the  $D\bar{D}$ -loop for the  $J/\Psi$  self-energy.

In Refs. [72, 73, 74]  $J/\Psi$  mass shift in nuclear matter was studied based on an effective Lagrangian approach, including the  $D, \bar{D}, D^*$  and  $\bar{D}^*$  mesons in the intermediate states for the  $J/\Psi$  self-energy. We update the results by including only the  $D\bar{D}$ -loop contribution for the  $J/\Psi$  self-energy as mentioned above. We report the updated results for the bound state single-particle energies, by solving the Schrödinger equation for the  $J/\Psi$  meson produced nearly at rest. The results for the  $\phi$ -nuclear bound

Table 6: The value of  $W_0$  in Eq. (110) for two values of the cutoff parameter  $r_{\text{vdW}}$  for the  $\eta_c N$  and  $J/\Psi$  systems. Also shown are the effective range parameters that are obtained with the potential  $W_{\varphi N}^{\text{latt}}(r)$  when the scattering lengths are fitted to the lattice values. Physical masses of the nucleon and charmonia are used. Units of  $r_{\text{vdW}}$  and  $r_e$  are fm and of  $W_0$  is MeV.

$r_{\text{vdW}}$	$\eta_c N$		$J/\Psi N$	
	$W_0$	$r_e$	$W_0$	$r_e$
0.3	252	1.4	288	1.2
0.5	74	1.7	95	1.4

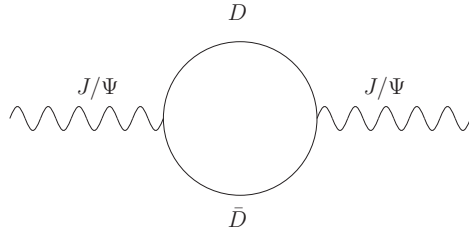


Figure 5:  $D\bar{D}$ -loop contribution to the  $J/\Psi$  self-energy.

states to be discussed in section 5, both solving the Klein-Gordon equation and the Schrödinger equation, have proven to be essentially the same. Thus, we solve the Schrödinger equation, which makes the numerical procedure simpler and can compare with the nonrelativistic QCD approach. However the differences are expected to be even smaller for the results obtained by solving the Klein-Gordon and Schrödinger equations for the  $J/\Psi$  meson, since  $J/\Psi$  is heavier than  $\phi$ . Note that, the structure of heavy nuclei, as well as the medium modification of the  $D$  mass ( $\bar{D}$  mass), are explicitly calculated by using the QMC model [92, 94].

A first estimate for the mass shifts for the  $J/\Psi$  meson (and  $\Psi(3686)$  and  $\Psi(3770)$ ) in nuclear medium including the effects of  $D\bar{D}$  loop in the  $J/\Psi$  self-energy – see Fig. 5 – was made in Ref. [71]. Employing a gauged effective Lagrangian for the coupling of  $D$  mesons to the charmonia, the mass shifts were found to be positive for  $J/\Psi$  and  $\psi(3770)$ , and negative for  $\psi(3660)$  at normal nuclear matter density  $\rho_0$ . These results were obtained for density-dependent  $D$  and  $\bar{D}$  masses that decrease linearly with density, such that at  $\rho_0$  they are shifted by 50 MeV. The loop integral in the self-energy (Fig. 5) is divergent and was regularized using form-factors derived from the  $^3P_0$  decay model with quark-model wave functions for  $\Psi$  and  $D$ . The positive mass shift is at first sight puzzling, since even with a 50 MeV reduction of the  $D$  masses, the intermediate state is still above threshold for the decay of  $J/\Psi$  into a  $D\bar{D}$  pair and so a second-order contribution should be negative. However, as we have shown in Ref. [72], this is a result of the interplay of the form factor used and the gauged nature of the interaction used in Ref. [71]. Focusing on these points, we update the study with the “the gauged term” more in detail. In the same way as done in Ref. [72], the mass shift of the  $J/\Psi$  is estimated, but including only the  $D\bar{D}$ -loop in the  $J/\Psi$  self-energy, using both non-gauged and gauged effective Lagrangians. It turns out that the sign of the  $J/\Psi$  mass shift in nuclear matter due to the  $D\bar{D}$ -loop, depends on the value of the cutoff in the form factor when the gauged term is employed. Reasonably large cutoff values still give the negative  $J/\Psi$  mass shift when including the gauged term.

We briefly discuss below how the  $J/\Psi$  scalar potential (mass shift) is calculated in nuclear matter [72] with the  $D\bar{D}$ -loop for the  $J/\Psi$  self-energy. We use the following phenomenological effective Lagrangian densities at the hadronic level, which are similar to those to be used for the  $\phi$ -meson in subsection 5.1, correspond to replacing  $\psi \rightarrow \phi$ ,  $D \rightarrow K$  and  $\bar{D} \rightarrow \bar{K}$  (in the following we denote by  $\psi$  the field representing  $J/\Psi$ ):

$$\mathcal{L}_{int} = \mathcal{L}_{\psi DD} + \mathcal{L}_{\psi\psi DD}, \quad (113)$$

$$\mathcal{L}_{\psi DD} = ig_{\psi DD} \psi^\mu [\bar{D}(\partial_\mu D) - (\partial_\mu \bar{D})D], \quad (114)$$

$$\mathcal{L}_{\psi\psi DD} = g_{\psi DD}^2 \psi_\mu \psi^\mu \bar{D}D. \quad (115)$$

Here our convention is

$$D = \begin{pmatrix} D^0 \\ D^+ \end{pmatrix}, \quad \bar{D} = (\bar{D}^0 \quad D^-). \quad (116)$$

We note that the Lagrangians are an  $SU(4)$  extension of light-flavor chiral-symmetric Lagrangians of pseudoscalar and vector mesons. In the light flavor sector, they have been motivated by a local

gauge symmetry, treating vector mesons either as massive gauge bosons or as dynamically generated gauge bosons. Local gauge symmetry implies in the contact interaction in Eq. (115) involving two pseudoscalar and two vector mesons. In view of the fact that  $SU(4)$  flavor symmetry is strongly broken in nature, and in order to stay as close as possible to phenomenology, we use experimental values for the charmed meson masses and use the empirically known meson coupling constants. For these reasons we choose not to use gauged Lagrangians – a similar attitude was followed in Ref. [146] in a study of hadronic scattering of charmed mesons. However, in order to compare results with Ref. [71] and assess the impact of a contact term of the form Eq. (115), we also present results for the  $J/\Psi$  mass shift including such a term. More detailed, similar discussions will be made for the  $\phi$ -meson case, below Eq. (130) in subsection 5.1. We mention that recent investigations of  $SU(4)$  flavor symmetry breaking in hadron couplings of charmed hadrons to light hadrons are not conclusive; while two studies based on the Dyson-Schwinger equations of QCD find large deviations from  $SU(4)$  symmetry [147, 148], studies using QCD sum rules [149, 150], a constituent quark model [151] and a holographic QCD model [152] find moderate deviations.

We are interested in the difference of the in-medium,  $m_\psi^*$ , and vacuum,  $m_\psi$ ,

$$\Delta m_\psi = m_\psi^* - m_\psi, \quad (117)$$

with the masses obtained from

$$m_\psi^2 = (m_\psi^0)^2 + \Sigma_{D\bar{D}}(k^2 = m_\psi^2). \quad (118)$$

Here  $m_\psi^0$  is the bare mass and  $\Sigma_{D\bar{D}}(k^2)$  is the total  $J/\Psi$  self-energy obtained from the  $D\bar{D}$ -loop contribution. The in-medium mass,  $m_\psi^*$ , is obtained likewise, with the self-energy calculated with medium-modified  $D$  meson mass calculated by the QMC model.

We take the averaged, equal masses for the neutral and charged  $D$  mesons, i.e.  $m_{D^0} = m_{D^\pm}$ . Averaging over the three polarizations of  $J/\Psi$ , one can calculate the  $D\bar{D}$ -loop contribution to the  $J/\Psi$  self-energy  $\Sigma_{D\bar{D}}$  as

$$\Sigma_{D\bar{D}}(m_\psi^2) = -\frac{g_\psi^2 DD}{3\pi^2} \int_0^\infty dq \vec{q}^2 F_{D\bar{D}}(\vec{q}^2) K_{D\bar{D}}(\vec{q}^2), \quad (119)$$

where  $F_{D\bar{D}}(\vec{q}^2)$  is the product of vertex form-factors (to be discussed later) and the  $K_{D\bar{D}}(\vec{q}^2)$  for the  $D\bar{D}$ -loop contribution is given by

$$K_{D\bar{D}}(\vec{q}^2) = \frac{\vec{q}^2}{\omega_D} \left( \frac{\vec{q}^2}{\omega_D^2 - m_\psi^2/4} - \xi \right), \quad (120)$$

where  $\omega_D = (\vec{q}^2 + m_D^2)^{1/2}$ ,  $\xi = 0$  for the non-gauged Lagrangian of Eq. (114) and  $\xi = 1$  with Eq. (115), for the gauged Lagrangian of Ref. [71].

Because of baryon number conservation, no vector potential should contribute to the  $D\bar{D}$ -loop integral. Recall that, for the  $K^+$  meson case,  $g_\omega^q$  associated with the vector potential had to be scaled  $1.4^2$  times to reproduce an empirically extracted repulsive potential of about 25 MeV at normal nuclear matter density [104]. The reason is that  $K$ -mesons may be regarded as pseudo-Goldstone bosons, and they are therefore difficult to describe by naive quark models as is also the case for pions. For this reason, in earlier work we explored the possibility of also scaling the  $g_\omega^q$  strength by a factor  $1.4^2$  for the  $D$  and  $\bar{D}$  mesons [107, 153]. In the present case, this possibility is irrelevant, since the vector potential does not contribute to the final results. Thus, we may focus on the effective masses of the  $D$ -mesons.

For completeness we show the effective masses of the  $D$  and  $D^*$  mesons calculated by the QMC model in Fig. 6. The net reductions of the  $D$  and  $D^*$  masses are nearly equal for a given density, as dictated by the *light quark number counting rule* [100]. (See also subsection 3.2.) This fact supports the assumption applied here that the  $J/\Psi$  self-energy involving any  $D^*$  ( $\bar{D}^*$ ) mesons intermediate states

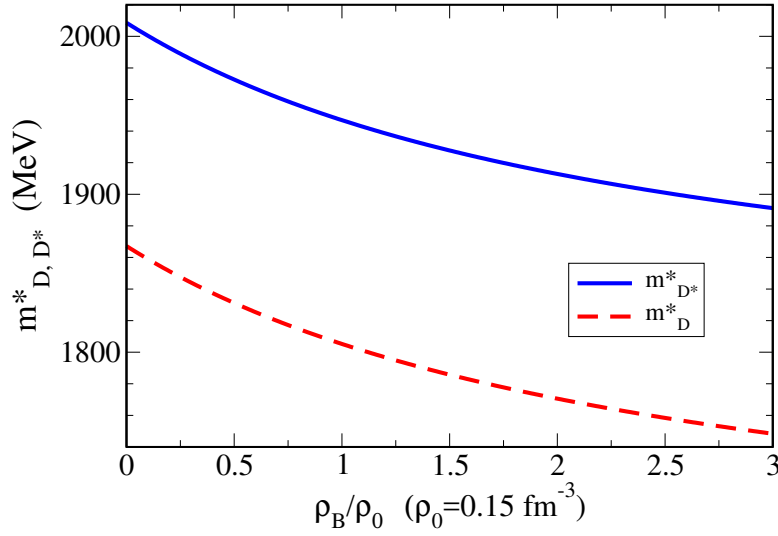


Figure 6:  $D$  (lower dashed line) and  $D^*$  (upper solid line) meson effective masses in symmetric nuclear matter.

should be less enhanced than that involving only the  $D$  ( $\bar{D}$ ) mesons as in vacuum—the reason why we update and ignore any intermediate states involving the  $D^*$  ( $\bar{D}^*$ ).

Amongst, one of the important ingredients in the present calculation is the phenomenological form factor, needed to regularize the self-energy loop integral in Eq. (119). Following previous experience with a similar calculation for the  $\rho$  self-energy [154] and the  $\phi$ -meson case, we use a dipole form for the vertex form factor,

$$u_D(\vec{q}^2) = \left( \frac{\Lambda_D^2 + m_\psi^2}{\Lambda_D^2 + 4\omega_D^2(\vec{q})} \right)^2, \quad (121)$$

so that the  $F_{D\bar{D}}(\vec{q}^2)$  in Eq. (119) are given by

$$F_{D\bar{D}}(\vec{q}^2) = u_D^2(\vec{q}^2), \quad (122)$$

where  $\Lambda_D$  is a cutoff mass. Obviously the main uncertainty here is the value of this cutoff mass. In a simple-minded picture of the vertex the cutoff mass is related to the extension of the overlap region of  $J/\Psi$  and  $D$  meson at the vertex, and therefore should depend upon the size of the wave function of this meson. One can have a rough estimate of  $\Lambda_D$  by using a quark model calculation of the form factors. Using a  $^3P_0$  model for quark-pair creation [155] and Gaussian wave functions for the mesons, the vertex form factor can be written as [71]

$$u_{QM}(\vec{q}^2) = e^{-\vec{q}^2/4(\beta_D^2 + 2\beta_\psi^2)}, \quad (123)$$

where  $\beta_D$  and  $\beta_\psi$  are respectively the Gaussian size parameters of the  $D$  and  $J/\Psi$  wave functions. Demanding that the  $u_D(\vec{q}^2)$  of Eq. (121) and  $u_{QM}(\vec{q}^2)$  have the r.m.s. radii  $\langle r^2 \rangle^{1/2}$ , with

$$\langle r^2 \rangle = -6 \left. \frac{d \ln u(q^2)}{dq^2} \right|_{\vec{q}^2=0}, \quad (124)$$

one obtains

$$\Lambda_D^2 = 32(\beta_D^2 + 2\beta_\psi^2) - 4m_D^2. \quad (125)$$

Using  $m_D = 1867.2$  MeV and for the  $\beta_{D,\psi}$  the values used in Ref. [71],  $\beta_D = 310$  MeV and  $\beta_\psi = 520$  MeV, one obtains  $\Lambda_D = 2537$  MeV. Admittedly this is a somewhat rough estimate and it is made solely to obtain an order of magnitude estimate, since we do not expect that Gaussian form factors should be

very accurate at high  $\vec{q}^2$ . In view of this and to gauge uncertainties of our results, we allow the value of  $\Lambda_D$  vary in the range  $2000 \text{ MeV} \leq \Lambda_D \leq 6000 \text{ MeV}$ . We have studied much larger range of the values for  $\Lambda_D$  [75] than before [72, 73, 74].

There remain to be fixed the bare  $J/\Psi$  mass  $m_\psi^0$  and the coupling constants. The bare mass is fixed by fitting the physical mass  $m_{J/\Psi} = 3096.9 \text{ MeV}$  using Eq. (118). For the coupling constants we use  $g_{\psi DD} = 7.64$ , which is obtained by the use of isospin symmetry [156].

We calculate the in-medium self-energy using the in-medium  $D$  meson mass calculated by the QMC model presented in Fig. 6. We present results for both  $\xi = 0$  (no gauge coupling) and for  $\xi = 1$  (with gauge coupling). In Fig. 7 we show the contribution of the  $D\bar{D}$ -loop to the  $J/\Psi$  mass shift for  $\xi = 0$  (left panel), and the comparison with  $\xi = 0$  and  $\xi = 1$  (right panel). As the cutoff mass value increases in the form factor, obviously the  $D\bar{D}$ -loop contribution becomes larger.

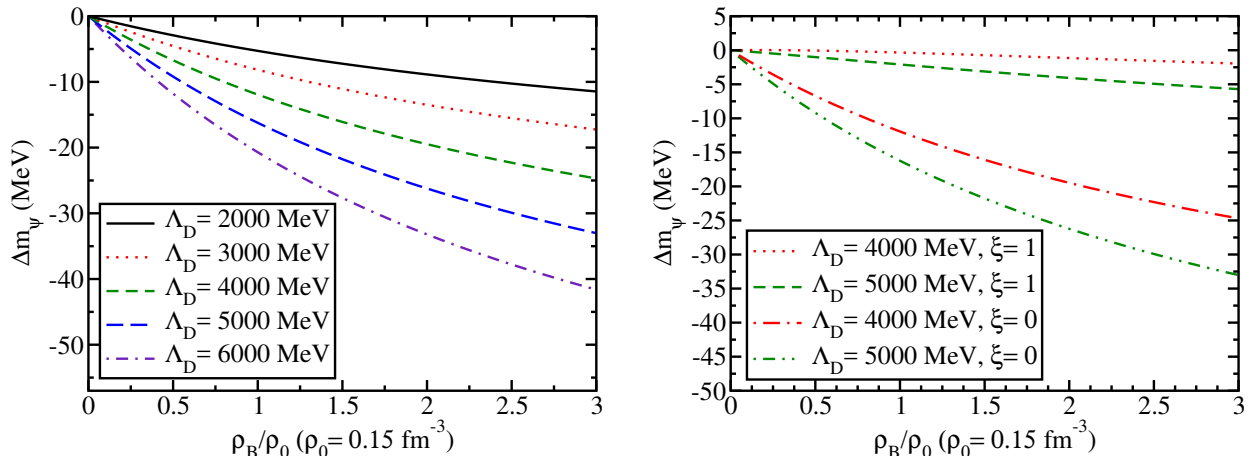


Figure 7: Contribution from the  $DD$ -loop to the  $J/\Psi$  mass shift  $\Delta m_\psi = m_\psi^* - m_\psi$  in symmetric nuclear matter without the gauge term ( $\xi = 0$ ) for five different values of the cutoff  $\Lambda_D$  (left panel), and the comparison with including the gauge term ( $\xi = 1$ ) for two values of  $\Lambda_D$  (right panel).

First, from the result shown in the left panel in Fig. 7 without the gauge term ( $\xi = 0$ ), one can see that the  $J/\Psi$  gets the attractive potential for all the values of the cutoff  $\Lambda_D$ , 2000 – 6000 MeV. In contrast, one can see from the right panel in Fig. 7, that the effect of the gauge term tends to oppose the effect (repulsion) of the contribution of the  $D\bar{D}$ -loop as noticed in Ref. [72]. When the value of  $\Lambda_D$  is smaller, the mass shift becomes positive. (Note that in Tab. 1 of Ref. [72], since the  $J/\Psi$  bare mass  $m_\psi^0$  was calculated including all the  $DD$ -,  $DD^*$ -,  $\bar{D}D^*$ - and  $D^*\bar{D}^*$ -loops, the dependence of the  $J/\Psi$  mass shift on the applied  $\Lambda_D$  values was slightly different from the present case with the inclusion of only the  $D\bar{D}$ -loop.)

The results shown in Fig. 7 reveal a negative mass shift (attractive potential) for the  $J/\Psi$  in symmetric nuclear matter in all cases. A negative self-energy for  $\Delta m_\psi$  means that the nuclear mean field provides attraction to  $J/\Psi$ . Using for  $m = m_\psi^*$  and  $R = 5 \text{ fm}$  in Eq. (107), one sees that the values of  $\Delta m_\psi$  shown in Fig. 7 are much larger than the lower bound minimum  $V_0 > 1 \text{ MeV}$ . Of course, as mentioned previously, the nuclear surface plays an important role and a detailed investigation is required.

### 4.3 Predictions for $\eta_c$ - and $J/\Psi$ -nucleus binding energies

We now present predictions for the binding energies of  $\eta_c$  and  $J/\Psi$  in selected nuclei, ranging from small- to large-sized:  ${}^4\text{He}$ ,  ${}^{12}\text{C}$ ,  ${}^{40}\text{Ca}$ ,  ${}^{48}\text{Ca}$ ,  ${}^{90}\text{Zr}$  and  ${}^{208}\text{Pb}$ . We present first the predictions obtained with the quarkonium-nucleon potentials discussed in section 4.1 and then those based on the potentials due to the  $D\bar{D}$ -loop for  $J/\Psi$  self-energy discussed in section 4.2. The nucleon density distributions

used for  $^{12}\text{C}$ ,  $^{16}\text{O}$ ,  $^{40}\text{Ca}$ ,  $^{90}\text{Zr}$  and  $^{208}\text{Pb}$  are calculated by the QMC model [98]. For  $^4\text{He}$ , we use the parametrization for the density distribution obtained in Ref. [157]. The  $J/\Psi$  potentials from the  $D\bar{D}$ -loop are calculated using a local density approximation. Recall that also the in-medium mass of  $D$  meson, which is necessary in this case, is consistently calculated in the QMC model without changing any parameters. We stress that we limit the discussion to the situation that the quarkonium is produced nearly at rest in the interior of the nucleus (recoilless kinematics in experiments).

Since in free space the width of  $J/\Psi$  meson is  $\sim 93$  keV [15], we can ignore this tiny natural width in the following. When the  $J/\Psi$  meson is produced nearly at rest, its dissociation process via  $J/\Psi + N \rightarrow \Lambda_c^+ + \bar{D}$  is forbidden in the nucleus, as the threshold energy in free space is about 115 MeV above. This is because the same number of light quarks three, participates in the initial and final states and hence, the effects of the partial restoration of chiral symmetry which reduces mostly the amount of the light quark condensates, would affect a similar total mass reduction for the initial and final states [100, 107]. (See subsection 3.2, and Fig. 4.) Thus, the relative energy ( $\sim 115$  MeV) to the threshold would not be modified significantly.

We also note that once the  $J/\Psi$  meson is bound in the nucleus, the total energy of the system is below threshold for nucleon knock-out and the whole system is stable. The exception to this is the process  $J/\Psi + N \rightarrow \eta_c + N$ , which is exothermic. Reference [158] has provided an estimate of this cross section from which we deduce a width for the bound  $J/\Psi$  of order 0.8 MeV (nuclear matter density at  $\rho_B = \rho_0/2$ ). We therefore expect that the bound  $J/\Psi$ , while not being completely stable under the strong interaction, should be narrow enough to be clearly observed. It would be worthwhile to investigate this further. Then, provided that experiments can be performed to produce the  $J/\Psi$  meson in recoilless kinematics, the  $J/\Psi$  meson is expected to be captured by the nucleus into one of the bound states, which has no strong-interaction originated width.  $\eta_c$  has a total decay width which is larger than that of  $J/\Psi$ , but still relatively small,  $\sim 31.8$  MeV. Therefore, the situation of heavy quarkonia is completely different and advantageous compared to that of lighter quarkonium  $\phi$  and also  $\eta$  and  $\omega$ , to be discussed in sections 5 and 6.2, respectively. This justifies neglecting their widths in calculating the single-particle energy levels in a nucleus.

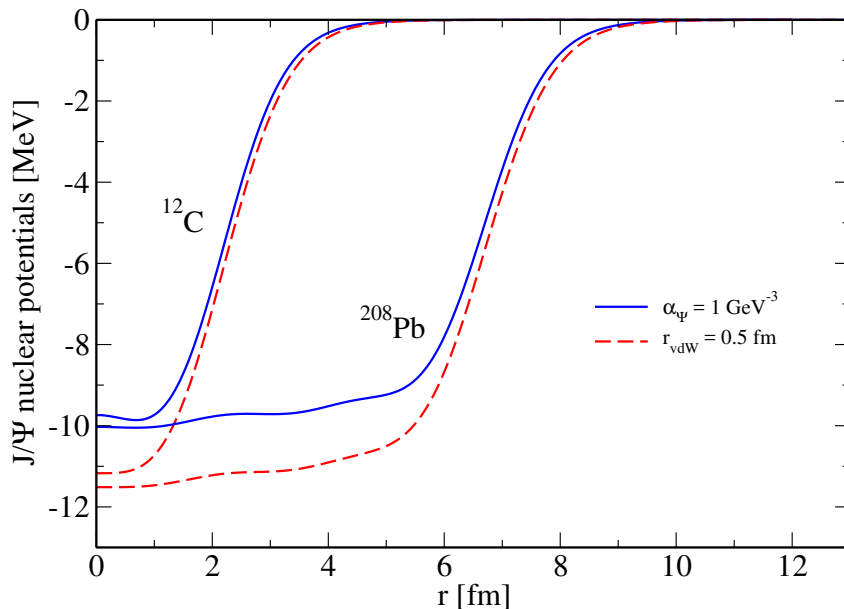


Figure 8:  $J/\Psi$  nuclear potentials  $W_{J/\Psi A}^{\text{pol}}(\vec{r})$  (solid line) for a polarizability  $\alpha_{J/\Psi} = 1 \text{ GeV}^{-3}$  and  $W_{J/\Psi A}^{\text{latt}}(\vec{r})$  (dashed line) from a fit to the lattice data with a cutoff  $r_{\text{vdW}} = 0.5$  fm.

Initially, we compare in Fig. 8 the potentials  $W_{\varphi A}^{\text{pol}}(\vec{r})$  and  $W_{\varphi A}^{\text{latt}}(\vec{r})$ , defined respectively by Eqs. (106)

and (112). We make the comparison for  $J/\Psi$  in the  $^{12}\text{C}$  and  $^{208}\text{Pb}$ . We recall that while  $W_{\varphi A}^{\text{pol}}(\vec{r})$  is proportional to the nuclear density  $\rho_A(\vec{r})$ ,  $W_{\varphi A}^{\text{latt}}(\vec{r})$  is a convolution of the density with the finite-range potential that gives the lattice spin-averaged value for the  $J/\Psi N$  interaction in free space. Not surprisingly, the shapes of both nuclear potentials are similar, essentially following the shape of the density.

Table 7: Predictions for  $J/\Psi$  single-particle energies in several nuclei obtained with the polarization potential  $W_{J/\Psi A}^{\text{pol}}(\vec{r})$ , defined in Eq. (105).

	$^4_{J/\Psi}\text{He}$	$^{12}_{J/\Psi}\text{C}$	$^{16}_{J/\Psi}\text{O}$	$^{40}_{J/\Psi}\text{Ca}$	$^{48}_{J/\Psi}\text{Ca}$	$^{90}_{J/\Psi}\text{Zr}$	$^{208}_{J/\Psi}\text{Pb}$
$\alpha_{J/\Psi} = 1 \text{ GeV}^{-3}$							
1s	n	-3.36	-4.41	-6.77	-6.84	-7.91	-8.38
1p	n	n	-0.39	-3.47	-3.95	-5.71	-7.05
2s	n	n	n	-0.26	-0.59	-2.70	-5.01
2p	n	n	n	n	n	-0.21	-2.94
3s	n	n	n	n	n	n	-0.70
$\alpha_{J/\Psi} = 2 \text{ GeV}^{-3}$							
1s	-4.49	-10.76	-12.62	-16.41	-16.16	-17.70	-17.27
1p	n	-3.98	-6.54	-11.95	-12.44	-14.95	-16.30
2s	n	n	-0.54	-6.74	-7.50	-11.07	-13.95
2p	n	n	n	-1.62	-2.52	-7.33	-11.41
3s	n	n	n	n	n	-2.71	-8.28

Table 7 contains the predictions for  $J/\Psi$  single-particle energies for several nuclei obtained by solving the Schrödinger equation, Eq. (96), with the polarization potential given in Eq. (106). The states are denoted by  $nl$ , where  $n = 1, 2, 3, \dots$  is the principal quantum number, and  $l = 0(\text{s}), 1(\text{p}), 2(\text{d}), \dots$ . When the single-particle energy is less than  $10^{-2}$  MeV, we consider there is no bound state and denote this with “n” in the tables. We present results for two typical values of the polarizability:  $\alpha_{J/\Psi} = 2 \text{ GeV}^{-3}$ , which is an estimate made in Refs. [68, 115], and  $\alpha_{J/\Psi} = 1 \text{ GeV}^{-3}$ , which is the upper value for  $\alpha_{\eta_b}$  obtained in Ref. [64] in the context of pNRQCD; they correspond respectively to scattering lengths  $a_{J/\Psi N} = -0.37 \text{ fm}$  and  $a_{J/\Psi N} = -0.19 \text{ fm}$ . The table reveals that while relatively deep  $J/\Psi$  bound states, with more than 10 MeV, can happen in all nuclei when  $\alpha_{J/\Psi} = 2 \text{ GeV}^{-3}$ , when  $\alpha_{J/\Psi} = 1 \text{ GeV}^{-3}$  they can happen only for the largest nucleus,  $^{208}\text{Pb}$ . We also mention that with a scattering length  $a_{J/\Psi N} = -0.05 \text{ fm}$ , the value extracted from  $J/\Psi p$  scattering [137], the binding of  $J/\Psi$  to nuclei is about 1 MeV for the largest nuclei, being close to 2 MeV in  $^{208}\text{Pb}$ .

Predictions for  $\eta_c$  and  $J/\Psi$  single-particle energies for several nuclei from the potential using lattice QCD input, given in Eq. (112), are presented in Tab. 8. We recall that the  $\eta_c N$  and  $J/\Psi N$  potentials fit the lattice scattering lengths and incorporate the Yuakwa tail from the fit from lattice data. Results for  $^4\text{He}$  are not displayed because there are no bound states and  $^{12}\text{C}$  are similar to those for  $^{12}\text{C}$  like in the previous case. One first conclusion can be drawn from the results displayed is that the nuclear potentials are rather weak. The finite range of the quarkonium-nucleon interaction clearly influences the nuclear potentials; although they give a larger quarkonium-nucleon scattering length than the contact-interaction with  $\alpha_{J/\Psi} = 1 \text{ GeV}^{-3}$  (i.e.  $a_{J/\Psi N} = -0.19 \text{ fm}$ ), the nuclear surface cuts off the tail of the finite-range potentials.

Next, we present results from calculations based on the in-medium  $J/\Psi$  self-energy calculated with meson Lagrangians. As mentioned previously, the  $J/\Psi$ -meson-nucleus effective potential is calculated

Table 8: Single-particle energies of  $\eta_c$  and  $J/\Psi$  in selected nuclei. The  $\eta_c N$  and  $J/\Psi N$  potentials fit the lattice scattering lengths and incorporate the Yuakwa tail from the fit from lattice data.

	$^{16}_{\eta_c}\text{O}$	$^{40}_{\eta_c}\text{Ca}$	$^{90}_{\eta_c}\text{Zr}$	$^{290}_{\eta_c}\text{Pb}$	$^{16}_{J/\Psi}\text{O}$	$^{40}_{J/\Psi}\text{Ca}$	$^{90}_{J/\Psi}\text{Zr}$	$^{290}_{J/\Psi}\text{Pb}$
$r_{\text{vdW}} = 0.3 \text{ fm}$								
1s	-2.92	-5.15	-6.32	-6.88	-3.62	-5.92	-7.10	-7.62
1p	n	-2.06	-4.17	-5.55	n	-2.74	-4.93	-6.29
2s	n	n	-1.40	-3.53	n	n	-2.06	-4.29
2p	n	n	n	-1.50	n	n	n	-2.30
$r_{\text{vdW}} = 0.5 \text{ fm}$								
1s	-3.62	-5.99	-7.23	-7.79	-5.23	-7.95	-9.24	-9.74
1p	n	-2.72	-4.99	-6.41	-0.87	-4.41	-6.90	-8.33
2s	n	n	-2.04	-4.33	n	-0.82	-3.71	-6.20
2p	n	n	n	-2.28	n	n	-0.92	-4.03

in a local density approximation using the  $J/\Psi$ -meson mass shift in nuclear matter, together with the nuclear density profile  $\rho_A(r)$  of a nucleus  $A$  calculated in the QMC model; specifically:

$$V_{J/\Psi A}(r) = m_{J/\Psi}^*(\rho_A(r)) - m_{J/\Psi} = \Delta m_{J/\Psi}(\rho_A(r)), \quad (126)$$

where  $r$  is the distance from the center of the nucleus  $A$ . We solve the Schrödinger equation, Eq. (96), with the nuclear potential given by Eq. (126). Also, we use the reduced mass of the system instead of  $m_{J/\Psi}$ , which is important for  $^4\text{He}$ .

In the situation of recoilless kinematics, it should be a very good approximation to neglect the possible energy difference between the longitudinal and transverse components [159] of the  $J/\Psi$  wave function ( $\phi_{\Psi}^{\mu}$ ) as was assumed for the  $\omega$  meson case [159]. After imposing the Lorentz condition,  $\partial_{\mu}\phi_{\Psi}^{\mu} = 0$ , to solve the Proca equation, aside from a possible width, becomes equivalent to solving the Klein-Gordon equation. We have solved the Schrödinger equation, and compared the results obtained with those obtained in solving the Klein-Gordon equation for some cases. We have confirmed that the two methods (without an imaginary part in the potential) yield nearly identical results within the accuracy of a few percent as we have tested also the lighter  $\phi$ -meson case.

The results in Tab. 9 show that the  $J/\Psi$  are expected to form  $J/\Psi$ -nuclear bound states for nearly all the nuclei considered, but some cases for  $^4\text{He}$ . This is insensitive to the values of cutoff mass values used in the form factor. It will be possible to search for the bound states in a  $^{208}\text{Pb}$  nucleus at JLab after the 12 GeV upgrade. In addition, one can expect quite rich spectra for medium and heavy mass nuclei. Of course, the main issue is to produce the  $J/\Psi$  meson with nearly stopped kinematics, or nearly zero momentum relative to the nucleus. Since the present results imply that many nuclei should form  $J/\Psi$ -nuclear bound states, it may be possible to find such kinematics by careful selection of the beam and target nuclei.

We have been able to set the strong interaction width of the  $J/\Psi$  to be zero (and neglect its tiny natural width of  $\sim 93$  keV in free space). Combined with the generally advocated color-octet gluon-based attraction, or QCD color van der Waals forces, one can expect that the  $J/\Psi$  meson will form nuclear bound states, and that the signal for the formation should be experimentally very clear, provided that the  $J/\Psi$  meson is produced in recoilless kinematics.

The  $J/\Psi$ - $D$  coupling constants are taken as determined from vector meson dominance, and the cutoff masses are varied over a large range of values. The QMC model predicts a 62 MeV downward



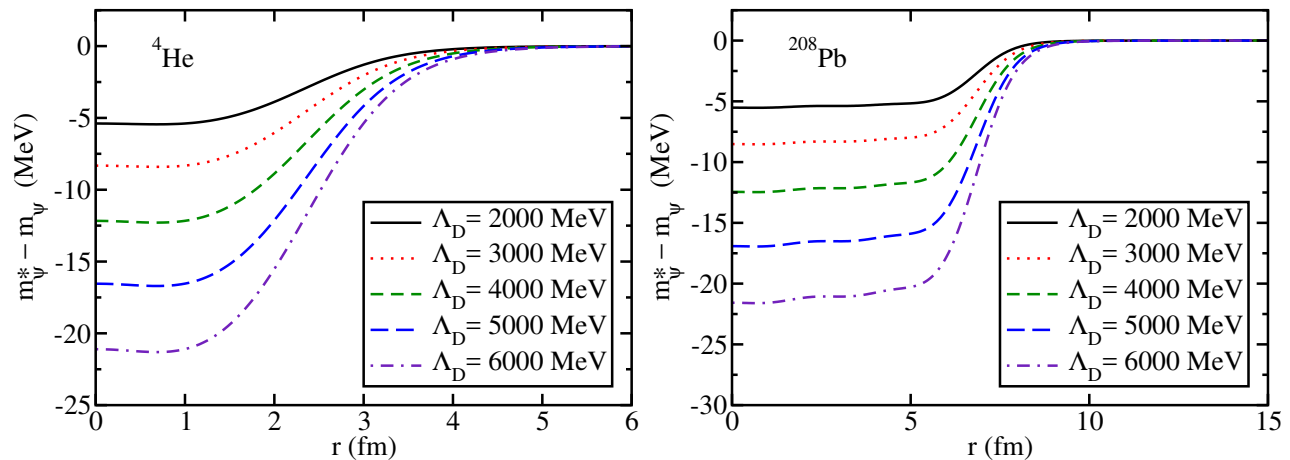


Figure 9: Potentials felt by  $J/\Psi$  in a  ${}^4\text{He}$  nucleus (left panel) and in a  ${}^{208}\text{Pb}$  nucleus (right panel) for five values of the cutoff mass in the form factors,  $\Lambda_D = 2000, 3000, 4000, 5000$  and  $6000$  MeV.

mass shift for the  $D$ -meson at normal nuclear matter density. The  $D$ -meson mass shift leads to a corresponding in-medium  $J/\Psi$  downward mass shift varying between  $-5$  MeV and  $-22$  MeV in  ${}^4\text{He}$  and  ${}^{208}\text{Pb}$  nuclei, for cutoff mass values in the range of  $2000$  MeV and  $6000$  MeV. Such a mass shift is large enough to bind a  $J/\Psi$  to a nucleus for a  $J/\Psi$  produced at low momentum in the rest frame of the nucleus.

We note that it is unclear whether the two mechanisms underlying both approaches we have discussed for heavy quarkonium binding are independent from each other and their predictions should be combined. This is because a quark-gluon-based interaction of a quarkonium with light hadrons can, in principle, be matched to a hadron-based interaction. This is nicely illustrated by the derivation of the van der Waals force in the quarkonium-quarkonium interaction with a chiral EFT derived from gWEFT that, in turn, is derived from pNRQCD, the latter being a quark-gluon based theory. In the same way, the matching of gWEFT to an EFT involving couplings of quarkonia to  $D$  mesons would lead to an approach in which the quarkonium interacts with the medium via virtual  $D\bar{D}$  loops. On the other hand, the interaction generated by the  $D\bar{D}$  loop is of shorter range (of the order of  $1/2M_D$ ) as compared with the range of a van der Waals force and, therefore, both mechanisms are expected to contribute. Such an EFT involving quarkonium and  $D$  mesons has not been derived from pNRQCD so far and, therefore, for now one has to resort to a phenomenological Lagrangian approach.

Although the present results point to the possible existence of  $\eta_c$  and  $J/\Psi$  nuclear bound states, some issues clearly require further investigation. Amongst the most important ones are the calculation of effective  $\eta_c$  and  $J/\Psi$  potentials with taking into account momentum dependence. In the context of the  $D\bar{D}$ -loop calculation, the width of the  $D$ -meson needs to be taken into account. Recent calculations [160] of in-medium  $D$  and  $D^*$  widths based on meson-exchange models have obtained somewhat contradictory results and further study is required. Still in this context, as emphasized in Refs. [161, 162, 163], the lack of experimental information on the free-space interaction of  $D$  mesons with nucleons is a major impediment for constraining models and the use of symmetry principles and exploration of the interplay between quark-gluon and baryon-meson degrees of freedom is essential in this respect. Another issue is the dissociation of  $\eta_c$  and  $J/\Psi$  in matter by collisions with nucleons and light mesons. This subject has been studied vigorously in the last years using different approaches, like meson exchange [164] and quark models [165], QCD sum rules [166], and the NJL model [167]. Finally, as already discussed in detail in subsection 4.1, we stress the need for a deeper understanding of the  $J/\Psi N$  interaction, including its long-range van der Waals behavior and its relation to the  $D\bar{D}$ -loop mechanism within the context of the strongly interacting many-nucleon system. The construction of an EFT for the quarkonium-nucleon

Table 9:  $J/\Psi$ –nucleus bound state energies taking into account the change in the self-energy in medium, calculated with the Schrödinger equation. All dimensioned quantities are given in MeV.

		Bound state energies				
		$\Lambda_D = 2000$	$\Lambda_D = 3000$	$\Lambda_D = 4000$	$\Lambda_D = 5000$	$\Lambda_D = 6000$
${}^4_{J/\Psi}\text{He}$	1s	n	n	-0.70	-2.70	-5.51
${}^{12}_{J/\Psi}\text{C}$	1s	-0.52	-1.98	-4.47	-7.67	-11.26
	1p	n	n	n	-1.38	-3.84
${}^{16}_{J/\Psi}\text{O}$	1s	-1.03	-2.87	-5.72	-9.24	-13.09
	1p	n	n	-0.94	-3.48	-6.60
${}^{40}_{J/\Psi}\text{Ca}$	1s	-2.78	-5.44	-9.14	-13.50	-18.12
	1p	-0.38	-2.32	-5.43	-9.32	-13.56
	1d	n	n	-1.52	-4.74	-8.49
	2s	n	n	-1.27	-4.09	-7.60
${}^{48}_{J/\Psi}\text{Ca}$	1s	-2.96	-5.62	-9.28	-13.55	-18.08
	1p	-0.73	-2.83	-6.03	-9.95	-14.18
	1d	n	n	-2.46	-5.87	-9.73
	2s	n	-0.07	-1.90	-5.00	-8.65
${}^{90}_{J/\Psi}\text{Zr}$	1s	-3.64	-6.40	-10.12	-14.41	-18.92
	1p	-1.93	-4.42	-7.92	-12.03	-16.40
	1d	-0.03	-2.13	-5.31	-9.18	-13.37
	2s	-0.02	-1.56	-4.51	-8.26	-12.37
	2p	n	n	-1.52	-4.71	-8.45
${}^{208}_{J/\Psi}\text{Pb}$	1s	-4.25	-7.08	-10.82	-15.11	-19.60
	1p	-3.16	-5.86	-9.52	-13.74	-18.18
	1d	-1.84	-4.38	-7.90	-12.01	-16.37
	2s	-1.41	-3.81	-7.25	-11.30	-15.61
	2p	-0.07	-1.95	-5.10	-8.97	-13.14

system wherein light quark degrees of freedom are incorporated via chiral EFTs, possibly trailing a path similar to that in the derivation of a color van der Waals force with pNRQCD and gWEFT, is a challenge that seems worth facing in the coming years.

## 5 Nuclear-bound $\phi$

Several experiments have focused on the light vector mesons  $\rho$ ,  $\omega$ , and  $\phi$ , since their mean-free paths can be comparable with the size of a nucleus after being produced inside the nucleus. However, a unified consensus has not yet been reached among the different experiments—see Refs. [168, 169, 42] for comprehensive reviews of the current status.

For the  $\phi$ -meson, although the precise values are different, a large in-medium broadening of the width has been reported by most of the experiments performed, while only a few of them find evidence for a substantial mass shift. For example, the KEK-E325 collaboration [170] reported a mass reduction of 3.4% and an in-medium decay width of  $\approx 14.5$  MeV at normal nuclear matter density. The latter disagrees with the SPring8 [171] result, which reported a large in-medium  $\phi N$  cross section leading to a decay width of 35 MeV. But this 35 MeV is in close agreement with the two JLab CLAS collaboration measurements reported in Refs. [172] and [173].

In an attempt to clarify the situation, the CLAS collaboration at JLab [174] performed new measurements of nuclear transparency ratios, and estimated in-medium widths in the range of 23-100 MeV. These values overlap with that of the SPring8 measurement [171]. More recently, the ANKE-COSY collaboration [175] has measured the  $\phi$ -meson production from proton-induced reactions on various nuclear targets. The comparison of data with model calculations suggests an in-medium  $\phi$  width of  $\approx 50$  MeV. This result is consistent with that of SPring8 [171], as well as the one deduced from CLAS at JLab [174]. However, the value is clearly larger than that of the KEK-E325 collaboration [170].

Thus, it is obvious that the search for evidence of a light vector meson mass shift is indeed complicated. It certainly requires further experimental efforts to understand better the changes of  $\phi$ -meson properties in a nuclear medium. For example, the J-PARC E16 collaboration [176] intends to perform a more systematic study for the mass shift of vector mesons with higher statistics. Furthermore, the E29 collaboration at J-PARC has recently put forward a proposal [177, 178] to study the in-medium mass modification of the  $\phi$ -meson via the possible formation of  $\phi$ -nucleus bound states [179], using the primary reaction  $\bar{p}p \rightarrow \phi\phi$ . Finally, there is a proposal at JLab, following the 12 GeV upgrade, to study the binding of  $\phi$  (and  $\eta$ ) to  ${}^4\text{He}$  [180].

On the theoretical side, various authors predict a downward shift of the in-medium  $\phi$ -meson mass and a broadening of the decay width. The possible decrease of the light vector meson masses in a nuclear medium was first predicted by Brown and Rho [181]. Thereafter, many theoretical investigations have been conducted, some of them focused on the self-energies of the  $\phi$ -meson due to the kaon-antikaon loop. Ko et al. [70] used a density-dependent kaon mass determined from chiral perturbation theory and found that at normal nuclear matter density,  $\rho_0$ , the  $\phi$ -meson mass decreases very little, by at most 2%, and the width  $\Gamma_\phi \approx 25$  MeV and broadens drastically for large densities. However, their estimate has an uncertainty of factor of two for the in-medium kaon (and antikaon) mass used. Hatsuda and Lee calculated the in-medium  $\phi$ -meson mass based on the QCD sum rule approach [182, 183], and predicted a decrease of 1.5%-3% at normal nuclear matter density. Other investigations also predict a large broadening of the  $\phi$ -meson width: Ref. [184] reports a negative mass shift of  $< 1\%$  and a decay width of 45 MeV at  $\rho_0$ ; Ref. [185] predicts a decay width of 22 MeV but does not report a result on the mass shift; and Ref. [186] gives a rather small negative mass shift of  $\approx 0.81\%$  and a decay width of 30 MeV. More recently, Ref. [187] reported a downward mass shift of  $< 2\%$  and a large broadening width of 45 MeV; and finally, in Ref. [188], extending the work of Refs. [185, 186], the authors reported a negative mass shift of 3.4% and a large decay width of 70 MeV at  $\rho_0$ . The reason for these differences may lie in the different approaches used to estimate the kaon-antikaon loop contributions for the  $\phi$ -meson self-energy.

In this section we discuss possible formation of  $\phi$ -nucleus bound states, the strange quarkonium-nuclear bound states of  $s\bar{s}$ -nucleus. The results presented here are from Refs. [76, 189]. The method to estimate the  $\phi$ -meson-nuclear potential is similar to that for  $J/\Psi$ -meson, except that the  $\phi$ -meson has finite widths both in vacuum and in medium, due to the large decay branches of more than 80 % to kaon-antikaon pairs.

## 5.1 $\phi$ self-energy

We use the effective Lagrangian of Refs. [70, 190] to compute the  $\phi$  self-energy; the interaction Lagrangian  $\mathcal{L}_{int}$  involves  $\phi K \bar{K}$  and  $\phi\phi K \bar{K}$  couplings dictated by a local gauge symmetry principle:

$$\mathcal{L}_{int} = \mathcal{L}_{\phi K \bar{K}} + \mathcal{L}_{\phi\phi K \bar{K}}, \quad (127)$$

where

$$\mathcal{L}_{\phi K \bar{K}} = ig_\phi \phi^\mu [\bar{K}(\partial_\mu K) - (\partial_\mu \bar{K})K], \quad (128)$$

and

$$\mathcal{L}_{\phi\phi K \bar{K}} = g_\phi^2 \phi^\mu \phi_\mu \bar{K} K. \quad (129)$$

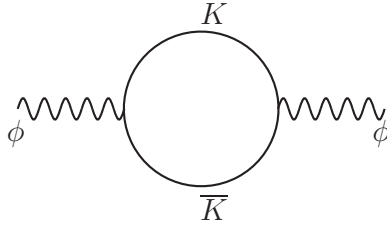


Figure 10:  $K\bar{K}$ -loop contribution to the  $\phi$ -meson self-energy.

We use the convention:

$$K = \begin{pmatrix} K^+ \\ K^0 \end{pmatrix}, \quad \bar{K} = (K^- \bar{K}^0). \quad (130)$$

We note that the use of the effective interaction Lagrangian of Eq. (127) without the term given in Eq. (129) may be considered as being motivated by the hidden gauge approach in which there are no four-point vertices, such as (129), that involves two pseudoscalar mesons and two vector mesons [146, 191]. This is in contrast to the approach of using the minimal substitution to introduce vector mesons as gauge particles where such four-point vertices do appear. However, these two methods have been shown to be consistent if both the vector and axial vector mesons are included [192, 193, 194, 195]. Therefore, we present results with and without such an interaction.

We first consider the contribution from the  $\phi K\bar{K}$  coupling given by Eq. (128) to the scalar part of the  $\phi$  self-energy,  $\Pi_\phi(p)$ ; Fig. 10 depicts this contribution. For a  $\phi$ -meson at rest, it is given by

$$i\Pi_\phi(p) = -\frac{8}{3}g_\phi^2 \int \frac{d^4q}{(2\pi)^4} \vec{q}^2 D_K(q) D_K(q-p), \quad (131)$$

where  $D_K(q) = (q^2 - m_K^2 + i\epsilon)^{-1}$  is the kaon propagator;  $p = (p^0 = m_\phi, \vec{0})$  is the  $\phi$ -meson four-momentum vector, with  $m_\phi$  the  $\phi$ -meson mass;  $m_K (= m_{\bar{K}})$  is the kaon mass. When  $m_\phi < 2m_K$  the self-energy  $\Pi_\phi(p)$  is real. However, when  $m_\phi > 2m_K$ , which is the case here,  $\Pi_\phi(p)$  acquires an imaginary part. The mass of the  $\phi$  is determined from the real part of  $\Pi_\phi(p)$ ,

$$m_\phi^2 = (m_\phi^0)^2 + \text{Re } \Pi_\phi(m_\phi^2), \quad (132)$$

with  $m_\phi^0$  being the bare mass of the  $\phi$  and

$$\text{Re } \Pi_\phi = -\frac{2}{3}g_\phi^2 \mathcal{P} \int \frac{d^3q}{(2\pi)^3} \vec{q}^2 \frac{1}{E_K(E_K^2 - m_\phi^2/4)}. \quad (133)$$

Here  $\mathcal{P}$  denotes the Principal Value part of the integral Eq. (131) and  $E_K = (\vec{q}^2 + m_K^2)^{1/2}$ . The decay width of  $\phi$  to a  $K\bar{K}$  pair is given in terms of the imaginary part of  $\Pi_\phi(p)$ ,

$$\text{Im } \Pi_\phi = -\frac{g_\phi^2}{24\pi} m_\phi^2 \left(1 - \frac{4m_K^2}{m_\phi^2}\right)^{3/2}, \quad (134)$$

as

$$\Gamma_\phi = -\frac{1}{m_\phi} \text{Im } \Pi_\phi = \frac{g_\phi^2}{24\pi} m_\phi \left(1 - \frac{4m_K^2}{m_\phi^2}\right)^{3/2}. \quad (135)$$

The integral in Eq. (133) is divergent and needs regularization; we use a phenomenological form factor, with a cutoff parameter  $\Lambda_K$ , as in Ref. [72]. The coupling constant  $g_\phi$  is determined by the experimental width of the  $\phi$  in vacuum [15]. For the  $\phi$  mass,  $m_\phi$ , we use its experimental value:

$m_\phi^{\text{expt}} = 1019.461$  MeV [15]. For the kaon mass  $m_K$ , there is a small ambiguity since  $m_{K^+} \neq m_{K^0}$ , as a result of charge symmetry breaking and electromagnetic interactions. The experimental values for the  $K^+$  and  $K^0$  meson masses in vacuum are  $m_{K^+}^{\text{expt}} = 493.677$  MeV and  $m_{K^0}^{\text{expt}} = 497.611$  MeV, respectively [15]. For definiteness we use the average of  $m_{K^+}^{\text{expt}}$  and  $m_{K^0}^{\text{expt}}$  as the value of  $m_K$  in vacuum. The effect of this tiny mass ambiguity on the in-medium kaon (antikaon) properties is negligible. Then, we get the coupling  $g_\phi = 4.539$ , and can fix the bare mass  $m_\phi^0$ .

## 5.2 $\phi$ nuclear bound states

The in-medium  $\phi$  mass is calculated by solving Eq. (132) by replacing  $m_K$  by  $m_K^*$  and  $m_\phi$  by  $m_\phi^*$ , and the width is obtained by using the solutions in Eq. (135). In-medium kaon mass  $m_K^*$  is calculated in the QMC model [104] explained in Sec. 3. We regularize the associated loop integral with a dipole form factor using a cutoff mass parameter  $\Lambda_K$ . In principle, this parameter may be determined phenomenologically using, for example, a quark model—see Ref. [72] for more details. However, for simplicity we keep it free and vary its value over a wide interval, namely 1000-4000 MeV.

Table 10:  $\phi$  mass and width at normal nuclear matter density,  $\rho_0$ . All quantities are given in MeV.

	$\Lambda_K = 1000$	$\Lambda_K = 2000$	$\Lambda_K = 3000$	$\Lambda_K = 4000$
$m_\phi^*$	1009.3	1000.9	994.9	990.5
$\Gamma_\phi^*$	37.7	34.8	32.8	31.3

In Tab. 10, we present the values for  $m_\phi^*$  and  $\Gamma_\phi^*$  at normal nuclear matter density  $\rho_0$ . A negative kaon mass shift of 13% induces only maximum of  $\approx 3\%$  downward mass shift of the  $\phi$ . On the other hand,  $\Gamma_\phi^*$  is very sensitive to the change in the kaon mass; at  $\rho_B = \rho_0$ , the broadening of the  $\phi$  becomes an order of magnitude larger than its vacuum value and it increases rapidly with increasing nuclear density, up to a factor of  $\sim 20$  enhancement for the largest nuclear matter density treated,  $\rho_B = 3\rho_0$ .

We present the in medium mass shift of the  $\phi$  and its width without the gauge term, ( $\xi = 0$ ) in the upper panel in Fig. 11. The effect of the in-medium kaon mass change gives a negative shift of the  $\phi$ -meson mass. However, even for the largest value of density treated, namely  $3\rho_0$ , the downward mass shift is only a few percent for all values of the cutoff parameter  $\Lambda_K$ .

To conclude and for completeness, we show the impact the  $\phi\phi K\bar{K}$  interaction of Eq. (129) on the in-medium  $\phi$  mass and width. The lower panels in Fig. 11 present the results. We have used the notation that  $\xi = 1(0)$  means that this interaction is (not) included in the calculation of the  $\phi$  self-energy. One still gets a downward shift of the in-medium  $\phi$  mass when  $\xi = 1$ , although the absolute value is slightly different from  $\xi = 0$ . The in-medium width is not very sensitive to this interaction.

Next, we present our predictions for the single-particle energies and half widths for  $\phi$ -nucleus bound states for seven nuclei selected. We solve the Klein-Gordon equation for complex  $\phi$ -nucleus potentials obtained by a local-density approximation using the nucleon density distributions calculated by the QMC model. This leads to use the following complex  $\phi$ -nucleus (A) potential,

$$V_{\phi A}(r) = \Delta m_\phi^*(\rho_B(r)) - (i/2)\Gamma_\phi^*(\rho_B(r)), \quad (136)$$

$$\equiv U_\phi(r) - \frac{i}{2}W_\phi(r), \quad (137)$$

where  $U_\phi(r) \equiv \Delta m_\phi^*(\rho_B(r)) \equiv m_\phi^*(\rho_B(r)) - m_\phi$ ,  $r$  is the distance from the center of the nucleus and  $\rho_B(r)$  is the baryon density profile of the given nucleus calculated by the QMC model. As examples, we show in Fig. 12 the  $\phi$ -nuclear potentials  $U_\phi(r)$  and width  $W_\phi(r)$  in  ${}^4\text{He}$  and  ${}^{208}\text{Pb}$  nuclei, for three values of the cutoff parameter values of  $\Lambda_K$ .

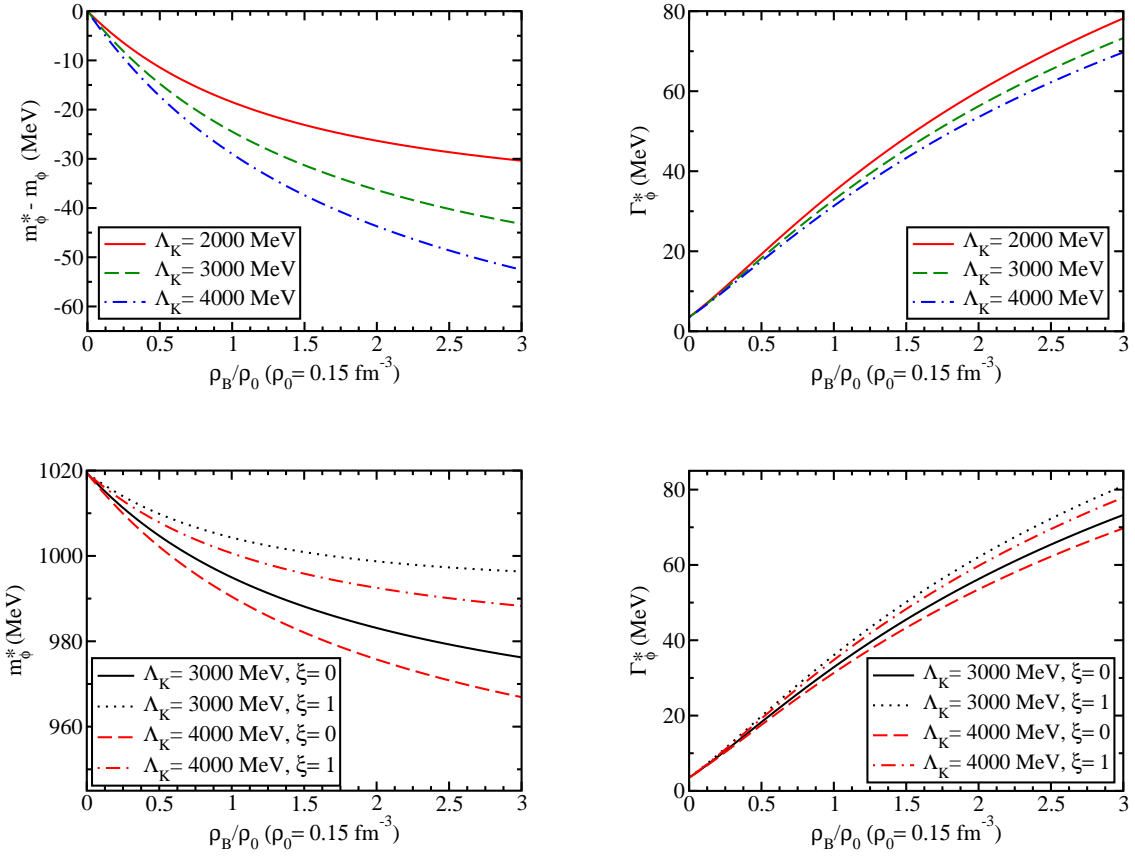


Figure 11: In-medium  $\phi$  mass shift (upper left panel) and width (upper right panel) without the gauge term,  $\xi = 0$ , and the comparison of these with the gauge term ( $\xi = 1$ ) (lower panels) for different values of the cutoff parameter  $\Lambda_K$ . Figures are taken from Refs. [76, 189].

Using the  $\phi$ -meson potentials obtained in this manner, we calculate the  $\phi$ -meson–nuclear bound state energies and absorption widths for the seven nuclei selected. Before proceeding, a few comments on the use of Eq. (138) (below) are in order. In this study we consider the situation where the  $\phi$ -meson is produced nearly at rest; therefore, the same remarks made in the previous section on neglecting a possible energy difference between the longitudinal and transverse components of the  $J/\Psi$  apply to the present case of the  $\phi$ . We solve the Klein-Gordon equation ( $\phi$ -meson wave function is represented by  $\phi(\vec{r})$  here),

$$\left(-\nabla^2 + \mu^2 + 2\mu V(\vec{r})\right) \phi(\vec{r}) = \mathcal{E}^2 \phi(\vec{r}), \quad (138)$$

where  $\mu = m_\phi m_A / (m_\phi + m_A)$  is the reduced mass of the  $\phi$ -meson-nucleus system with  $m_\phi$  ( $m_A$ ) the mass of the  $\phi$ -meson (nucleus  $A$ ) in vacuum, and  $V(\vec{r})$  is the complex  $\phi$ -meson-nucleus potential of Eq. (137). This equation is solved by using the momentum space methods developed in Ref. [196]. Here, Eq. (138) is first converted to momentum space representation via a Fourier transform, followed by a partial wave-decomposition of the Fourier-transformed potential. Then, for a given value of angular momentum, the eigenvalues of the resulting equation are found by the inverse iteration eigenvalue algorithm. The calculated bound state energies ( $E$ ) and widths ( $\Gamma$ ), which are related to the complex energy eigenvalue  $\mathcal{E}$  by  $E = \text{Re } \mathcal{E} - \mu$  and  $\Gamma = -2 \text{Im } \mathcal{E}$ , are listed in Tab. 11 for three values of the cutoff parameter  $\Lambda_K$ , with and without the imaginary part of the potential,  $W_{\phi A}(r)$ .

Table 11 shows the results for the real and imaginary parts of the single-particle energies  $\mathcal{E} = E - (i/2)\Gamma$  in seven nuclei selected. We present results with and without the imaginary (absorptive)

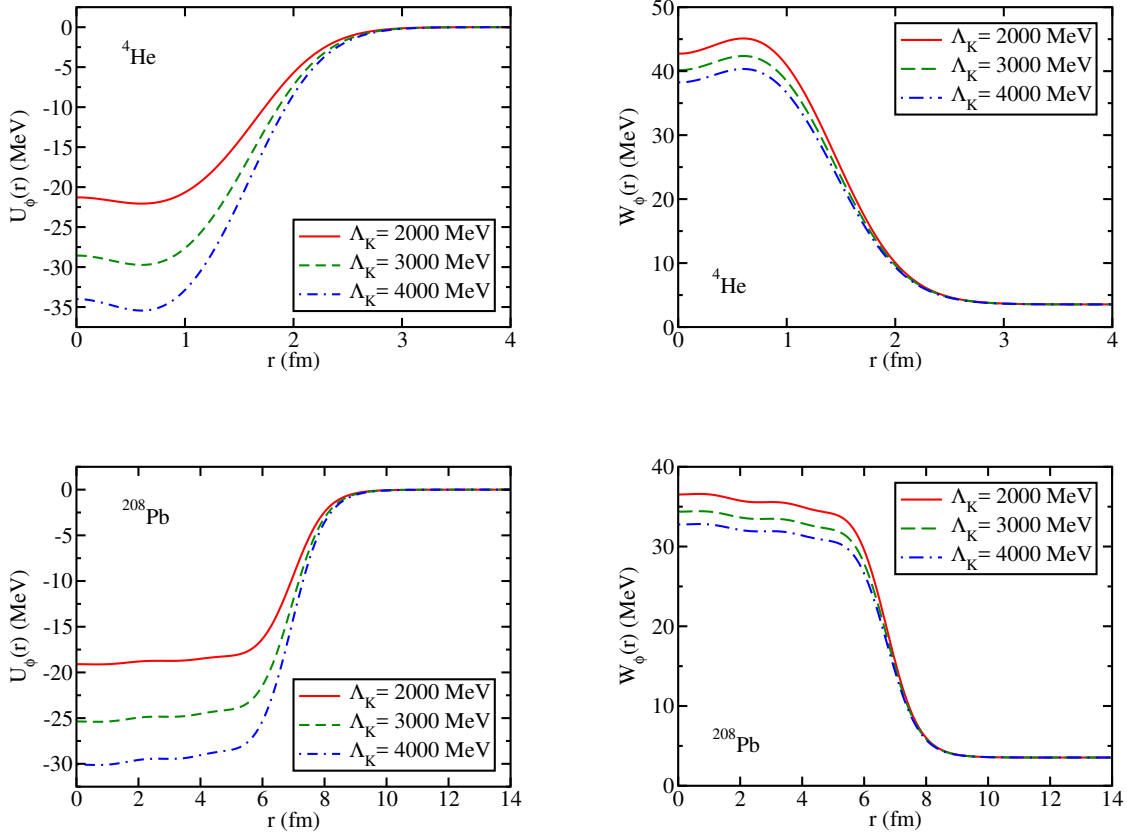


Figure 12: Potential (left panel) and width (right panel) for  $\phi$ -meson in  ${}^4\text{He}$  (upper panel), and for  ${}^{208}\text{Pb}$  (lower panel), respectively for three values of the cutoff parameter  $\Lambda_K$ , from Ref. [189].

part of the  $\phi$ -nucleus potential  $V_{\phi A}(r)$ . One sees that  $\phi$  is not bound to  ${}^4\text{He}$  when the imaginary part of the potential is included. For larger nuclei, the  $\phi$  does bind but while the binding is substantial the energy levels are quite broad; the half widths being roughly the same size as the central values of the real parts.

We first discuss the case in which the imaginary part of the  $\phi$ -nucleus potential  $W_\phi(r)$  is set to zero. The results are listed in the brackets in Tab. 11. From the values shown in brackets, we see that the  $\phi$ -meson is expected to form bound states with all the seven nuclei selected, for all values of the cutoff parameter  $\Lambda_K = 2000, 3000$  and  $4000$  MeV. (For the variation in the potential depths due to the  $\Lambda_K$  values, see Fig. 12.) However, the bound state energy is obviously dependent on  $\Lambda_K$ , as expected.

Next, we discuss the results obtained with the full potential, including the imaginary part  $W_\phi(r)$ . Adding the absorptive part of the potential, the situation changes appreciably. From the results presented in Tab. 11 we note that, for the largest value of the cutoff parameter  $\Lambda_K = 4000$  MeV which yields the deepest attractive potentials, the  $\phi$ -meson is expected to form bound states in all the seven nuclei selected, including the lightest  ${}^4\text{He}$  nucleus. However, whether or not the bound states can be observed experimentally, is sensitive to the value of the cutoff parameter  $\Lambda_K$ . One can also observe that the width of the bound state is insensitive to the values of  $\Lambda_K$  for all nuclei. Furthermore, since the imaginary part induces a repulsive potential, the bound states disappear completely in some cases, even though the bound states are found when the absorptive part is set to zero. This feature is obvious for the  ${}^4\text{He}$  nucleus. Thus, it would be very interesting for the future experiments planned at J-PARC and JLab, using light and medium-heavy nuclei [179, 180, 197, 198].

Here we comment that we have also solved the Schrödinger equation with the potential Eq. (137)

Table 11:  $\phi$ -nucleus single-particle energy  $E$  and half width  $\Gamma/2$  obtained, with and without the imaginary part of the potential  $W_\phi(r)$ , for three values of the cutoff parameter  $\Lambda_K$ . When only the real part is included, where the corresponding single-particle energy  $E$  is given inside the brackets,  $\Gamma = 0$  for all nuclei. “n” denotes that no bound state is found. All quantities are given in MeV.

		$\Lambda_K = 2000$		$\Lambda_K = 3000$		$\Lambda_K = 4000$	
		$E$	$\Gamma/2$	$E$	$\Gamma/2$	$E$	$\Gamma/2$
${}^4_\phi\text{He}$	1s	n (-0.8)	n	n (-1.4)	n	-1.0 (-3.2)	8.3
${}^{12}_\phi\text{C}$	1s	-2.1 (-4.2)	10.6	-6.4 (-7.7)	11.1	-9.8 (-10.7)	11.2
${}^{16}_\phi\text{O}$	1s	-4.0 (-5.9)	12.3	-8.9 (-10.0)	12.5	-12.6 (-13.4)	12.4
	1p	n (n)	n	n (n)	n	n (-1.5)	n
${}^{40}_\phi\text{Ca}$	1s	-9.7 (-11.1)	16.5	-15.9 (-16.7)	16.2	-20.5 (-21.2)	15.8
	1p	-1.0 (-3.5)	12.9	-6.3 (-7.8)	13.3	-10.4 (-11.4)	13.3
	1d	n (n)	n	n (n)	n	n (-1.4)	n
${}^{48}_\phi\text{Ca}$	1s	-10.5 (-11.6)	16.5	-16.5 (-17.2)	16.0	-21.1 (-21.6)	15.6
	1p	-2.5 (-4.6)	13.6	-7.9 (-9.2)	13.7	-12.0 (-12.9)	13.6
	1d	n (n)	n	n (-0.8)	n	-2.1 (-3.6)	11.1
${}^{90}_\phi\text{Zr}$	1s	-12.9 (-13.6)	17.1	-19.0 (-19.5)	16.4	-23.6 (-24.0)	15.8
	1p	-7.1 (-8.4)	15.5	-12.8 (-13.6)	15.2	-17.2 (-17.8)	14.8
	1d	-0.2 (-2.5)	13.4	-5.6 (-6.9)	13.5	-9.7 (-10.6)	13.4
	2s	n (-1.4)	n	-3.4 (-5.1)	12.6	-7.4 (-8.5)	12.7
	2p	n (n)	n	n (n)	n	n (-1.1)	n
${}^{208}_\phi\text{Pb}$	1s	-15.0 (-15.5)	17.4	-21.1 (-21.4)	16.6	-25.8 (-26.0)	16.0
	1p	-11.4 (-12.1)	16.7	-17.4 (-17.8)	16.0	-21.9 (-22.2)	15.5
	1d	-6.9 (-8.1)	15.7	-12.7 (-13.4)	15.2	-17.1 (-17.6)	14.8
	2s	-5.2 (-6.6)	15.1	-10.9 (-11.7)	14.8	-15.2 (-15.8)	14.5
	2p	n (-1.9)	n	-4.8 (-6.1)	13.5	-8.9 (-9.8)	13.4
	2d	n (n)	n	n (-0.7)	n	-2.2 (-3.7)	11.9

with and without the imaginary part, and obtained the single-particle energies and widths, and compared with those given in Tab. 11. The results found for both, with and without the imaginary part, are essentially the same.

To summarize, essential to the calculation of the  $\phi$ -nucleus bound states is the in-medium kaon mass which is calculated in the QMC model, where the scalar and vector meson mean fields couple directly to the light  $u$  and  $d$  quarks (antiquarks) in the  $K$  ( $\bar{K}$ ) meson.

At normal nuclear matter density, allowing for a very large variation of the cutoff parameter  $\Lambda_K$ , although one finds a sizable negative mass shift of 13% in the kaon mass, this induces only a few percent downward shift of the  $\phi$ -meson mass. On the other hand, it induces an order-of-magnitude broadening of the decay width.

Given the nuclear matter results, a local density approximation was used to infer the position dependent  $\phi$ -nucleus (A) complex scalar potential,  $V_{\phi A}(\rho_B(r)) = U_\phi(r) - (i/2)W_\phi(r)$ , in a finite nucleus. This allowed us to study the binding and absorption of a number of  $\phi$ -nuclear systems, given the nuclear density profiles,  $\rho_B(r)$ , calculated using the QMC model.

The Klein-Gordon equation has been solved to obtain the bound state single-particle energies for seven nuclei selected. While the results found in here show that one should expect the  $\phi$ -meson to bound in all but the lightest nuclei, the broadening of these energy levels, which is comparable to the amount of binding, suggests that it may be challenging to observe such states experimentally.



## 6 Nuclear-bound of $\omega$ , $\eta$ and $\eta'$ mesons

As mentioned already, to study the medium modification of the light vector ( $\rho$ ,  $\omega$  and  $\phi$ ) meson masses is very interesting since it can provide us with information on partial restoration of chiral symmetry in a nuclear medium. Such experiments carried out by the CERES and HELIOS collaborations at the CERN/SPS [199], and those at JLab [200, 201] and GSI [202, 203], are closely related to this issue. An alternative approach to study meson mass shifts in nuclei was suggested by Hayano *et al.* [204] to produce  $\eta$  and  $\omega$  mesons with nearly zero recoil, which inspired the theoretical investigations of  $\eta$ - and  $\omega$ -mesic nuclei [205, 206]. We review here the results for  $\omega$ -,  $\eta$ - and  $\eta'$ -mesic nuclei, those studied using the quark-meson coupling (QMC) model [107, 206].

In this section we discuss the nuclear binding of the  $\omega$ ,  $\eta$  and  $\eta'$  mesons. These mesons contain the *hidden light-quark* ( $q\bar{q}$ ) components, while the  $D$  and  $\bar{D}$  mesons, which will be discussed in next section, are respectively represented by  $c\bar{q}$  and  $\bar{c}q$  mesons. Since the interactions of the mesons with the nuclear medium, or nuclear many-body systems are mainly mediated by the scalar-isoscalar  $\sigma$  and vector-isoscalar  $\omega$  mean fields which directly couple to the light quarks in the QMC model, the treatment for these mesons is different from that for the hidden strange meson  $\phi$ , and hidden charm meson  $J/\Psi$ . Thus, at first order, they directly interact with the surrounding nuclear environment, not necessary through the higher order process such as appeared in the self-energy diagrams for  $\phi$  and  $J/\Psi$ .

### 6.1 In-medium masses of $\omega$ , $\eta$ and $\eta'$ mesons

First, we discuss the  $\omega$ ,  $\eta$ , and  $\eta'$  meson masses in symmetric nuclear matter, since the treatments need some more explanations in addition to those given in subsection 3.2. They are calculated in Ref. [206] (see also Eq. (88)):

$$m_{\eta,\omega}^*(\vec{r}) = \frac{2[a_{P,V}^2\Omega_q^*(\vec{r}) + b_{P,V}^2\Omega_s(\vec{r})] - z_{\eta,\omega}}{R_{\eta,\omega}^*} + \frac{4}{3}\pi R_{\eta,\omega}^{*3}B, \quad (\text{for } \eta', a_P \leftrightarrow b_P), \quad (139)$$

$$\left. \frac{\partial m_j^*(\vec{r})}{\partial R_j} \right|_{R_j=R_j^*} = 0, \quad (j = \omega, \eta, \eta'), \quad (140)$$

$$a_{P,V} \equiv \sqrt{1/3} \cos \theta_{P,V} - \sqrt{2/3} \sin \theta_{P,V}, \quad b_{P,V} \equiv \sqrt{2/3} \cos \theta_{P,V} + \sqrt{1/3} \sin \theta_{P,V}, \quad (141)$$

where  $\theta_{P,V}$  are the octet and singlet mixing angles for the pseudoscalar and vector mesons, respectively.

In Fig. 13 we show the calculated in-medium to vacuum mass ratios of the mesons in symmetric nuclear matter [107, 206]. The masses for the physical  $\omega$ ,  $\eta$  and  $\eta'$  are calculated using the corresponding octet ( $\eta_8$ ) and singlet ( $\eta_1$ ) mixing angles,  $\theta_P = -10^\circ$  for ( $\eta, \eta'$ ), and  $\theta_V = 39^\circ$  for ( $\phi, \omega$ ) [15]. Note that for the  $\omega$  and  $\phi$  mesons, they are known to be nearly *ideal-mixing*, so the mixing effect for their in-medium masses are expected to be negligible, and in fact they have been treated as  $q\bar{q}$  and  $s\bar{s}$  mesons, respectively. The masses for the octet and singlet states without the mixing effect for calculating the  $\eta$  and  $\eta'$  system are also shown (the dotted lines indicated by  $\eta_8$  and  $\eta_1$ ).

### 6.2 $\omega$ -, $\eta$ - and $\eta'$ -nuclear bound states

To calculate the bound state energies for the mesons with the situation of almost zero momenta, we solve the Klein-Gordon equation [105, 107, 206]:

$$[\nabla^2 + (E_j^* - V_v^j(r))^2 - \tilde{m}_j^{*2}(r)] \phi_j(\vec{r}) = 0, \quad (j = \omega, \eta, \eta', D, \bar{D}), \quad (142)$$

$$\tilde{m}_j^*(r) \equiv m_j^*(r) - \frac{i}{2} [(m_j - m_j^*(r))\gamma_j + \Gamma_j^0] \equiv m_j^*(r) - \frac{i}{2}\Gamma_j^*(r), \quad (143)$$

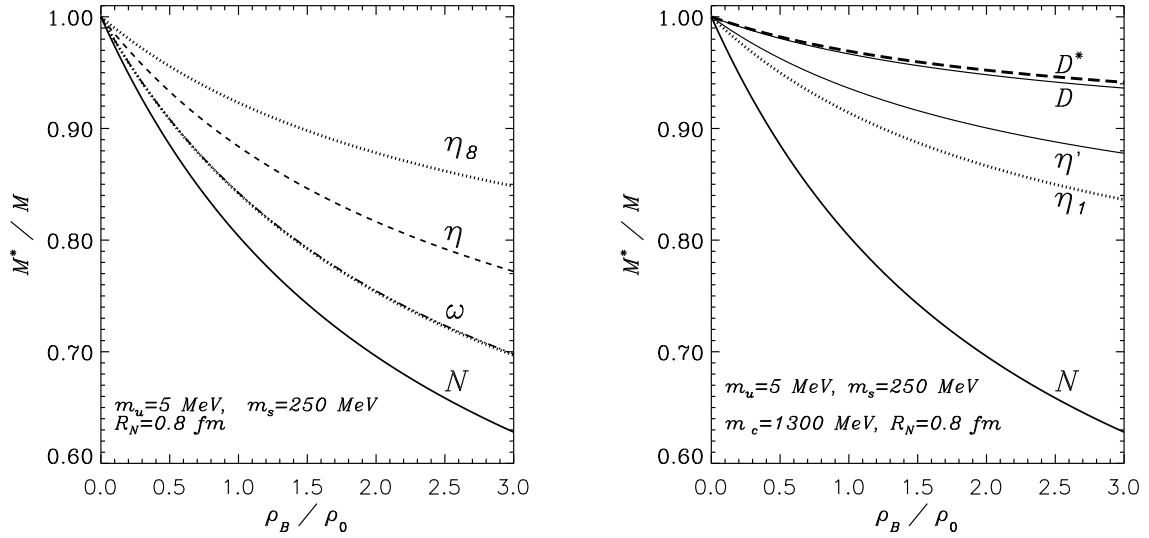


Figure 13: Effective mass ratios in medium to those in vacuum in symmetric nuclear matter ( $\rho_0 = 0.15 \text{ fm}^{-3}$ ).  $\eta_8$  and  $\eta_1$  are respectively the octet and singlet states without the effect of the mixing angle  $\theta_P$ .

where  $E_j^*$  is the total energy of the meson,  $V_v^j(r)$ ,  $m_j$  and  $\Gamma_j^0$  are respectively the sum of the vector and Coulomb potentials, the corresponding masses and widths in free space, and  $\gamma_j$  are treated as phenomenological parameters to describe the in-medium meson widths,  $\Gamma_j^*(r)$  [206]. Note that, for the  $\eta'$ -meson, any effects of in-medium width has been ignored. Thus, for the  $\eta'$ -meson, the results may have larger uncertainties due to the lack of including the possible widths in nucleus. We discuss this issue below based on recent experimental developments.

We show the nuclear bound state energies calculated for  $\eta$ ,  $\omega$  and  $\eta'$  mesons respectively for  $\gamma_\eta = 0.5$ ,  $\gamma_\omega = 0.2$  and  $\gamma_{\eta'} = 0$ . This order seems to be experimentally promising. For the  $\eta$  and  $\omega$  cases, they are expected to correspond best with experiment according to the estimates in Refs. [204, 207], although for  $\eta'$ , no clue existed when it was studied [105]. The bound state single-particle energies obtained are listed in Tab. 12.

We first discuss the  $\eta$ -nuclear bound states. Studies of the  $\eta$ -nuclear bound states have a relatively long history following the studies in Refs. [208, 209]. Later in Ref. [205] experimental feasibility of observing the  $\eta$ -nuclear bound states was studied. The results for the  $\eta$  in Tab. 12 show that the  $\eta$ -meson will be bound in all nuclei considered. However, the half widths ( $\Gamma_\eta/2$ ) obtained are relatively large compared to the corresponding binding energies. A similar conclusion was also derived in Ref. [205]. They argued that, despite the relatively large widths of the bound states, it would be feasible to experimentally observe the  $\eta$  mesic nuclei in the excitation energy spectrum.  $\eta$  bound states in nuclei was also studied focusing on the  $\eta$ - $\eta'$  mixing and flavor-singlet dynamics in Refs. [47, 48].

As for the  $\omega$ -nuclear bound states, the results in Tab. 12 indicate that one may expect deeper bound state energies and smaller widths than those for the  $\eta$ . A similar trend was also found in the study made based on QHD [210]. However, as already discussed in section 5, the present situation for the vector meson properties in nuclear medium, is still controversial [168, 169, 42].

As already mentioned, we have shown the result for the  $\eta'$ -nuclear bound state energies calculated for some nuclei, by setting the possible width to be zero. (Based on the QCD symmetry, the  $\eta'$  (and  $\eta$ ) mesic nuclei was further studied in Ref. [46].) However, a recent experimental study of the  $\eta'$ -nucleus optical potential by the photoproduction of  $\eta'$  (and  $\omega$ ) off carbon and niobium nuclei [211], found the imaginary part of the  $\eta'$ -nuclear potential to be about three times smaller than the real part. Thus, one can extract the main features of the  $\eta'$ -nuclear bound states from the results shown in Tab. 12, the results obtained by setting the width to be zero.

Table 12:  $\eta$ ,  $\omega$  and  $\eta'$  bound state single-particle energies (in MeV),  $E_j = \text{Re}(E_j^* - m_j)$  ( $j = \eta, \omega, \eta'$ ), where all widths for the  $\eta'$  are set to zero. The eigenenergies are given by,  $E_j^* = E_j + m_j - i\Gamma_j/2$ .

		$\gamma_\eta = 0.5$		$\gamma_\omega = 0.2$		$\gamma_{\eta'} = 0$
		$E_\eta$	$\Gamma_\eta$	$E_\omega$	$\Gamma_\omega$	$E_{\eta'}$
${}^6_j\text{He}$	1s	-10.7	14.5	-55.6	24.7	* (not calculated)
${}^{11}_j\text{B}$	1s	-24.5	22.8	-80.8	28.8	*
${}^{26}_j\text{Mg}$	1s	-38.8	28.5	-99.7	31.1	*
	1p	-17.8	23.1	-78.5	29.4	*
	2s	—	—	-42.8	24.8	*
${}^{16}_j\text{O}$	1s	-32.6	26.7	-93.4	30.6	-41.3
	1p	-7.72	18.3	-64.7	27.8	-22.8
${}^{40}_j\text{Ca}$	1s	-46.0	31.7	-111	33.1	-51.8
	1p	-26.8	26.8	-90.8	31.0	-38.5
	2s	-4.61	17.7	-65.5	28.9	-21.9
${}^{90}_j\text{Zr}$	1s	-52.9	33.2	-117	33.4	-56.0
	1p	-40.0	30.5	-105	32.3	-47.7
	2s	-21.7	26.1	-86.4	30.7	-35.4
${}^{208}_j\text{Pb}$	1s	-56.3	33.2	-118	33.1	-57.5
	1p	-48.3	31.8	-111	32.5	-52.6
	2s	-35.9	29.6	-100	31.7	-44.9

Theoretically, the  $\eta'$ -nucleus bound states were studied in Refs. [105, 212, 213, 214], where some of them focused on the reactions involving a  ${}^{12}\text{C}$  nucleus. However, recent measurement of excitation spectra in the  ${}^{12}\text{C}(p, d)$  reaction near the  $\eta'$  emission threshold, observed no distinct structure associated with the formation of  $\eta'$ -nucleus bound states [215, 216]. Thus, we need to wait for further experimental efforts, ideally in low recoil momentum conditions, to draw a definite conclusion, possibly using heavier nuclear targets.

## 7 Nuclear-bound heavy-flavor hadrons

Very little is presently known about the strength of the interaction of charmed hadrons with ordinary baryons and mesons. For the feasibility of experimental studies of formation of nuclear bound states, the production rate for charmed hadrons is a key factor. For the specific case of experiments of antiproton annihilation on the nucleon and nuclei, as those planned to be conducted by the  $\overline{\text{PANDA}}$  collaboration [217] at the FAIR facility, several predictions have been made in recent years. These include predictions for charmed mesons and baryons in free space [218, 219, 220, 221, 222, 223, 224, 226, 225, 227, 228, 229, 230, 231] and  $D\overline{D}$  production in nuclei [232] and formation of  $\Lambda_c^+$ -hypernuclei [233]. Systematic studies were made on the property changes of heavy hadrons which contain a charm or a bottom quark in nuclear matter [100] (see subsection 3.2), and on  $\Lambda_c^+$ - and  $\Lambda_b$ -hypernuclei [101]. Furthermore, production of  $D\overline{D}$  meson pair in nucleus [232], These results suggest that it is quite likely to form the charmed and bottom hypernuclei, which were predicted first in mid 70's [234, 235]. The experimental possibilities were also studied later [236]. For the strange hypernuclei including recent development, see Refs. [99, 237, 238, 239]. In addition, the  $B^-$ -nuclear (atomic) bound states were also predicted, based on the analogy with the kaonic atoms [240], and a study made for the  $D^-$ - and  $\overline{D}$ -nuclear bound states [107] (subsection 7.1) using the QMC model [92, 93, 94, 98] (section 3).

The issue of charmed mesic nuclei [107] is in some ways even more exciting, in that it promises more specific information on the relativistic mean fields in nuclei and the nature of dynamical chiral symmetry breaking. We focus on systems containing an anti-charm quark and a light quark,  $\bar{c}q$  ( $q = u, d$ ), which have no strong decay channels if bound. If we assume that dynamical chiral symmetry breaking is the same for the light quark in the charmed meson as in purely light-quark systems, we expect the same coupling constant  $g_s^q$ , in the QMC model. Thus, the  $D$  and  $\bar{D}$  mesons can provide very nice systems to study the dynamical symmetry breaking due to their light-quark components. That is, whether or not the light quarks in the  $D$  and  $\bar{D}$  mesons reveal the same dynamical symmetry breaking in a nuclear medium, as those in nucleons.

We note that, in the absence of any strong interaction, the  $D^-$  will form atomic states, bound by the Coulomb potential. The resulting binding for, say, the  $1s$  level in  $^{208}\text{Pb}$  is between 10 and 30 MeV and should provide a very clear experimental signature. On the other hand, although we expect the  $D$ -meson (systems of  $\bar{q}c$ ) will form deeply bound  $D$ -nucleus states, they will also couple strongly to open channels such as  $DN \rightarrow B_c(\pi's)$ , with  $B_c$  a charmed baryon. Unfortunately, because our present knowledge does not permit an accurate calculation of the  $D$ -meson widths in a nucleus, results for the  $D$ -mesic nuclei may not give useful information for experimenters.

In the following we discuss the nuclear binding of  $D$ ,  $\bar{D}$ ,  $\Lambda_c^+$  and  $\Lambda_b$  heavy hadrons. One of the interests to study such systems is dynamically symmetry breaking of light quarks inside the heavy flavored hadrons, whether or not the light quarks inside the heavy hadrons feel the same forces with those in light hadrons (nucleons and light mesons). The role of the light quarks in heavy hadrons in connection with the partial restoration of chiral symmetry in a nuclear medium, is one of the very interesting issues in this section—we refer the reader to Ref. [12] for an extended overview on this topic.

## 7.1 Predictions for $D$ - and $\bar{D}$ -mesic nuclei in $^{208}\text{Pb}$

In this subsection we discuss the possible formation of  $D$ - and  $\bar{D}$ -nuclear bound states in a  $^{208}\text{Pb}$  nucleus. The reason we consider the  $^{208}\text{Pb}$  nucleus is that, it induces sufficient attractive Coulomb potential for the negatively charged  $D^-$  meson, and this can assist to form the  $D^-$ - $^{208}\text{Pb}$  bound state, namely, a Coulomb-assisted mesic nuclei (nuclear bound states). Theoretically, possible nuclear bound states involving the  $D$  and  $\bar{D}$  mesons were studied in Refs. [107, 241, 242].

Because the role of the Coulomb potential for the  $D^-$ -meson is important, we explicitly give potentials for the  $D$  and  $\bar{D}$  mesons also including the Coulomb potential. But we do not show the potential for  $D^+$ , since the Coulomb repulsion for  $D^+$  would not allow the  $D^+$ - $^{208}\text{Pb}$  bound states. The potentials are given by:

$$V_s^D(r) = m_D^*(r) - m_D, \quad (144)$$

$$V_v^{D^-}(r) = V_\omega^q(r) - \frac{1}{2}V_\rho^q(r) - A(r), \quad (145)$$

$$V_v^{\bar{D}^0}(r) = V_\omega^q(r) + \frac{1}{2}V_\rho^q(r), \quad (146)$$

$$V_v^{D^0}(r) = -V_\omega^q(r) - \frac{1}{2}V_\rho^q(r), \quad (147)$$

where  $A(r)$  is the Coulomb potential associated with the  $D^-$  and  $^{208}\text{Pb}$ . Note that the  $\rho$ -meson mean field potential,  $V_\rho^q(r)$ , is negative in a nucleus with a neutron excess, such as e.g.,  $^{208}\text{Pb}$ , the present case. To discuss the effects of the larger  $\omega$ -meson coupling suggested by  $K^+$ -nucleus scattering,  $V_\omega^q(r)$  is replaced by  $\tilde{V}_\omega^q(r) = 1.4^2 V_\omega^q(r)$  [104, 107].

Before showing the calculated potentials for the  $D^-$  in  $^{208}\text{Pb}$ , which are particularly interesting in view of the strong Coulomb field, recall that we have already shown in Figs. 6 and 13 (right panel) the mass shift of  $D(\bar{D})$  calculated in symmetric nuclear matter.

In Fig. 14 we show respectively the Coulomb potential felt by  $D^-$  in  $^{208}\text{Pb}$  calculated by the QMC model (left panel), and the total potential, including the Coulomb and  $\rho$ -mean field potentials (right panel), the sum of the potentials for the two choices of  $V_s^{D^-}(r) + V_v^{D^-}(r)$  (the dashed line corresponds to  $\tilde{V}_\omega^q(r) = 1.4^2 V_\omega^q(r)$ , and the dotted line to the usual  $V_\omega^q(r)$ ). Because the  $D^-$  meson is heavy and may be described well in the (nonrelativistic) Schrödinger equation, one expects the existence of the  $D^-$ - $^{208}\text{Pb}$  bound states just from inspection of the naive sum of the potentials, in a way which does not distinguish the Lorentz vector or scalar character.

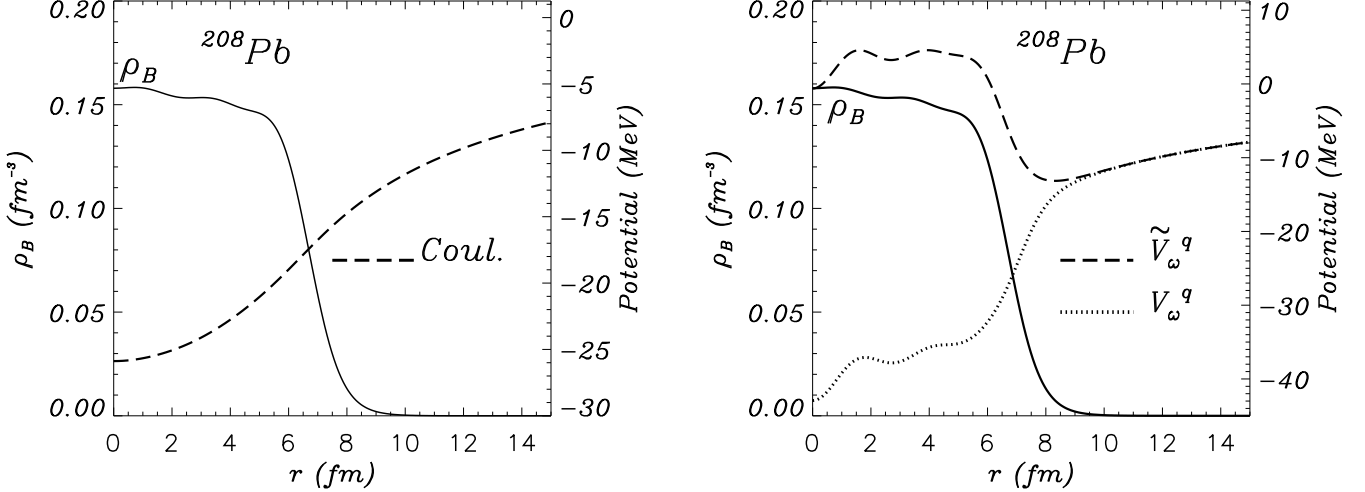


Figure 14: Coulomb potential in a  $^{208}\text{Pb}$  (left panel) and sum of the scalar, vector and Coulomb potentials for the  $D^-$  meson in  $^{208}\text{Pb}$  (right panel) for two cases,  $(m_{D^-}^*(r) - m_{D^-}) + \tilde{V}_\omega^q(r) - 1/2V_\rho^q(r) - A(r)$  (the dashed line) and  $(m_{D^-}^*(r) - m_{D^-}) + V_\omega^q(r) - 1/2V_\rho^q(r) - A(r)$  (the dotted line), where  $\tilde{V}_\omega^q(r) = 1.4^2 V_\omega^q(r)$ .

Now we are in a position to calculate the bound state energies for the  $D$  and  $\bar{D}$  in  $^{208}\text{Pb}$ , using the potentials calculated in the QMC model. For the  $D^-$  and  $\bar{D}^0$ , the widths are set to zero which is (nearly) exact. There are several variants of the dynamical equation for a bound meson-nucleus system. Consistent with the mean field picture of QMC, we solve the Klein-Gordon equation,

$$[\nabla^2 + (E_j - V_v^j(r))^2 - m_j^{*2}(r)] \phi_j(\vec{r}) = 0, \quad (148)$$

where  $E_j$  is the total energy of the meson  $j$  (the binding energy is  $E_j - m_j$ ). To deal with the long range Coulomb potential, we first expand the quadratic term (the zeroth component of Lorentz vector) as ,  $(E_j - V_v^j(r))^2 = E_j^2 + A^2(r) + V_{\omega\rho}^2(r) + 2A(r)V_{\omega\rho}(r) - 2E_j[A(r) + V_{\omega\rho}(r)]$ , where  $V_{\omega\rho}(r)$  is the combined potential due to  $\omega$  and  $\rho$  meson mean fields ( $V_{\omega\rho}(r) = V_\omega^q(r) - 1/2V_\rho^q(r)$  for  $D^-$ ). Then Eq. (148) can be rewritten as an effective Schrödinger-like equation,

$$\left[ -\frac{\nabla^2}{2m_j} + V_j(E_j, r) \right] \Phi_j(r) = \frac{E_j^2 - m_j^2}{2m_j} \Phi_j(r), \quad (149)$$

where  $\Phi_j(r) = 2m_j\phi_j(r)$  and  $V_j(E_j, r)$  is an effective energy-dependent potential which can be split into three pieces (Coulomb, vector and scalar parts),

$$V_j(E_j, r) = \frac{E_j}{m_j} A(r) + \frac{2E_j V_{\omega\rho}^j(r) - (A(r) + V_{\omega\rho}^j(r))^2}{2m_j} + \frac{m_j^{*2}(r) - m_j^2}{2m_j}. \quad (150)$$

Note that, only the first term in this equation is a long-range interaction and thus needs special treatment, while the second and third terms are short range interactions. In practice, Eq. (149) is first

converted into momentum space representation via a Fourier transformation and is then solved using the Kwan-Tabakin-Landé technique [196]. It should be emphasized that no reduction has been made to derive the Schrödinger-like equation, so that all relativistic corrections are included in the calculation. The calculated meson-nucleus bound state energies for  $^{208}\text{Pb}$ , are listed in Tab. 13.

Table 13:  $D^-$ ,  $\overline{D}^0$  and  $D^0$  bound state energies (in MeV). The widths are all set to zero.

State	$D^-(\tilde{V}_\omega^q)$	$D^-(V_\omega^q)$	$D^-(V_\omega^q, \text{no Coulomb})$	$\overline{D}^0(\tilde{V}_\omega^q)$	$\overline{D}^0(V_\omega^q)$	$D^0(V_\omega^q)$
1s	-10.6	-35.2	-11.2	unbound	-25.4	-96.2
1p	-10.2	-32.1	-10.0	unbound	-23.1	-93.0
2s	-7.7	-30.0	-6.6	unbound	-19.7	-88.5

The results in Tab. 13 show that both the  $D^-$  and  $\overline{D}^0$  are bound in  $^{208}\text{Pb}$  with the usual QMC  $\omega$  coupling constant,  $g_\omega^q$ . For  $D^-$  the Coulomb force provides roughly 24 MeV of attractive potential for the 1s state, and is strong enough to bind the system even with the much more repulsive  $\omega$  coupling  $1.4^2 g_\omega^q$  (viz.,  $\tilde{V}_\omega^q = 1.4^2 V_\omega^q$ ). The  $\overline{D}^0$  with the stronger  $\omega$  coupling  $1.4^2 g_\omega^q$  is not bound. Note that the difference between  $\overline{D}^0$  and  $D^-$  without the Coulomb force is due to the interaction with the  $\rho$ -meson mean field  $\frac{1}{2}V_\rho^q$ , which is attractive for the  $\overline{D}^0$  but repulsive for the  $D^-$ . For completeness, we have also calculated the binding energies for the  $D^0$ , which is deeply bound since the  $\omega$  interaction with the light antiquarks is attractive. However, the expected large width associated with strong absorption may render it experimentally inaccessible. It is an extremely important experimental challenge to see whether it can be detected.

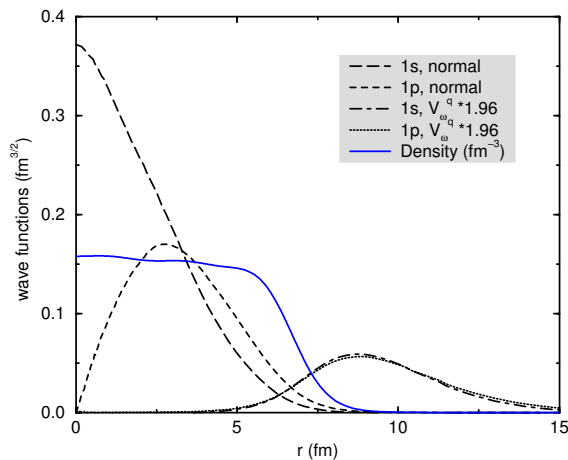


Figure 15: The  $D^-$ -meson bound state wave functions in  $^{208}\text{Pb}$  obtained by solving the Schrödinger-like equation Eq. (149) for two different  $\omega$  meson coupling strengths,  $g_\omega^q$  and  $1.4^2 g_\omega^q = 1.96 g_\omega^q$ . See also the caption of Fig. 14. The wavefunction is normalized as,  $\int_0^\infty dr 4\pi r^2 |\Phi(r)|^2 = 1$ .

The  $D^-$  bound state wave functions obtained by solving the Schrödinger-like equation Eq. (149) are shown in Fig. 15, together with the baryon density distribution in  $^{208}\text{Pb}$ . For the usual  $\omega$  coupling  $g_\omega^q$ , the eigenstates (1s and 1p) are well within the nucleus, and behave as expected at the origin. For the stronger  $\omega$  coupling  $1.4^2 g_\omega^q$ , however, the  $D^-$  meson is considerably pushed out of the nucleus. In this case, the bound state (an atomic state) is formed solely due to the Coulomb force. An experimental determination of whether this is a nuclear state or an atomic state would give a strong constraint on the  $\omega$  coupling. We note, however, that because it is very difficult to produce  $D$ -mesic nuclei with

small momentum transfer, and also the  $D$ -meson production cross subsection is small compared with the background from other channels, it will be a challenging task to detect such bound states experimentally.

It should be emphasized again that, whether or not the  $\overline{D}^0$ - $^{208}\text{Pb}$  bound states exist, would give new information as to whether the interactions of light quarks in a heavy meson are the same as those in a nucleon in nucleus. The enormous difference between the binding energies of the  $D^0$  ( $\sim 100$  MeV) and the  $\overline{D}^0$  ( $\sim 10$  MeV) is a simple consequence of the presence of a strong Lorentz vector mean-field, while the existence of any binding at all would give us important information concerning the role of the Lorentz scalar  $\sigma$  field (and hence dynamical symmetry breaking) in heavy-flavor hadron systems. In spite of the perceived experimental difficulties, we feel that the search for these bound systems should have a very high priority.

To summarize, the  $D^-$  meson should be bound in  $^{208}\text{Pb}$ , due to two different mechanisms, namely, the scalar and attractive  $\sigma$  mean field for the case of  $V_\omega^q(r)$  even without the Coulomb force, or solely due to the Coulomb force for the case of  $\tilde{V}_\omega^q(r) = 1.4^2 V_\omega^q(r)$ . The existence of any bound states at all would give us important information concerning the role of the Lorentz scalar  $\sigma$  field, and hence dynamical symmetry breaking.

## 7.2 $\Lambda_c^+$ - and $\Lambda_b$ -hypernuclei

Systematic studies were made on the property changes of heavy hadrons which contain a charm or a bottom quark in nuclear matter [100] (subsection 3.2), and on  $\Lambda_c^+$ - and  $\Lambda_b$ -hypernuclei [101]. Furthermore, production of  $D\overline{D}$  meson pair in nucleus [232], and formation reaction of  $\Lambda_c^+$ -hypernuclei [233] were studied. These results suggest that it is quite likely to form the charmed and bottom hypernuclei, which were predicted first in mid 70's [234, 235]. The experimental possibilities were also studied later [236]. (For the strange hypernuclei including recent development, see Refs. [99, 237, 238, 239].) In addition, the  $B^-$ -nuclear (atomic) bound states were also predicted, based on analogy with kaonic atom [240], and a study made for the  $D^-$ - and  $\overline{D}^-$ -nuclear bound states [107] (subsection 7.1) using the QMC model [92, 93, 98, 94] (section 3).

We discuss in the following subsections some results for  $\Lambda_c^+$ - and  $\Lambda_b$ -hypernuclei. The results are obtained by solving a system of coupled differential equations for finite nuclei, embedding a  $\Lambda_c^+$  or a  $\Lambda_b$  to a closed-shell nucleus in Hartree mean-field approximation. (See section 3.) The results are compared with those for the  $\Lambda$ -hypernuclei [99], which were also studied in the QMC model. It is shown that, although the scalar and vector potentials felt by the  $\Lambda$ ,  $\Lambda_c^+$  and  $\Lambda_b$  in the corresponding hypernuclear multiplet with the same baryon numbers are quite similar, the wave functions obtained, e.g., for  $1s_{1/2}$  state are very different. Namely, the  $\Lambda_c^+$  baryon density distribution in  $^{209}\text{Pb}$  is much more pushed away from the center than that for the  $\Lambda$  in  $^{209}\text{Pb}$  due to the repulsive Coulomb force. On the contrary, the  $\Lambda_b$  baryon density distributions in  $\Lambda_b$ -hypernuclei are much more centralized than those for the  $\Lambda$  in the corresponding  $\Lambda$ -hypernuclei due to its heavy mass. Furthermore, the level spacing for the  $\Lambda_b$  single-particle energies is much smaller than that for the  $\Lambda$  and  $\Lambda_c^+$ , which may imply many interesting new phenomena, that will possibly be discovered in experiments. The studies for such heavy-flavor-hypernuclei open a new possibility of experiments, for the facilities such as JLab, J-PARC, and FAIR.

## 7.3 Description of $\Lambda_c^+$ - and $\Lambda_b$ -hypernuclei

Let us start to consider static, (approximately) spherically symmetric charmed and bottom hypernuclei (closed shell plus one heavy baryon configuration) ignoring small non-spherical effects due to the embedded heavy baryon in Hartree mean-field approximation. In this approximation,  $\rho NN$  tensor coupling gives a spin-orbit force for a nucleon bound in a static spherical nucleus, although in Hartree-Fock it can give a central force which contributes to the bulk symmetry energy [93, 98]. Furthermore, it gives no

contribution for nuclear matter, since the meson fields are independent of position and time. Thus, we ignore the  $\rho NN$  tensor coupling in this study as usually adopted in the Hartree treatment of quantum hadrodynamics (QHD) [95, 96].

Here we recall the effective Pauli potential discussed in subsection 3.1. (See Eq. (75).) This potential is regard to reflect the Pauli blocking effects originating from the underlying quark structure of hyperons. As explained already, for the strange hyperon sector, it includes the effects of the  $\Sigma N - \Lambda N$  channel coupling, as well as those to reproduce the observed  $^{208}\text{Pb}$   $1s$  state single-particle energy of  $\cong -27$  MeV [99]. For the  $\Lambda_c^+$ - and  $\Lambda_b$ -hypernuclei, the same effective Pauli potential is included.

Next, we briefly discuss the spin-orbit force in QMC [93]. The origin of the spin orbit force for a composite nucleon moving through scalar and vector fields which vary with position, was explained in detail in Ref. [93]. The situation for the  $\Lambda$  and also for other hyperons are discussed in detail in Ref. [99, 101]. In order to include the spin-orbit potential (approximately) properly, for example, for the  $\Lambda_c^+$ -hypernuclei, it is added perturbatively the correction due to the vector potential,

$$-\frac{2}{2M_{\Lambda_c^+}^{*2}(\vec{r})r} \left( \frac{d}{dr} g_{\omega}^{\Lambda_c^+} \omega(\vec{r}) \right) \vec{l} \cdot \vec{s}, \quad (151)$$

to the single-particle energies obtained by solving the Dirac equation, in the same way as that added in Ref. [99]. This may correspond to a correct spin-orbit force which is calculated by the underlying quark model [93, 99]:

$$V_{S.O.}^{\Lambda_c^+}(\vec{r})\vec{l} \cdot \vec{s} = -\frac{1}{2M_{\Lambda_c^+}^{*2}(\vec{r})r} \left( \frac{d}{dr} [M_{\Lambda_c^+}^*(\vec{r}) + g_{\omega}^{\Lambda_c^+} \omega(\vec{r})] \right) \vec{l} \cdot \vec{s}, \quad (152)$$

since the Dirac equation at the hadronic level solved in usual QHD-type models leads to,

$$V_{S.O.}^{\Lambda_c^+}(\vec{r})\vec{l} \cdot \vec{s} = -\frac{1}{2M_{\Lambda_c^+}^{*2}(\vec{r})r} \left( \frac{d}{dr} [M_{\Lambda_c^+}^*(\vec{r}) - g_{\omega}^{\Lambda_c^+} \omega(\vec{r})] \right) \vec{l} \cdot \vec{s}, \quad (153)$$

which has the opposite sign for the vector potential,  $g_{\omega}^{\Lambda_c^+} \omega(\vec{r})$ . The correction to the spin-orbit force, which appears naturally in the QMC model, may also be modeled at the hadronic level of the Dirac equation by adding a tensor interaction, motivated by the quark model [243, 244]. Here, we should make a comment that, as was discussed in detail Ref. [245], a one boson exchange model with underlying (approximate) SU(3) symmetry in the strong interaction, also leads to weaker spin-orbit forces for the (strange) hyperon-nucleon ( $YN$ ) than that for the nucleon-nucleon ( $NN$ ).

However, in practice, because of its heavy mass  $M_{\Lambda_c^+}^*$ , the contribution to the single-particle energies from the spin-orbit potential with or without including the correction term, turned out to be even smaller than that for the  $\Lambda$ -hypernuclei, and further smaller for the  $\Lambda_b$ -hypernuclei. Contribution from the spin-orbit potential with the correction term is typically of order 0.01 MeV, and even the largest case is  $\cong 0.1$  MeV. This can be understood when one considers the limit,  $M_{\Lambda_c^+}^* \rightarrow \infty$  in Eq. (152), where the quantity inside the square brackets varies smoothly from an order of hundred MeV to zero near the surface of the hypernucleus, and the derivative with respect to  $r$  is finite. (See also Fig. 17 presented below.)

## 7.4 Predictions for single-particle energies in $\Lambda_c^+$ - and $\Lambda_b$ -hypernuclei

Now we discuss the results. First, in Fig. 16 we show the total baryon density distributions in  $^{41}_j\text{Ca}$  and  $^{209}_j\text{Pb}$  ( $j = \Lambda, \Lambda_c^+, \Lambda_b$ ), for  $1s_{1/2}$  configuration in each hypernucleus. Note that because of the self-consistency, the total baryon density distributions are dependent on the configurations of the embedded hyperons. The total baryon density distributions are quite similar for the  $\Lambda$ -,  $\Lambda_c^+$ - and  $\Lambda_b$ -hypernuclear



multiplet with the same baryon numbers,  $A$ , since the effect of  $\Lambda, \Lambda_c^+$  and  $\Lambda_b$  is  $\cong 1/A$  for each hypernucleus. Nevertheless, one can notice that the  $\Lambda_b$ -hypernuclear density near the center is slightly higher than the corresponding  $\Lambda$ - and  $\Lambda_c^+$ -hypernucleus. This is because the  $\Lambda_b$  is heavy and localized nearer the center, and contributes to the total baryon density there. The baryon (probability) density distributions for the  $\Lambda, \Lambda_c^+$  and  $\Lambda_b$  in the corresponding hypernuclei will be shown later.

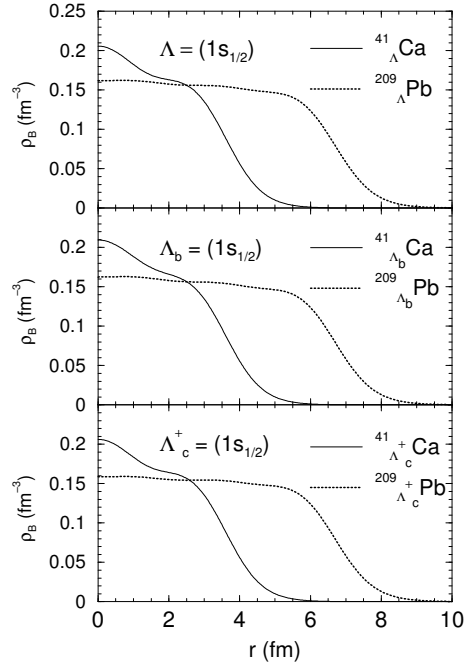


Figure 16: Total baryon density distributions in  ${}^4_1\text{Ca}$  and  ${}^{209}_j\text{Pb}$  ( $j = \Lambda, \Lambda_c^+, \Lambda_b$ ), for  $1s_{1/2}$  configuration for the  $\Lambda, \Lambda_c^+$  and  $\Lambda_b$ .

Next, in Fig. 17, it is shown the scalar, vector, and effective Pauli-blocking potentials (denoted by Pauli) felt by the  $\Lambda, \Lambda_c^+$  and  $\Lambda_b$  for  $1s_{1/2}$  state in  ${}^4_1\text{Ca}$  (left panel) and  ${}^{209}_j\text{Pb}$  (right panel) [ $j = \Lambda, \Lambda_c^+, \Lambda_b$ ]. For the  $\Lambda_c^+$ -hypernuclei, the Coulomb potentials are also shown. The corresponding probability density distributions are shown in Fig. 18.

As for the case of the nuclear matter [100], the scalar and vector potentials felt by these particles in hypernuclear multiplet with the same baryon numbers are also quite similar. (See subsection 3.2.) Thus, as far as the total baryon density distributions and the scalar and vector potentials are concerned,  $\Lambda$ -,  $\Lambda_c^+$ - and  $\Lambda_b$ -hypernuclei show quite similar features within the multiplet. However, as shown in Fig. 18, the wave functions obtained for  $1s_{1/2}$  state are very different. The  $\Lambda_c^+$  baryon density distribution in  ${}^{209}_{\Lambda_c^+}\text{Pb}$  is much more pushed away from the center than that for the  $\Lambda$  in  ${}^{209}_{\Lambda}\text{Pb}$  due to the Coulomb force. On the contrary, the  $\Lambda_b$  baryon density distributions in  $\Lambda_b$ -hypernuclei are much larger near the origin than those for the  $\Lambda$  in the corresponding  $\Lambda$ -hypernuclei due to its heavy mass.

Having obtained reasonable ideas about the potentials felt by  $\Lambda, \Lambda_c^+$  and  $\Lambda_b$ , we show the calculated single-particle energies in Tabs. 14 and 15 [101]. Results for the  $\Lambda$ -hypernuclei are from Ref. [99]. In these calculations, effective Pauli blocking, the effect of the  $\Sigma_{c,b}N - \Lambda_{c,b}N$  channel coupling, and correction to the spin-orbit force based on the underlying quark structure, are all included in the same way as adopted in Ref. [99]. However, the correction term for the spin-orbit force, as well as the contribution from the spin-orbit force itself are small, their effects on the final result are very small. Note that since the mass difference of the  $\Lambda_c^+$  and  $\Sigma_c$  is larger than that of the  $\Lambda$  and  $\Sigma$ , and it is also true for the  $\Lambda_b$  and  $\Sigma_b$ , we expect the effect of the channel coupling for the charmed and bottom hypernuclei is smaller than those for the strange hypernuclei, although the same parameters were used.

In addition, the single-particle states were searched up to the same highest state as that of the core neutrons in each hypernucleus, since the deeper levels are usually easier to observe in experiment.

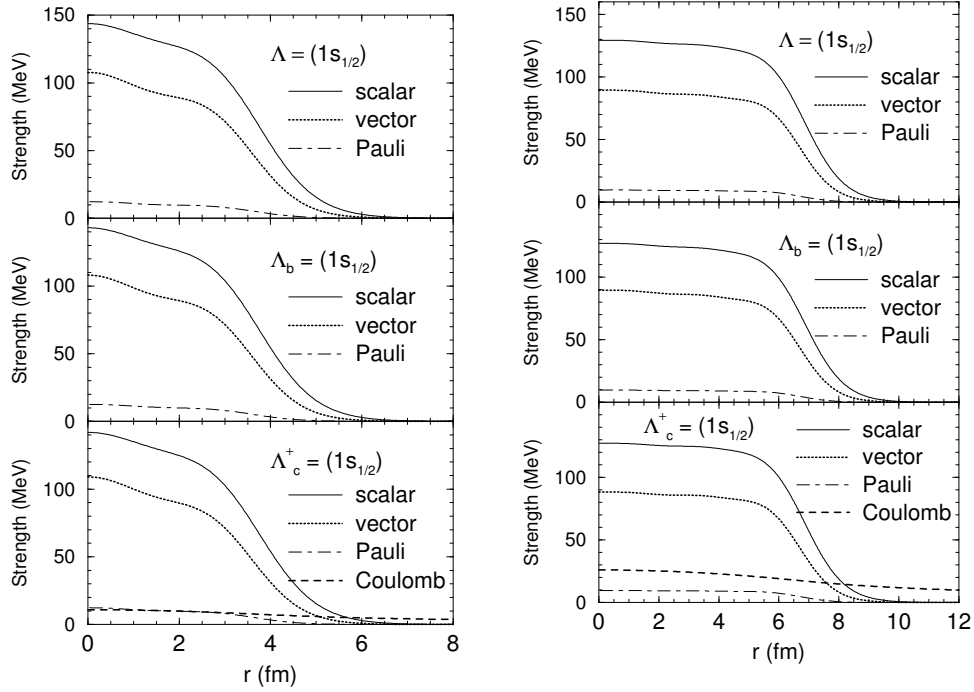


Figure 17: Potential strengths for  $1s_{1/2}$  state felt by the  $\Lambda$ ,  $\Lambda_c^+$  and  $\Lambda_b$  in  $^{41}\text{Ca}$  (left panel) and those in  $^{209}\text{Pb}$  ( $j = \Lambda, \Lambda_c^+, \Lambda_b$ ). "Pauli" stands for the effective, repulsive, potential representing the Pauli blocking at the quark level plus the  $\Sigma_{c,b}N - \Lambda_{c,b}N$  channel coupling, introduced at the baryon level phenomenologically [99].

From the results listed in Tabs. 14 and 15, first, it is clear that the  $\Lambda_c^+$  single-particle energy levels are higher than the corresponding levels for the  $\Lambda$  and  $\Lambda_b$ . This is a consequence of the Coulomb force. This feature becomes stronger as the proton number in the core nucleus increases.

Second, the level spacing for the  $\Lambda_b$  single-particle energies is much smaller than that for the  $\Lambda$  and  $\Lambda_c^+$ . This is ascribed to its heavy effective mass,  $M_b^*$ . In the Dirac equation for the  $\Lambda_b$ , the mass term dominates more than that of the term proportional to Dirac's  $\kappa$ , which classifies the states, or single-particle wave functions. (See Refs. [98, 99] for detail.) This small level spacing would make it very difficult to distinguish the states in experiment, or to achieve such high resolution. On the other hand, this may imply also many new phenomena. It will have a large probability to trap a  $\Lambda_b$  among one of those many states, especially in a heavy nucleus such as lead (Pb). What are the possible consequences? Maybe the  $\Lambda_b$  weak decay happens inside a heavy nucleus with a very low probability? Does it emit many photons when the  $\Lambda_b$  gradually makes transitions from a deeper state to a shallower state? All these questions may raise a lot of interesting issues.

To summarize, a quantitative study for  $\Lambda_c^+$ - and  $\Lambda_b$ -hypernuclei in the QMC model has shown that, although the scalar and vector potentials felt by the  $\Lambda$ ,  $\Lambda_c^+$  and  $\Lambda_b$  are quite similar in the corresponding hypernuclear multiplet with the same baryon numbers, the single-particle wave functions, and single-particle energy level spacings are quite different. For the  $\Lambda_c^+$ -hypernuclei, the Coulomb force plays a crucial role, and so does the heavy  $\Lambda_b$  mass for the  $\Lambda_b$ -hypernuclei. It should be emphasized that the values used for the coupling constants of  $\sigma$  (or  $\sigma$ -field dependent strength),  $\omega$  and  $\rho$  to the  $\Lambda$ ,  $\Lambda_c^+$  and  $\Lambda_b$ , are determined automatically based on the underlying quark model, the same as for the nucleon and other baryons. (Recall that the values for the vector  $\omega$  fields to any baryons can be obtained by

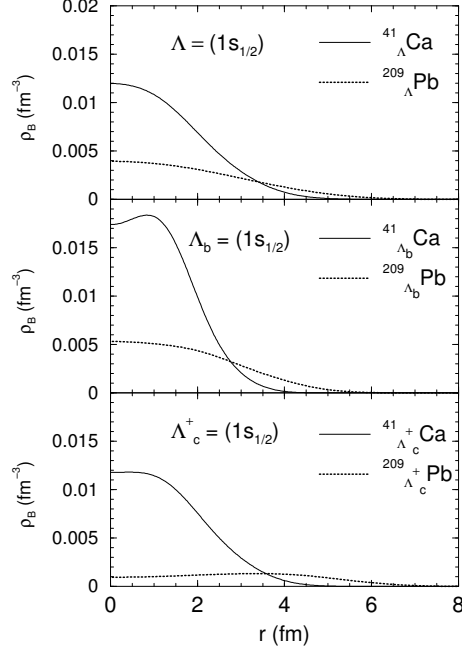


Figure 18:  $\Lambda, \Lambda_c^+$  and  $\Lambda_b$  baryon (probability) density distributions for  $1s_{1/2}$  state in  ${}^{41}_j\text{Ca}$  and  ${}^{209}_j\text{Pb}$  ( $j = \Lambda, \Lambda_c^+, \Lambda_b$ ).

Table 14: Single-particle energies (in MeV) for  ${}^{17}_j\text{O}$ ,  ${}^{41}_j\text{Ca}$  and  ${}^{49}_j\text{Ca}$  ( $j = \Lambda, \Lambda_c^+, \Lambda_b$ ). Single-particle energy levels are calculated up to the same highest states as that of the core neutrons. Results for the hypernuclei are taken from Ref. [99]. Experimental data for  $\Lambda$ -hypernuclei are taken from Ref. [246], where spin-orbit splittings for  $\Lambda$ -hypernuclei are not well determined by the experiments.

	${}^{16}_\Lambda\text{O}$ (Exp.)	${}^{17}_\Lambda\text{O}$	${}^{17}_{\Lambda_c^+}\text{O}$	${}^{17}_{\Lambda_b}\text{O}$	${}^{40}_\Lambda\text{Ca}$ (Exp.)	${}^{41}_\Lambda\text{Ca}$	${}^{41}_{\Lambda_c^+}\text{Ca}$	${}^{41}_{\Lambda_b}\text{Ca}$	${}^{49}_\Lambda\text{Ca}$	${}^{49}_{\Lambda_c^+}\text{Ca}$	${}^{49}_{\Lambda_b}\text{Ca}$
$1s_{1/2}$	-12.5	-14.1	-12.8	-19.6	-20.0	-19.5	-12.8	-23.0	-21.0	-14.3	-24.4
$1p_{3/2}$	-2.5	-5.1	-7.3	-16.5	-12.0	-12.3	-9.2	-20.9	-13.9	-10.6	-22.2
$1p_{1/2}$	( $1p_{3/2}$ )	-5.0	-7.3	-16.5	( $1p_{3/2}$ )	-12.3	-9.1	-20.9	-13.8	-10.6	-22.2
$1d_{5/2}$						-4.7	-4.8	-18.4	-6.5	-6.5	-19.5
$2s_{1/2}$						-3.5	-3.4	-17.4	-5.4	-5.3	-18.8
$1d_{3/2}$						-4.6	-4.8	-18.4	-6.4	-6.4	-19.5
$1f_{7/2}$									—	-2.0	-16.8

Table 15: Single-particle energies (in MeV) for  ${}_{j}^{91}\text{Zr}$  and  ${}_{j}^{208}\text{Pb}$  ( $j = \Lambda, \Lambda_c^+, \Lambda_b$ ). Experimental data are taken from Ref. [247]. See caption of Table 14 for other explanations.

	${}_{\Lambda}^{89}\text{Yb}$ (Exp.)	${}_{\Lambda}^{91}\text{Zr}$	${}_{\Lambda_c^+}^{91}\text{Zr}$	${}_{\Lambda_b}^{91}\text{Zr}$	${}_{\Lambda}^{208}\text{Pb}$ (Exp.)	${}_{\Lambda}^{209}\text{Pb}$	${}_{\Lambda_c^+}^{209}\text{Pb}$	${}_{\Lambda_b}^{209}\text{Pb}$
$1s_{1/2}$	-22.5	-23.9	-10.8	-25.7	-27.0	-27.0	-5.2	-27.4
$1p_{3/2}$	-16.0	-18.4	-8.7	-24.2	-22.0	-23.4	-4.1	-26.6
$1p_{1/2}$	( $1p_{3/2}$ )	-18.4	-8.7	-24.2	( $1p_{3/2}$ )	-23.4	-4.0	-26.6
$1d_{5/2}$	-9.0	-12.3	-5.8	-22.4	-17.0	-19.1	-2.4	-25.4
$2s_{1/2}$	—	-10.8	-3.9	-21.6	—	-17.6	—	-24.7
$1d_{3/2}$	( $1d_{5/2}$ )	-12.3	-5.8	-22.4	( $1d_{5/2}$ )	-19.1	-2.4	-25.4
$1f_{7/2}$	-2.0	-5.9	-2.4	-20.4	-12.0	-14.4	—	-24.1
$2p_{3/2}$	—	-4.2	—	-19.5	—	-12.4	—	-23.2
$1f_{5/2}$	( $1f_{7/2}$ )	-5.8	-2.4	-20.4	( $1f_{7/2}$ )	-14.3	—	-24.1
$2p_{1/2}$		-4.1	—	-19.5	—	-12.4	—	-23.2
$1g_{9/2}$		—	—	-18.1	-7.0	-9.3	—	-22.6
$1g_{7/2}$					( $1g_{9/2}$ )	-9.2	—	-22.6
$1h_{11/2}$						-3.9	—	-21.0
$2d_{5/2}$						-7.0	—	-21.7
$2d_{3/2}$						-7.0	—	-21.7
$1h_{9/2}$						-3.8	—	-21.0
$3s_{1/2}$						-6.1	—	-21.3
$2f_{7/2}$						-1.7	—	-20.1
$3p_{3/2}$						-1.0	—	-19.6
$2f_{5/2}$						-1.7	—	-20.1
$3p_{1/2}$						-1.0	—	-19.6
$1i_{13/2}$						—	—	-19.3

the number of light quarks in a baryon, but those for the  $\sigma$  are different as shown in Eq. (76).) Phenomenology would determine ultimately whether or not the coupling constants (strengths) determined by the underlying quark model actually work for  $\Lambda_c^+$  and  $\Lambda_b$ . This also provides us with the information on dynamical chiral symmetry breaking for the light quarks inside the different heavy-flavor baryons. Although one may speculate about some aspects of the present results, they clearly show that the  $\Lambda_c^+$ - and  $\Lambda_b$ -hypernuclei should exist in realistic experimental conditions. Experiments at facilities like JLab, J-PARC and FAIR would provide further inputs to gain a better understanding of the interaction of  $\Lambda_c^+$  and  $\Lambda_b$  with the nuclear matter. The study of the presence of  $\Lambda_c^+$  and  $\Lambda_b$  in finite nuclei experimentally is expected to be realized in the near future. Careful investigations, both theoretical and experimental, would lead to a much better understanding of the role of heavy quarks in a nuclear medium (finite nuclei).

## 8 Conclusions and Perspectives

We have presented a review of the theoretical ideas underlying the study of quarkonia in atomic nuclei, along with the latest experimental information. This is an exciting field which promises to provide a far deeper understanding of how QCD works. It is an field where experimental interest is high and important new results may be expected in the near future.

In the context of understanding whether or not one can expect to find  $J/\Psi$  mesons bound to atomic nuclei, we reviewed the predictions of both heavy quark effective field theory and lattice QCD for the attraction they might be expected to feel. The current expectation is for an attractive nuclear potential from a few MeV up to as much as 20 MeV, certainly sufficient to lead to bound states. Further support for this suggestion comes when one also calculates the reduction in the  $J/\Psi$  effective mass which arises through the modification of self-energy loops in-medium, calculated within the QMC model. These effects combined lead one to anticipate substantial binding energies in medium and large nuclei. We stress that these states should also be expected to be rather narrow, with widths below 1 MeV. That should improve the chances of finding them if one can produce the  $J/\Psi$  mesons in essentially recoilless conditions.

Even though there have been rather more experiments aimed at examining the interaction of  $\phi$  mesons with nuclei, the situation is currently quite uncertain. While it is clear that there is substantial broadening of the resonance, there is as yet no consensus as to whether or not the real part of the interaction is attractive. Our review of recent theoretical progress leads us to expect that one should find  $\phi$ -nucleus bound states for almost all nuclei. A number of experiments aimed at finding such states were described. It was also pointed out that these experiments are made even more challenging because the widths are expected to be comparable with the amount of binding.

For mesons which are not strictly quarkonia, like the  $\omega$ ,  $\eta$  and  $\eta'$ , there has also been a great deal of experimental work at laboratories such as CERN/SPS, GSI, JLab and Mami. There are hints of binding for both the  $\omega$  and  $\eta$  that strongly suggest more work would be valuable. There is compelling theoretical evidence that the real part of their interaction with nuclei is attractive but the possibility of strong absorption clouds those predictions, making the need for new experimental work even greater.

Other systems involving naked, rather than hidden, heavy quarks such as the  $D$  and  $\bar{D}$  mesons, as well as  $\Lambda_c^+$  and  $\Lambda_b$  baryons have also been reviewed. In some cases there are predictions of remarkably deep binding. In any case, there is considerable interest in the study of the binding of such systems because of the information which it may provide concerning dynamical symmetry breaking and the partial restoration of chiral symmetry in a nuclear medium.

The various theoretical predictions discussed here are of direct relevance for the existing modern experimental facilities such as FAIR, Jefferson Lab at 12 GeV and J-PARC, and we await the future experimental results with great anticipation. On the theoretical side, we look forward to the new

information that one may expect lattice QCD simulations will be able to provide concerning the binding of heavy-flavor-quarkonia and (heavy-flavor) baryons to atomic nuclei.

## 9 Acknowledgments

The authors would like to thank J.J. Cobos-Martínez for the updated  $J/\Psi$  results presented in this article. G.K. thanks Jaume Tarrús-Castellá for discussions. This work was partially supported by Conselho Nacional de Desenvolvimento Científico e Tecnológico - CNPq, Grant Nos. 305894/2009-9 (G.K.), 313800/2014-6 (A.W.T), 400826/2014-3 and 308088/2015-8 (K.T.), and Fundação de Amparo à Pesquisa do Estado de São Paulo - FAPESP, Grant Nos. 2013/0197-0 (G.K.) and 2015/17234 (K.T.). This research was also supported by the Australian Research Council through the ARC Centre of Excellence for Particle Physics at the Terascale (CE110001104), and through Grant No. DP151103101 (A.W.T.).

## References

- [1] S. Durr *et al.*, *Science* 322 (2008) 1224.
- [2] R. L. Jaffe, *Phys. Rev. Lett.* 38 (1977) 195; Erratum: [*Phys. Rev. Lett.* 38 (1977) 617].
- [3] P. J. Mulders and A. W. Thomas, *J. Phys. G* 9 (1983) 1159.
- [4] H. Clement, *Prog. Part. Nucl. Phys.* 93 (2017) 195.
- [5] R. De Vita *et al.* [CLAS Collaboration], *Phys. Rev. D* 74 (2006) 032001.
- [6] R. Aaij *et al.* [LHCb Collaboration], *Phys. Rev. Lett.* 115 (2015) 072001.
- [7] L. Maiani, *Nuovo Cim. C* 39 (2017) 319.
- [8] J. M. M. Hall, W. Kamleh, D. B. Leinweber, B. J. Menadue, B. J. Owen, A. W. Thomas and R. D. Young, *Phys. Rev. Lett.* 114 (2015) 132002.
- [9] Z. W. Liu, W. Kamleh, D. B. Leinweber, F. M. Stokes, A. W. Thomas and J. J. Wu, *Phys. Rev. D* 95 (2017) 034034.
- [10] J. Segovia, B. El-Bennich, E. Rojas, I. C. Cloet, C. D. Roberts, S. S. Xu and H. S. Zong, *Phys. Rev. Lett.* 115 (2015) 171801.
- [11] R. F. Lebed, R. E. Mitchell and E. S. Swanson, *Prog. Part. Nucl. Phys.* 93 (2017) 143.
- [12] A. Hosaka, T. Hyodo, K. Sudoh, Y. Yamaguchi and S. Yasui, arXiv:1606.08685 [hep-ph].
- [13] A. S. Kronfeld, *Phys. Rev. D* 58 (1998) 051501.
- [14] J. Collins, *Foundations of perturbative QCD* (Cambridge University Press, Cambridge, 2011)
- [15] C. Patrignani *et al.* (Particle Data Group), *Chin. Phys. C* 40 (2016) 100001.
- [16] D. J. Gross and F. Wilczek, *Phys. Rev. Lett.* 30 (1973) 1343.
- [17] H. D. Politzer, *Phys. Rev. Lett.* 30 (1973) 1346.

- [18] M. S. Chanowitz and J. R. Ellis, *Phys. Lett. B* 40 (1972) 397.
- [19] M. S. Chanowitz and J. R. Ellis, *Phys. Rev. D* 7 (1973) 2490.
- [20] R.J. Crewther, *Phys. Rev. Lett.* 28 (1972) 1421.
- [21] D. Z. Freedman, I. J. Muzinich and E. J. Weinberg, *Annals Phys.* 87 (1974) 95.
- [22] J. C. Collins, A. Duncan and S. Joglekar, *Phys. Rev. D* 16 (1977) 16.
- [23] M. B. Voloshin and V. I. Zakharov, *Phys. Rev. Lett.* 45 (1980) 688.
- [24] V.A. Novikov, M. A. Shifman, *Z. Phys. C* 8 (1981) 43.
- [25] A. Deur, S. J. Brodsky and G. F. de Teramond, *Prog. Part. Nucl. Phys.* 90 (2016) 1.
- [26] T. Appelquist and J. Carazzone, *Phys. Rev. D* 11 (1975) 2856.
- [27] J. F. Donoghue, E. Golowich and B. R. Holstein, *Dynamics of the standard model* (Cambridge University Press, Cambridge, 1996).
- [28] A. V. Smilga, *Lectures on quantum chromodynamics* (World Scientific, Singapore, 2001).
- [29] D. Kharzeev, *Proc. Int. Sch. Phys. Fermi* 130 (1996) 105.
- [30] X. D. Ji, *Phys. Rev. Lett.* 74 (1995) 1071.
- [31] A. V. Manohar and M. B. Wise, *Heavy quark physics* (Cambridge University Press, Cambridge, 2000).
- [32] C. D. Roberts and C. Mezrag, *EPJ Web Conf.* 137 (2017) 01017.
- [33] A. S. Kronfeld, *Lattice Gauge Theory and the Origin of Mass in One Hundred Years of Subatomic Physics*, ed. E.M. Henley and S.D. Ellis (World Scientific, Singapore, 2013)
- [34] I. C. Cloet and C. D. Roberts, *Prog. Part. Nucl. Phys.* 77 (2014) 1.
- [35] G. Eichmann, H. Sanchis-Alepuz, R. Williams, R. Alkofer and C. S. Fischer, *Prog. Part. Nucl. Phys.* 91 (2016) 1.
- [36] S. Scherer and M. R. Schindler, *A Primer for Chiral Perturbation Theory* (Springer, Berlin, 2012).
- [37] A. Bazavov *et al.*, *Phys. Rev. D* 85 (2012) 054503.
- [38] J. Gasser and H. Leutwyler, *Phys. Lett. B* 184 (1987) 83.
- [39] P. Gerber and H. Leutwyler, *Nucl. Phys. B* 321 (1989) 387.
- [40] E. G. Drukarev and E. M. Levin, *Prog. Part. Nucl. Phys.* 27 (1991) 77.
- [41] T. D. Cohen, R. J. Furnstahl and D. K. Griegel, *Phys. Rev. C* 45 (1992) 1881.
- [42] G. Krein, *AIP Conf. Proc.* 1701 (2016) 020012.
- [43] S. L. Adler, *Phys. Rev.* 177 (1969) 2426.
- [44] J. S. Bell and R. Jackiw, *Nuovo Cim. A* 60 (1969).

- [45] K. Fujikawa, *Phys. Rev. Lett.* 42 (1979) 1195.
- [46] S. D. Bass and A. W. Thomas, *Acta Phys. Polon.* B 45 (2014) 627.
- [47] S. D. Bass and A. W. Thomas, *Acta Phys. Polon.* B **41**, 2239 (2010) [arXiv:1007.0629 [hep-ph]].
- [48] S. D. Bass and A. W. Thomas, *Phys. Lett.* B 634 (2006) 368.
- [49] W. E. Caswell and G. P. Lepage, *Phys. Lett.* B 167 (1986) 437.
- [50] A. Pineda and J. Soto, *Nucl. Phys. B, Proc. Suppl.* 64 (1998) 428.
- [51] N. Brambilla, A. Pineda, J. Soto, and A. Vairo, *Nucl. Phys.* B 566 (2000) 275.
- [52] N. Brambilla, A. Pineda, J. Soto and A. Vairo, *Rev. Mod. Phys.* 77 (2005) 1423.
- [53] I. I. Y. Bigi, Y. L. Dokshitzer, V. A. Khoze, J. H. Kuhn and P. M. Zerwas, *Phys. Lett.* B 181 (1986) 157.
- [54] G. Paz, *Mod. Phys. Lett.* A 30 (2015) 1550128.
- [55] A. V. Manohar, *Phys. Rev.* D 56 (1997) 230.
- [56] G. Passarino, *Eur. Phys. J. Plus* 132 (2017) 16.
- [57] T. Kinoshita and M. Nio, *Phys. Rev.* D 53 (1996) 4909.
- [58] G. T. Bodwin, E. Braaten and G. P. Lepage, *Phys. Rev.* D 51 (1995) 1125, [Erratum: *Phys. Rev.* D 55 (1997) 5853].
- [59] A. Pineda and J. Soto, *Phys. Rev.* D 58 (1998) 114011.
- [60] B. A. Thacker and G. P. Lepage, *Phys. Rev.* D 43 (1991) 196.
- [61] S. Hashimoto and T. Onogi, *Ann. Rev. Nucl. Part. Sci.* 54 (2004) 451.
- [62] A. Pineda, *Prog. Part. Nucl. Phys.* 67 (2012) 735.
- [63] A. Vairo, in *Quark Confinement and the Hadron Spectrum IV*, edited by W. Lucha and K. M. Maung (World Scientific, Singapore, 2002), p. 221.
- [64] N. Brambilla, G. Krein, J. Tarrús Castellà and A. Vairo, *Phys. Rev.* D 93 (2016) 054002.
- [65] N. Brambilla, V. Shtabovenko, J. Tarrs Castell and A. Vairo, arXiv:1704.03476 [hep-ph].
- [66] B. R. Holstein, *Phys. Rev.* D 78 (2008) 013001.
- [67] H. Fujii and D. Kharzeev, *Phys. Rev.* D 60 (1999) 114039.
- [68] M. B. Voloshin, *Prog. Part. Nucl. Phys.* 61 (2008) 455.
- [69] J. Tarrús-Castellà, private communication.
- [70] C. M. Ko, P. Levai, X. J. Qiu and C. T. Li, *Phys. Rev.* C 45 (1992) 1400.
- [71] S. H. Lee, C. M. Ko, *Phys. Rev.* C 67 (2003) 038202.
- [72] G. Krein, A. W. Thomas and K. Tsushima, *Phys. Lett.* B 697 (2011) 136.



- [73] K. Tsushima, D. H. Lu, G. Krein and A. W. Thomas, *AIP Conf. Proc.* 1354 (2011) 39.
- [74] K. Tsushima, D. H. Lu, G. Krein and A. W. Thomas, *Phys. Rev. C* 83 (2011) 065208.
- [75] J. J. Cobos-Martínez, K. Tsushima, G. Krein and A. W. Thomas, “ $\eta_c$ - and  $J/\Psi$ -nucleus bound states” in preparation.
- [76] J. J. Cobos-Martínez, K. Tsushima, G. Krein and A. W. Thomas, *Phys. Lett. B* 771 (2017) 113
- [77] G. Krein, *EPJ Web Conf.* 137 (2017) 06012.
- [78] M. B. Voloshin, *Nucl. Phys. B* 154 (1979) 365.
- [79] M. E. Peskin, *Nucl. Phys. B* 156 (1979) 365.
- [80] G. Bhanot and M. E. Peskin, *Nucl. Phys. B* 156 (1979) 391.
- [81] H. Leutwyler, *Phys. Lett. B* 98 (1981) 447.
- [82] A. B. Kaidalov and P. E. Volkovitsky, *Phys. Rev. Lett.* 69 (1992) 3155.
- [83] A. W. Thomas and G. Krein, *Phys. Lett. B* 456 (1999) 5.
- [84] A. W. Thomas and G. Krein, *Phys. Lett. B* 481 (21) 2000.
- [85] P. J. A. Bicudo, G. Krein and J. E. F. T. Ribeiro, *Phys. Rev. C* 64 (2001) 025202.
- [86] R. J. Perry, M. E. Carrillo-Serrano and A. W. Thomas, arXiv:1703.01032 [nucl-th].
- [87] M. Berwein, N. Brambilla, J. Tarrús Castellà and A. Vairo, *Phys. Rev. D* 92 (2015) 114019.
- [88] M. Giordano and E. Meggiolaro, *Phys. Rev. D* 92 (2015) 096007.
- [89] M. Karliner, S. Nussinov and J. L. Rosner, *Phys. Rev. D* 95 (2017) 034011.
- [90] J. M. Richard, A. Valcarce and J. Vijande, *Phys. Rev. D* 95 (2017) 054019.
- [91] Y. Bai, S. Lu and J. Osborne, arXiv:1612.00012 [hep-ph].
- [92] P. A. M. Guichon, *Phys. Lett. B* 200 (1998) 235.
- [93] P. A. M. Guichon, K. Saito, E. N. Rodionov and A. W. Thomas, *Nucl. Phys. A* 601 (1996) 349.
- [94] K. Saito, K. Tsushima and A. W. Thomas, *Prog. Part. Nucl. Phys.* 58 (2007) 1.
- [95] J.D. Walecka, *Ann. Phys. (N.Y.)* 83 (1974) 491.
- [96] B.D. Serot and J.D. Walecka, *Adv. Nucl. Phys.* 16 (1986) 1.
- [97] A.W. Thomas, P.A.M. Guichon, D.B. Leinweber, and R.D. Young, *Prog. Theor. Phys. Suppl.* 124 (2004) 156.
- [98] K. Saito, K. Tsushima and A. W. Thomas, *Nucl. Phys. A* 609 (1996) 339.
- [99] K. Tsushima, K. Saito, A.W. Thomas, *Phys. Lett. B* 411 (1997) 9; (E) *ibid.* 421 (1998) 413; K. Tsushima, K. Saito, J. Haidenbauer, A.W. Thomas, *Nucl. Phys. A* 630 (1998) 691.
- [100] K. Tsushima and F. C. Khanna, *Phys. Lett. B* 552 (2003) 138.

- [101] K. Tsushima and F.C. Khanna, *Phys. Rev. C* 67 (2003) 015211.
- [102] D. L. Whittenbury, M. E. Carrillo-Serrano and A. W. Thomas, *Phys. Lett. B* 762 (2016) 467.
- [103] M. E. Bracco, G. Krein and M. Nielsen, *Phys. Lett. B* 432 (1998) 258.
- [104] K. Tsushima, K. Saito, A.W. Thomas, S.V. Wright, *Phys. Lett. B* 429 (1998) 239; (E) *ibid.* B 436 (1998) 453;  
K. Tsushima, A. Sibirtsev, A.W. Thomas, *Phys. Rev. C* 62 (2000) 064904;  
K. Tsushima, A. Sibirtsev, A.W. Thomas, *J. Phys. G* 27 (2001) 349.
- [105] K. Tsushima, *Nucl. Phys. A* 670 (2000) 198.
- [106] K. Tsushima, A. Sibirtsev, K. Saito, A. W. Thomas and D. H. Lu, *Nucl. Phys. A* 680 (2001) 280.
- [107] K. Tsushima, D.H. Lu, A.W. Thomas, K. Saito, R.H. Landau, *Phys. Rev. C* 59 (1999) 2824.
- [108] P. A. M. Guichon, H. H. Matevosyan, N. Sandulescu and A. W. Thomas, *Nucl. Phys. A* 772 (2006) 1.
- [109] M. Dutra *et al.*, *Phys. Rev. C* 90 (2014) 055203.
- [110] S. J. Brodsky, I. A. Schmidt and G. F. de Teramond, *Phys. Rev. Lett.* 64 (1990) 1011.
- [111] D. A. Wasson, *Phys. Rev. Lett.* 67 (1991) 2237.
- [112] S. J. Brodsky and G. A. Miller, *Phys. Lett. B* 412 (1997) 125.
- [113] M. E. Luke, A. V. Manohar and M. J. Savage, *Phys. Lett. B* 288 (1992) 355.
- [114] G. F. de Teramond, R. Espinoza and M. Ortega-Rodriguez, *Phys. Rev. D* 58 (1998) 034012.
- [115] A. Sibirtsev and M. B. Voloshin, *Phys. Rev. D* 71 (2005) 076005.
- [116] F. Klingl, S. Kim, S. H. Lee, P. Morath and W. Weise, *Phys. Rev. Lett.* 82 (1999) 339; [*Erratum-ibid.* 83 (1999) 4224].
- [117] A. Hayashigaki, *Prog. Theor. Phys.* 101 (1999) 923.
- [118] S. Kim and S. H. Lee, *Nucl. Phys. A* 679 (2001) 517.
- [119] V. B. Belyaev, N. V. Shevchenko, A. I. Fix and W. Sandhas, *Nucl. Phys. A* 780 (2006) 100.
- [120] A. Yokota, E. Hiyama and M. Oka, *Prog. Theor. Exp. Phys.* 2013 (2013) 113D01.
- [121] S. R. Beane, E. Chang, S. D. Cohen, W. Detmold, H.-W. Lin, K. Orginos, A. Parreño and M. J. Savage, *Phys. Rev. D* 91 (2015) 114503.
- [122] M. Alberti, G. S. Bali, S. Collins, F. Knechtli, G. Moir and W. Söldner, *Phys. Rev. D* 95 (2017) 074501.
- [123] K. Yokokawa, S. Sasaki, T. Hatsuda and A. Hayashigaki, *Phys. Rev. D* 74 (2006) 034504.
- [124] L. Liu, H. W. Lin and K. Orginos, *PoS LATTICE* (2008) 112.
- [125] T. Kawanai and S. Sasaki, *Phys. Rev. C* 82 (2010) 091501.

- [126] T. Kawanai and S. Sasaki, *PoS LATTICE* 156 2010
- [127] J. C. Bernauer *et al.* [A1 Collaboration], *Phys. Rev. C* 90 (2014) 015206.
- [128] V. F. Weisskopf, *Science* 113 (1951) 101.
- [129] M. Betz, G. Krein and T. A. J. Maris, *Nucl. Phys. A* 437 (1985) 509.
- [130] G. Krein and T. A. J. Maris, *Phys. Rev. C* 36 (1987) 365.
- [131] E. Eichten, K. Gottfried, T. Kinoshita, J. B. Kogut, K. D. Lane and T. M. Yan, *Phys. Rev. Lett.* 34 (1975) 369; Erratum: [*Phys. Rev. Lett.* 36 (1976) 1276].
- [132] E. Eichten, K. Gottfried, T. Kinoshita, K. D. Lane and T. M. Yan, *Phys. Rev. D* 17 (1978) 3090; Erratum: [*Phys. Rev. D* 21 (1980) 313].
- [133] J. W. Negele and H. Orland, *Quantum Many Particle Systems* (Addison-Wesley, Redwood City, 1988).
- [134] H. Kamada *et al.*, *Phys. Rev. C* 64 (2001) 044001.
- [135] M. Kamimura, *Phys. Rev. A* 38 621 1988.
- [136] E. Hiyama, Y. Kino and M. Kamimura, *Prog. Part. Nucl. Phys.* 51 223 2003.
- [137] O. Gryniuk and M. Vanderhaeghen, *Phys. Rev. D* **94** (2016) 074001.
- [138] O. Lakhina and E. S. Swanson, *Phys. Lett. B* 582 (2004) 172.
- [139] C. W. Xiao and U.-G. Meiner, *Phys. Rev. D* 92 (2015) 114002.
- [140] See, for example, L.I. Schiff, *Quantum Mechanics*, 3rd. edition (McGraw-Hill, 1968), Sec. 15.
- [141] M. Luscher, *Nucl. Phys. B* 354 (1991) 531.
- [142] P. F. Bedaque, *Phys. Lett. B* 593 (2004) 82.
- [143] N. Ishii, S. Aoki and T. Hatsuda, *Phys. Rev. Lett.* 99 (2007) 022001.
- [144] F. Calogero, *Variable phase approach to potential scattering* (Elsevier, New York, 1967).
- [145] S. Dubynskiy and M. B. Voloshin, *Phys. Lett. B* 666 (2008) 344.
- [146] Z. w. Lin, C. M. Ko and B. Zhang, *Phys. Rev. C* 51 (2000) 024904.
- [147] B. El-Bennich, G. Krein, L. Chang, C. D. Roberts and D. J. Wilson, *Phys. Rev. D* 85 (2012) 031502.
- [148] B. El-Bennich, M. A. Paracha, C. D. Roberts and E. Rojas, *Phys. Rev. D* 95 (2017) 034037.
- [149] F. S. Navarra and M. Nielsen, *Phys. Lett. B* 443 (1998) 285.
- [150] A. Khodjamirian, C. Klein, T. Mannel and Y.-M. Wang, *JHEP* 1109 (2011) 106.
- [151] C. E. Fontoura, J. Haidenbauer and G. Krein, *Eur. Phys. J.* 53 (2017) 92.
- [152] A. Ballon-Bayona, G. Krein and C. Miller, arXiv:1702.08417 [hep-ph].

- [153] A. Sibirtsev, K. Tsushima and A. W. Thomas, *Eur. Phys. J. A* 6 (1999) 351.
- [154] D. B. Leinweber, A. W. Thomas, K. Tsushima and S. V. Wright, *Phys. Rev. D* 64 (2001) 094502.
- [155] A. Le Yaouanc, L. Oliver, O. Pene, J.-C. Raynal *Phys. Rev. D* 8 (1973) 2223; *ibid* 9 (1974) 1415; 11 (1974) 1272;  
E. S. Ackleh, T. Barnes, and E. S. Swanson, *Phys. Rev. D* 54 (1996) 6811;  
T. Barnes and E. S. Swanson, *Phys. Rev. C* 77 (2008) 055206.
- [156] Z. w. Lin and C. M. Ko, *Phys. Rev. C* 62 (2000) 034903.
- [157] K. Saito, K. Tsushima and A. W. Thomas, *Phys. Rev. C* 56 (1997) 566.
- [158] A. Sibirtsev, K. Tsushima and A. W. Thomas, *Phys. Rev. C* 63 (2001) 044906.
- [159] K. Saito, K. Tsushima, A. W. Thomas and A. G. Williams, *Phys. Lett. B* 433 (1998) 243.
- [160] L. Tolos, A. Ramos and E. Oset, *Phys. Rev. C* 74 (2006) 015203;  
L. Tolos, C. Garcia-Recio and J. Nieves, *Phys. Rev. C* 80 (2009) 065202.
- [161] J. Haidenbauer, G. Krein, U. G. Meissner and A. Sibirtsev, *Eur. Phys. J. A* 33 (2007) 107.
- [162] J. Haidenbauer, G. Krein, U. G. Meissner and A. Sibirtsev, *Eur. Phys. J. A* 37 (2008) 55.
- [163] J. Haidenbauer, G. Krein, U. G. Meissner and L. Tolos, *Eur. Phys. J. A* 47 (2011) 18.
- [164] S. G. Matinyan and B. Müller, *Phys. Rev. C* 58 (1998) 2994;  
A. Bourque and C. Gale, *Phys. Rev. C* 78 (2008) 035206;  
K. Haglin and C. Gale, *Phys. Rev. C* 63 (2001) 065201 (2001).
- [165] K. Martins, D. Blaschke, and E. Quack, *Phys. Rev. C* 51 (1995) 2723;  
T. Barnes, E. S. Swanson, C. Y. Wong, and X. M. Xu, *Phys. Rev. C* 68 (2003) 014903.
- [166] F. S. Navarra, M. Nielsen, R. S. Marques de Carvalho and G. Krein, *Phys. Lett. B* 529 (2002) 87.
- [167] A. Bourque and C. Gale, *Phys. Rev. C* 80 (2009) 015204.
- [168] S. Leupold, V. Metag and U. Mosel, *Int. J. Mod. Phys. E* 19 (2010) 147.
- [169] R. S. Hayano and T. Hatsuda, *Rev. Mod. Phys.* 82 (2010) 2949.
- [170] R. Muto *et al.* [KEK-PS-E325 Collaboration], *Phys. Rev. Lett.* 98 (2007) 042501.
- [171] T. Ishikawa *et al.*, *Phys. Lett. B* 608 (2005) 215.
- [172] T. Mibe *et al.* [CLAS Collaboration], *Phys. Rev. C* 76 (2007) 052202.
- [173] X. Qian *et al.* [CLAS Collaboration], *Phys. Lett. B* 680 (2009) 417.
- [174] M. H. Wood *et al.* [CLAS Collaboration], *Phys. Rev. Lett.* 105 (2010) 112301.
- [175] A. Polyanskiy *et al.*, *Phys. Lett. B* 695 (2011) 74.
- [176] <http://rarfexp.riken.go.jp/yokkaich/paper/jparc-proposal-0604.pdf>.
- [177] [http://j-parc.jp/researcher/Hadron/en/pac\\_0907/pdf/Ohnishi.pdf](http://j-parc.jp/researcher/Hadron/en/pac_0907/pdf/Ohnishi.pdf).

- [178] [http://j-parc.jp/researcher/Hadron/en/pac\\_1007/pdf/KEK\\_J-PARC-PAC2010-02.pdf](http://j-parc.jp/researcher/Hadron/en/pac_1007/pdf/KEK_J-PARC-PAC2010-02.pdf).
- [179] K. Aoki [J-PARC E16 Collaboration], arXiv:1502.00703 [nucl-ex].
- [180] [https://www.jlab.org/exp\\_prog/PACpage/PAC42/PAC42\\_FINAL\\_Report.pdf](https://www.jlab.org/exp_prog/PACpage/PAC42/PAC42_FINAL_Report.pdf).
- [181] G. E. Brown and M. Rho, *Phys. Rev. Lett.* 66 (1991) 2720.
- [182] T. Hatsuda and S. H. Lee, *Phys. Rev. C* 46 (1992) R34.
- [183] T. Hatsuda, H. Shiomi and H. Kuwabara, *Prog. Theor. Phys.* 95 (1996) 1009.
- [184] F. Klingl, T. Waas and W. Weise, *Phys. Lett. B* 431 (1998) 254.
- [185] E. Oset and A. Ramos, *Nucl. Phys. A* 679 (2001) 616.
- [186] D. Cabrera and M. J. Vicente Vacas, *Phys. Rev. C* 67 (2003) 045203.
- [187] P. Gubler and W. Weise, *Phys. Lett. B* 751 (2015) 396.
- [188] D. Cabrera, A. N. Hiller Blin and M. J. Vicente Vacas, *Phys. Rev. C* 95 (2017) 015201.
- [189] J. J. Cobos-Martínez, K. Tsushima, G. Krein and A. W. Thomas, arXiv:1705.06653 [nucl-th].
- [190] F. Klingl, N. Kaiser and W. Weise, *Z. Phys. A* 356 (1996) 193.
- [191] S. H. Lee, C. Song and H. Yabu, *Phys. Lett. B* 341 (1995) 407.
- [192] K. Yamawaki, *Phys. Rev. D* 35 (1987) 412.
- [193] U. G. Meissner and I. Zahed, *Z. Phys. A* 327 (1987) 5.
- [194] U. G. Meissner, *Phys. Rept.* 161 (1988) 213.
- [195] S. Saito and K. Yamawaki, *NAGOYA, JAPAN: UNIV., PHYS. DEPT.* (1987) 225p.
- [196] Y. R. Kwan and F. Tabakin, *Phys. Rev. C* 18 (1978) 932.
- [197] P. Buhler *et al.*, *Prog. Theor. Phys. Suppl.* 186 (2010) 337.
- [198] H. Ohnishi *et al.*, *Acta Phys. Polon. B* 45 (2014) 819.
- [199] P. Wurm for the CERES collaboration,  
*Nucl. Phys. A* 590 (1995) 103c;  
 M. Masera for the HELIOS collaboration, *Nucl. Phys. A* 590 (1995) 93c.
- [200] P.Y. Bertin and P.A.M. Guichon, *Phys. Rev. C* 42 (1990) 1133.
- [201] M. H. Wood *et al.* [CLAS Collaboration], *Phys. Rev. C* 78 (2008) 015201.
- [202] G.J. Lolos *et al.*, *Phys. Rev. Lett.* 80 (1998) 241.
- [203] J. Friese [HADES Collaboration], *Prog. Part. Nucl. Phys.* 42 (1999) 235.
- [204] R. S. Hayano, S. Hirenzaki and A. Gillitzer, *In \*Pruhonice 1998, Mesons and light nuclei '98\**  
 473-477

- [205] R.S. Hayano, S. Hirenzaki and A. Gillitzer, *Eur. Phys. J A* 6 (1999) 99;  
F. Klingl, T. Waas and W. Weise, *Nucl. Phys. A* 650 (1999) 299.
- [206] K. Tsushima, D.H. Lu, A.W. Thomas, K. Saito, *Phys. Lett. B* 443 (1998) 26.
- [207] B. Friman, nucl-th/9801053;  
F. Klingl and W. Weise, hep-ph/9802211.
- [208] Q. Haider and L. C. Liu, *Phys. Lett. B* 172 (1986) 257.
- [209] L. C. Liu and Q. Haider, *Phys. Rev. C* 34 (1986) 1845.
- [210] K. Saito, K. Tsushima, D. H. Lu and A. W. Thomas, *Phys. Rev. C* 59 (1999) 1203.
- [211] S. Friedrich *et al.*, *Eur. Phys. J. A* 52 (2016) 297.
- [212] H. Nagahiro and S. Hirenzaki, *Phys. Rev. Lett.* 94 (2005) 232503.
- [213] H. Nagahiro, S. Hirenzaki, E. Oset and A. Ramos, *Phys. Lett. B* 709 (2012) 87.
- [214] H. Nagahiro, D. Jido, H. Fujioka, K. Itahashi and S. Hirenzaki, *Phys. Rev. C* 87 (2013) 045201.
- [215] Y. K. Tanaka *et al.* [n-PRiME/Super-FRS Collaboration], *Phys. Rev. Lett.* 117 (2016) 202501.
- [216] Y. K. Tanaka *et al.* [n-PRiME/Super-FRS Collaboration], arXiv:1705.10543 [nucl-ex].
- [217] U. Wiedner, *Prog. Part. Nucl. Phys.* 66 (2011) 477.
- [218] P. Kroll, B. Quadder and W. Schweiger, *Nucl. Phys. B* 316 (1989) 373.
- [219] B. Kerbikov and D. Kharzeev, *Phys. Rev. D* 51 (1995) 6103.
- [220] A. B. Kaidalov and P. E. Volkovitsky, *Z. Phys. C* 63 (1994) 517.
- [221] A. I. Titov and B. Kämpfer, *Phys. Rev. C* 78 (2008) 025201.
- [222] A. T. Goritschnig, P. Kroll and W. Schweiger, *Eur. Phys. J. A* 42 (2009) 43.
- [223] J. Haidenbauer and G. Krein, *Phys. Lett. B* 687 (2010) 314.
- [224] J. Haidenbauer and G. Krein, *Few Body Syst.* 50 (2011) 183.
- [225] A. Khodjamirian, C. Klein, T. Mannel and Y. M. Wang, *Eur. Phys. J. A* 48 (2012) 31.
- [226] A. I. Titov and B. Kämpfer, arXiv:1105.3847 [hep-ph].
- [227] A. T. Goritschnig, B. Pire and W. Schweiger, *Phys. Rev. D* 87 (2013) 014017, Erratum: *Phys. Rev. D* 88 (2013) 079903.
- [228] J. Haidenbauer and G. Krein, *Phys. Rev. D* 89 (2014) 114003.
- [229] R. Shyam and H. Lenske, *Phys. Rev. D* 90 (2014) 014017
- [230] Y. Y. Wang, Q. F. Lü, E. Wang and D. M. Li, *Phys. Rev. D* 94 (2016) 014025.
- [231] J. Haidenbauer and G. Krein, *Phys. Rev. D* 95 (2017) 01407.
- [232] R. Shyam and K. Tsushima, *Phys. Rev. D* 94 (2016) 074041.

- [233] R. Shyam and K. Tsushima, *Phys. Lett. B* 770 (2017) 236.
- [234] A.A. Tyapkin, *Sov. J. Nucl. Phys.* 22 (1976) 89.
- [235] C.B. Dover and S.H. Kahana, *Phys. Rev. Lett.* 39 (1977) 1506.
- [236] T. Bressani, F. Iazzi, *Nuovo. Cim.* 102 A (1989) 597;  
S.A. Buyatov, V.V. Lyukov, N.I. Strakov and V.A. Tsarev, *Nuovo. Cim.* 104 A (1991) 1361.
- [237] P. A. M. Guichon, A. W. Thomas and K. Tsushima, *Nucl. Phys. A* 814 (2008) 66.
- [238] K. Tsushima, P. A. M. Guichon, R. Shyam and A. W. Thomas, *Int. J. Mod. Phys. E* 19 (2010) 2546.
- [239] K. Tsushima and P. A. M. Guichon, *AIP Conf. Proc.* 1261 (2010) 232.
- [240] T.M. Ito et. al., *Phys. Rev. C* 58 (1998) 2366; M. Iwasaki, *Nucl. Phys. A* 670 (2000) 190c; S. Hirenzaki, Y. Okumura, H. Toki, E. Oset, and A. Ramos, *Phys. Rev. C* 61 (2000) 055205.
- [241] C. Garcia-Recio, J. Nieves and L. Tolos, *Phys. Lett. B* 690 (2010) 369.
- [242] C. Garcia-Recio, J. Nieves, L. L. Salcedo and L. Tolos, *Phys. Rev. C* 85 (2012) 025203.
- [243] B.K. Jennings, *Phys. Lett. B* 246 (1990) 325;  
M. Chiapparini, A.O. Gattone, B.K. Jennings, *Nucl. Phys. A* 529 (1991) 589.
- [244] J. Cohen and H.J. Weber, *Phys. Rev. C* 44 (1991) 1181.
- [245] C.B. Dover and A. Gal, *Prog. Part. Nucl. Phys.* 12 (1985) 171.
- [246] R.E. Chrien *Nucl. Phys. A* 478 (1988) 705c.
- [247] S. Ajimura et al., *Nucl. Phys. A* 585 (1985) 173.